Electron Interaction Effects in Some Correlated Transition Metal Perovskite Oxides Through Transport and Tunneling Experiments

A Thesis Submitted
in Partial Fulfillment of the Requirements
for the Degree of
Doctor of Philosophy

by

Ashutosh Tiwari

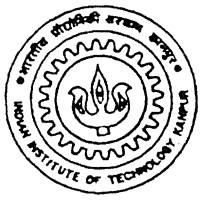

to the

DEPARTMENT OF PHYSICS
INDIAN INSTITUTE OF TECHNOLOGY, KANPUR

MAY, 1999

Certificate

It is certified that the work contained in this thesis entitled *"Electron Interaction Effects in Some Correlated Transition Metal Perovskite Oxides Through Transport and Tunneling Experiments"*, by *Ashutosh Tiwari*, has been carried out under my supervision and that this work has not been submitted elsewhere for a degree.

Dr. K. P. Rajeev
Assistant Professor
Department of Physics
Indian Institute of Technology
Kanpur

28 May, 1999

In this thesis an effort has been made to understand electrical transport in some disordered perovskite oxides. The thesis consists of two parts. The first part deals with the nickelates of the type $RNiO_3$ (R: La, Nd), chapters 3-6 belong to this part. The second part deals with the manganates of the type $La_{0.7}A_{0.3}MnO_3$ (A: Sr, Ba, Ca), chapter 7 belongs to this part. A brief outline of the thesis is given below:

Chapter 1 starts with an introduction to transition metal oxides. A brief discussion about Mott-Hubbard, Charge transfer and Anderson M-I transitions is given. Various aspects of disordered metallic systems are highlighted; the phenomena of weak localization and enhanced e-e interactions are discussed. This is followed by a short discussion on the role of disorder in transition metal oxides. Now a brief introduction to the nickelates of the type $RNiO_3$ (R: rare earth elements) is given and the earlier results on this system are reviewed. After this the manganates are discussed briefly. The phenomenon of double exchange interaction is explained. The previous results are reviewed and some peculiar features of the low temperature electrical conductivity of the system are pointed out.

Chapter 2 presents the details about the sample preparation, characterization, design and construction of cryostats, techniques and methodologies used in the measurements.

Chapter 3 is about $LaNiO_{3-\delta}$ ($0 \leq \delta \leq 0.14$) samples. This chapter contains the electrical resistivity ($2.5K \leq T \leq 300K$), thermopower ($5K \leq T \leq 300K$) and electron tunneling conductance (at T=1.2K) data of various samples. Stoichiometric $LaNiO_3$ behaves like a normal metal with positive temperature coefficient of resistivity (TCR) and an almost linear negative thermopower. As the oxygen deficiency increases the electrical resistivity (ρ) shows a minimum at low temperature which progressively shifts to higher temperature with increasing δ. The thermopower of the oxygen deficient samples is found to vary systematically with δ showing a sign reversal at low temperature, however its magnitude remains small throughout the whole temperature range which overrules the possibility of Kondo effect. In the low temperature limit the electrical conductivity follows a $T^{1/2}$ behavior. We also find a cusp-like dip in the tunneling conductance near zero bias voltage.

Both these features are attributed to enhanced interaction between the charge carriers in the system due to disorder.

Chapter 4 is about $NdNiO_{3-\delta}$ ($0.08 \leq \delta \leq 0.22$) samples. This chapter deals mainly with the electrical resistivity data ($1.2K \leq T \leq 300K$). A careful analysis of the data has been done and results are compared with earlier reports.

Chapter 5 is about $La_{1-x}Nd_xNiO_{3-\delta}$ ($0 \leq x \leq 1$) samples. In this chapter a detailed investigation of structure, electrical resistivity ($2.5K \leq T \leq 300K$), thermopower ($5K \leq T \leq 300K$), magnetoresistance ($0 < B \leq 4.5T$, $4.2\ K \leq T \leq 40K$) and electron tunneling conductance (at T=1.2K) has been done.

Chapter 6 is about $NdNi_{1-x}Fe_xNiO_{3-\delta}$ ($0.0 \leq x \leq 0.4$). This chapter contains the electrical resistivity ($2.5K \leq T \leq 300K$), thermopower ($5K \leq T \leq 300K$), magnetoresistance ($0 < B \leq 4.5T$, $4.2\ K \leq T \leq 40K$) and electron tunneling conductance (at T=1.2 K) of various samples. When Fe is doped in $NdNiO_{3-\delta}$ some interesting features appear. For 10% doping of Fe, instead of becoming more resistive the material becomes more conducting. For 20 % doping of Fe the material becomes highly resistive but is still metallic. For higher doping of Fe the material becomes fully insulating. The magnetoresistance in the system is negative. This presumably suggests that the magnetic field counteracts the disorder driven localization tendency of electrons.

Chapter 7 presents our results on manganates. The first part of this chapter contains a detailed study of the low temperature electrical resistivity and electron tunneling conductance of $La_{0.7}A_{0.3}MnO_3$ (A: Ca, Sr, Ba). The residual electrical resistivity of these materials is higher than the estimated Mott's maximum metallic resistivity and also the electrical resistivity of all the samples shows an upturn at around 30K. At low temperatures ($T < 15$ K) electrical resistivity follows $T^{1/2}$ dependence. For all the samples, an anomaly in the density of states, with a minimum at the Fermi energy is observed through electron tunneling conductance measurements. Both these features are the characteristics of a strongly interacting disordered metallic system. Various plausible mechanisms which might be responsible for the disorder in the system are discussed. The second part of this chapter

presents a systematic study of the effect of Fe doping at the Mn site in $La_{0.7}Sr_{0.3}MnO_3$. The doping of Fe at the Mn site does not cause any structural change, but the electrical transport in the system is strongly affected. As the concentration of Fe increases the system moves towards the insulating side and finally for 25% doping of Fe the material becomes fully insulating.

Chapter 8 presents the main conclusions drawn from the present investigations.

Acknowledgements

During the course of this thesis work I received enormous amount of help and support from a large number of people. I wish to acknowledge all of them. In Particular:

I wish to express my sincere gratitude to my thesis advisor Dr. K. P. Rajeev for his excellent guidance, help and blessings. His deep knowledge of cryogenics, electronics and computer programming has helped me at several occasions. The results presented in this thesis are an outcome of numerous discussions I have had with him. His sharp questions and incisive analysis widened my imagination and showed deeper insights. He has been extremely nice, kind and gentle to me, for which I thank him a lot.

I thank Prof. A. K. Majumdar for his help, suggestions and support. I have been greatly benefited by his vast knowledge and experience.

I thank Prof. R. C. Budhani for patiently attending my semester evaluations and for his probing questions.

I thank Prof. N. S. Gajbhiye for introducing me to several novel routes of sample preparation and characterization.

I thank Prof. A. K. Nigam for allowing me to do high field magnetoresistance measurements in his laboratory.

I thank Drs. C. V. Tomy, V. Subrahmanyam, S. Suder Manoharan, H. C. Verma, V. N. Kulkarni and Ravi Shankar for their valuable advice and suggestions at various stages

I thank all my labmates for their excellent cooperation. I mention T. K. Nath, N. Sudhakar, Gautam Sinha, Swapan, Gautam Mukherji and R. S. Patel in this regard. The association of Rabi Panda proved to be of immense value. The help provided by David, Gautam Mukherji and Patel in taking the final printout of the thesis can never be forgotten. Technical support provided by N. Sudhakar, Ram Ashray and Ram Prakash is worth appreciating.

I express my deep gratitude to my mother, father and sister for their love, support and blessings.

I thank CSIR India for providing me a research fellowship.

Contents

Synopsis i

Acknowledgments v

List of Figures xi

List of Tables xv

1.Introduction 1
1.1 Why are some oxides metallic and rest are not 2
1.2 Anderson Transition 4
1.3 Disordered metallic systems 5
1.3.1 Weak localization 6
1.3.2 Electron-electron interaction. 7
1.4 Disorder in Transition metal perovskite oxides 10
1.5 Nickelates 10
1.6 Manganates 12
1.7 Present study and motivation 15
1.8 The effect of polycrystallinity 17
1.9 Data analysis 18
1.10 Thesis Layout 18
References 20

2. Experimental 25
2.1 Sample preparation 25
2.1.1 Preparation of nickelates of the type $RNiO_3$ 25
2.1.2 Preparation of manganates 25
2.2 Characterization 26
2.2.1 X-ray diffraction 26
2.2.2 Iodometric titration 26
2.3 Design and construction of cryostats 27
2.3.1 A dipper cryostat for storage dewars 27
2.3.1 (A) Cryostat design and construction 28
2.3.1 (B) Sample holders 30
2.3.1 (C) Operation 31
2.3.1(D) Limitations of dipper cryostat 32
2.3.2 Conventional He^4 cryostat for glass dewar 33
2.3.3 A device for quick determination of Curie temperature 34
2.3.4 Construction of a specific heat set-up 35
2.4 Measurement techniques 35
2.4.1 Electrical resistivity 35

2.4.2 Thermopower 36
2.4.3 Tunneling conductance 37
2.4.4 Magnetoresistance 38
2.5 Automation and data acquisition 38
2.6 Miscellaneous 38
References 39

3. Electrical transport in $LaNiO_{3-\delta}$
3.1 Introduction 41
3.2 Experimental 42
3.3 Results 43
3.4 Discussion 47
3.4.1 Electrical resistivity 47
3.4.2 Tunneling spectroscopy 48
3.4.3 Thermopower 50
3.5 Conclusion 51
References 52

4. Electrical transport in $NdNiO_{3-\delta}$ **55**
4.1 Introduction 55
4.2 Experimental 56
4.3 Results and discussion 56
4.3.1 Electrical resistivity 58
4.3.2 Thermopower 65
4.3.3 Magnetization 66
4.4 Conclusion 67
References 68

5. Electrical transport in $La_{1-x}Nd_xNiO_{3-\delta}$ **71**
5.1 Introduction 71
5.2 Experimental 71
5.3 Results and discussion 72
5.3.1 Crystal structure 72
5.3.2 Electrical resistivity 74
5.3.3 Tunneling conductance 76
5.3.4 Magnetoresistance 78
5.3.5 Thermopower 79
5.4 Conclusion 80
References 81

6. Metal-insulator transition in $NdNi_{1-x}Fe_xO_{3-\delta}$ **83**
6.1 Introduction 83
6.2 Experimental 83
6.3 Results 84
6.4 Discussion 89

6.4.1 Electrical resistivity 89
6.4.2 Thermopower 90
6.4.3 Tunneling conductance 91
6.4.4 Magnetoresistance 92
6.5 Conclusion 92
References 93

7. Manganates 95
A. Low temperature electrical transport in $La_{0.7}A_{0.3}MnO_3$ (A: Ca, Sr, Ba) 96
7A.1 Experimental 96
7A.2 Results and discussion 96
7A.2.1 Electrical resistivity 96
7A.2.2 Electron tunneling conductance 100

B. Metal-Insulator transition in $La_{0.7}Sr_{0.3}Mn_{1-x}Fe_xO_3$ 103

7B.1 Introduction 103
7B.2 Results and discussion 103

The source of disorder 109

References 110

8. Conclusions 113

Appendix-I Design and construction of a calorimeter 117

Appendix-II Electron tunneling conductance and the density of states 125

Appendix-III Local Environment of Fe in $NdNi_{1-x}Fe_xO_{3-\delta}$ 127

Appendix-IV $LaMnO_{3+\delta}$ 133

List of Figures

1.1: A simple cubic perovskite structure. 1

1.2: Schematic illustration of energy levels for (a) Charge Transfer Insulator (b) Mott-Hubbard Insulator (c) Low Δ metal and (d) Low U metal. 3

1.3: (a) Random potential energy due to disorder (b) schematic diagram of the density of states vs. energy in an Anderson localized insulator (c) density of states vs. energy in a disordered metallic system. 4

1.4: Illustration of the mechanism of weak localization. 6

1.5: Single particle density of states (1) in a noninteracting electronic system (2) in an interacting electronic system. 9

1.6: (a) Resistivity vs. temperature for stoichiometric $NdNiO_3$ (after Granados *et al.* [30]) (b) resistance vs. temperature for sol-gel prepared nonstoichiometric $NdNiO_{3-\delta}$ (after Vassiliou *et al.* [36]). 11

1.7: Schematic illustration of double exchange interaction between Mn^{3+} and Mn^{+}. 13

1.8: (a) Temperature dependence of resistivity for $La_{1-x}Sr_xMnO_3$ crystals. Arrows show the critical temperature for the ferromagnetic phase transition. Anomalies indicated by triangles are due to the structural transition. (b) Electronic phase diagram of $La_{1-x}Sr_xMnO_3$. Open circles and filled triangles are the Neel (T_N) and Curie (T_c) temperatures, respectively. The abbreviations mean paramagnetic insulator (PI), paramagnetic metal (PM), spin-canted insulator (CNI), ferromagnetic insulator (FI), and ferromagnetic metal (FM) (after Urushibara *et al.*[45]). 14

2.1: Schematic diagram of dipper cryostat. 29

2.2: Sample holder for electrical resistivity measurement. 30

2.3: Sample holder for thermopower measurement. 30

2.4: Schematic diagram of He^4 cryostat 33

2.5: A Schematic diagram of Curie temperature device 34

2.6: Arrangement for the electrical resistivity measurement. 35

2.7: Arrangement for the thermopower measurement. 36

2.8: Thermopower of platinum measured using our thermopower setup. Symbols represent the present experimental data and solid line represents previously reported data[8]. 37

2.9: Arrangement for the electron tunneling conductance measurement. 37

3.1: X-ray diffraction pattern of $LaNiO_3$ taken with Cu K_α radiation. 42

3.2: Electrical resistivity of $LaNiO_{3-\delta}$ (δ=0.00, 0.06, 0.11, 0.14) from 2.5 K to 300 K. 44

3.3: Tunneling conductance (G) vs. the bias voltage for $LaNiO_{3-\delta}$ (δ=0.00, 0.06, 0.11, 0.14) at 1.2 K. The data have been normalized to unity at 100 mV and shifted vertically for clarity. Information about the absolute values is given in table 3.2. The inset shows the low bias (|V|<10 mV) experimental data for $LaNiO_3$, reflecting the signatures of the superconductivity gap of pb. 45

3.4: Thermopower of $LaNiO_{3-\delta}$ (δ=0.00, 0.06, 0.11, 0.14) from 5 K to 300 K. For δ=0.00, 0.06 and 0.11 the y-scale is on the left-hand side, while for δ=0.14, it is on the right hand side, The inset shows the fit for $LaNiO_{2.89}$ to $S = -\alpha T + \beta T^n$. 46

3.5: The variation of Δ with $\sigma(0)$. The solid curve represents the best fit to $\Delta = u + v.\sigma(0)^q$. 49

4.1: Structure of $NdNiO_{3-\delta}$, showing NiO_6 octahedra. Because of the orthorhombic distortion the Ni-O-Ni bond angles are less than 180^0. 57

4.2: Electrical resistivity of $NdNiO_{3-\delta}$ for various δ. Thin arrows represent whether the data was taken during cooling or heating. Not all the points are shown for clarity. 58

4.3: (a) Relative hysteresis $[(\rho_H - \rho_C)/\rho_C]$ vs. temperature for various δ, (b) max. relative hysteresis as a function of δ. When δ decreases relative hysteresis first increases and then starts decreasing. Solid circles show experimental data points. The line shown is a guide to the eye. 59

4.4: Low temperature (1.2 K < T < 16 K) conductivity data of $NdNiO_{2.88}$ and fits to eqs.(4.1)-(4.3). 62

4.5: Specific heat vs. temperature for $NdNiO_{3-\delta}$. After Blasco *et al.*[18]. 63

4.6: Time dependence of resistance for $NdNiO_{2.88}$, when the sample was maintained at 81 K during the cooling cycle. 64

4.7: Thermopower vs. temperature for $NdNiO_{2.92}$. 65

4.8: Magnetic susceptibility vs. temperature for $NdNiO_{2.88}$. The inset shows the variation of magnetization with field at 4.2 K and 40 K. 66

5.1: X-ray diffraction pattern of $La_{1-x}Nd_xNiO_{3-\delta}$ (x=0.0, 0.04, 0.06, 1.0). 72

5.2: Three-dimensional network of NiO_6 octahedra in (a) $LaNiO_3$ and in (b) $NdNiO_3$. 73

5.3: Electrical resistivity vs. temperature for $La_{1-x}Nd_xNiO_{3-\delta}$ ($0.0 \leq x \leq 1.0$). 74

5.4: Tunneling conductance vs. voltage for $La_{1-x}Nd_xNiO_{3-\delta}$ ($0.0 \leq x \leq 1.0$) at 1.2 K. The data have been normalized to unity at 100 mV and shifted vertically for clarity. Information about the absolute values is given in table 5.3. 76

5.5: Magnetoresistance [R(B)-R(0)]/R(0) vs. B for $La_{1-x}Nd_xNiO_{3-\delta}$ at 4.2 K. The inset shows the variation of magnetoresistance with temperature at B=4 T. 78

5.6: Thermopower of $La_{1-x}Nd_xNiO_{3-\delta}$ (x=0.0, 0.2, 0.4, 0.8, 1.0) from 5 K to 300 K. For x=0.0, 0.2 and 0.4 the y-scale is on the left hand side while for x=0.8 and 1.0 it is on the right hand side. 79

6.1: Electrical resistivity vs. temperature for $NdNi_{1-x}Fe_xNiO_{3-\delta}$. 85

6.2: Thermopower vs. temperature for $NdNi_{1-x}Fe_xNiO_{3-\delta}$. 86

6.3: Tunneling conductance vs. bias voltage for $NdNi_{1-x}Fe_xNiO_{3-\delta}$ at 1.2 K. The data has been normalized to unity at 100 mV and relatively shifted for clarity. 87

6.4: Magnetoresistance [R(B)-R(0)]/R(0) vs. B for $NdNi_{1-x}Fe_xNiO_{3-\delta}$ at 4.2 K. The inset shows the variation of magnetoresistance with temperature at B=4 T. 88

7.1: Temperature dependence of the electrical resistivity of $La_{0.7}A_{0.3}MnO_3$ (A: Ca, Sr, Ba). The inset shows the electrical resistivity of the samples below 50 K on an expanded scale. 97

7.2: Tunneling conductance vs. voltage for $La_{0.7}A_{0.3}MnO_3$ (A: Ca, Sr, Ba) at 1.2 K. The data have been normalized to unity at 100 mV and shifted

vertically for clarity. Information about the absolute values is given in table 7.2. The inset shows the superconductivity gap of Pb as seen in the low bias (|V| < 10 mV) tunneling conductance data of $La_{0.7}Sr_{0.3}MnO_3$. 101

7.3: Electrical resistivity of $La_{0.7}Sr_{0.3}MnO_3$ ($x \leq 0.25$). Inset shows the electrical resistivity of x=0.0 sample in an enlarged scale. 104

7.4: (a) Octahedral field splitting of d levels (b) schematic band structure of $La_{0.7}Sr_{0.3}MnO_3$ (c) band structure of Fe and Mn in $La_{0.7}Sr_{0.3}Mn_{1-x}Fe_xO_3$. 105

7.5: Tunneling conductance G(V) vs. bias voltage for $La_{0.7}Sr_{0.3}Mn_{1-x}Fe_xO_3$ ($x \leq 0.25$) at 1.2 K. The data have been normalized to unity at 100 mV and shifted vertically for clarity. Information about the absolute values is given in table 7.3. Inset shows the superconductivity gap of pb as seen in the low bias (|V| < 10 mV) tunneling conductance data of $La_{0.7}Sr_{0.3}MnO_3$. 107

AI.1: Schematic diagram of the cryostat used for specific heat measurement. 119

AI.2: Detailed diagram of the electronic circuit used for specific heat measurement. 120

AI.3: Sample temperature and heater power as a function of time. 122

AI.4: (a) Specific heat of Copper (b) specific heat of $La_{0.7}Sr_{0.3}Mn_{0.9}Cu_{0.1}O_3$, inset shows the magnetization vs T . 123

AII.1: Schematic illustration of the electron tunneling process. A thin insulating barrier separates the reference electrode and the sample. Φ_1 and Φ_2 represent the work functions and μ_1 and μ_2 represent the Fermi levels of the reference and sample respectively. V is the potential difference between the two electrodes. Conventionally if the sample voltage is greater than the reference electrode voltage, it is considered as a case of positive V. In this case the right side of the graph of dI/dV vs. V will represent empty states. 126

AIII.1: Room temperature Mössbauer spectrum of $NdNi_{1-x}Fe_xO_{3-\delta}$ for x<0.5. 127

AIII.2: Room temperature Mössbauer spectrum of $NdNi_{1-x}Fe_xO_{3-\delta}$ for x≥0.5. 127

AIV.1: A.C. susceptibility of $LaMnO_{3+\delta}$ samples as a function of temperature. Arrows indicate the temperature where $d\chi/dT$ is maximum. 134

List of Tables

3.1:Sintering conditions, oxygen nonstoichiometries (δ) and lattice parameters (a) for various $LaNiO_{3-\delta}$ samples. 43

3.2:Parameters used in fitting the low temperature (2.5K < T < 20K) conductivity data for $LaNiO_{3-\delta}$ to the empirical relation $\sigma(T) = \sigma(0) + bT^m - cT^n$. Number of data points used for fitting, N≈200. 48

3.3:Parameters used in fitting the tunneling conductance data for $LaNiO_{3-\delta}$ to $G(V) = G(0)\left[1 + (|V|/\Delta)^{0.5}\right]$. Data in the range 10 mV < V < 100 mV were used for fitting. Number of data points used for fitting, N≈100. 49

3.4 Parameters used in fitting the thermopower data (5 K < T < 300 K) to the experimental relation $S = -\alpha T + \beta T^n$. Number of data points used for fitting, N≈300. 50

4.1 Sintering conditions, δ, lattice parameters and Ni-O-Ni bond angles for various $NdNiO_{3-\delta}$ samples. 57

4.2:Parameters used in fitting the low temperature (1.2 K < T < 16 K) conductivity data of $NdNiO_{3-\delta}$ to eqs. (4.1)-(4.3). Number of data points used for fitting, N≈200. 61

5.1:Crystal structure, lattice parameters and oxygen contents for various $La_{1-x}Nd_xNiO_{3-\delta}$ samples. 73

5.2 Parameters used in fitting the low temperature (2.5 K < T < 20 K) conductivity data of $La_{1-x}Nd_xNiO_{3-\delta}$ to the empirical relation $\sigma(T) = \sigma(0) + bT^m - cT^n$. Number of data points used for fitting, N≈200. 75

5.3: Parameters used in fitting the tunneling conductance data of $La_{1-x}Nd_xNiO_{3-\delta}$ at 1.2 K to $G(V) = G(0)\left[1 + (|V|/\Delta)^{0.5}\right]$. Data in the range 10 mV < V < 100 mV were used for fitting. Number of data points used for fitting, N≈100. 77

6.1:Lattice parameters and oxygen contents for various $NdNi_{1-x}Fe_xO_{3-\delta}$ samples. 84

6.2:Parameters used in fitting the low temperature conductivity data of $NdNiO_{3-\delta}$ to eqs. (4.1)-(4.3). Number of data points used for fitting, N≈200. 89

6.3: Parameters used in fitting the tunneling conductance data of $NdNi_{1-x}Fe_xO_{3-\delta}$ ($x \leq 0.2$) to $G(V) = G(0)\left[1 + (|V|/\Delta)^n\right]$. Data in the range 10mV < V < 100 mV were used for fitting. Number of data points used for fitting, N≈100. 91

7.1 Parameters used in fitting the conductivity data of $La_{0.7}A_{0.3}MnO_3$ (A: Ca, Sr, Ba) to eq.(7.1) between 2.5 K and 15 K and to eq.(7.2) between 2.5 K and 100 K. Number of data points (N) used for fitting was ~300 in the first range and ~1000 in the second range. 98

7.2 Parameters used in fitting the tunneling conductance data of $La_{0.7}A_{0.3}MnO_3$ (A: Ca, Sr, Ba) to $G(V) = G(0)\left[1 + (|V|/\Delta)^n\right]$. Data in the range 10 mV < V < 100 mV were used for fitting. Number of data points used for fitting, N≈100. 101

7.3 T_p and parameters used in fitting the tunneling conductance data of $La_{0.7}Sr_{0.3}Mn_{1-x}Fe_xO_3$ to $G(V) = G(0)\left[1 + (|V|/\Delta)^n\right]$. Data in the range 10mV < V < 100 mV were used for fitting. Number of data points used for fitting, N≈100. 108

AIII.1: Lattice parameters and oxygen contents of $NdNi_{1-x}Fe_xO_{3-\delta}$ samples. 128

AIII.2: Isomer shift (IS), quadrupole splitting (QS), internal magnetic field and effective s-electron density at the iron nucleus for various $NdNi_{1-x}Fe_xO_{3-\delta}$ samples. 129

AIV.1: Mn^{3+}/Mn^{4+} ratio for different annealing conditions. 133

Chapter 1

Introduction

Transition metal oxides constitute one of the most interesting classes of solids, exhibiting a wide variety of structures, properties and phenomena[1]. They crystallize in several different structures, starting from well known ones like perovskite, pyrochlore and hexagonal ferrite to more complex structures like octahedral tunnel, lameller and low dimensional structures. The wide range of electrical transport properties exhibited by these oxides is equally outstanding. Some of them are metals (e.g. $LaNiO_3$, ReO_3), some are insulators (e.g. NiO, $BaTiO_3$) and some of them undergo an M-I transition as a function of temperature, pressure or composition (e.g. V_2O_3, $LaNi_{1-x}Co_xO_3$).

Recently, because of the discovery of some phenomena like high temperature superconductivity and giant magnetoresistance in oxides, they have become very popular. Both these phenomena, high temperature superconductivity as well as the giant magnetoresistance, are observed in perovskite oxides ABO_3 (see figure 1.1).

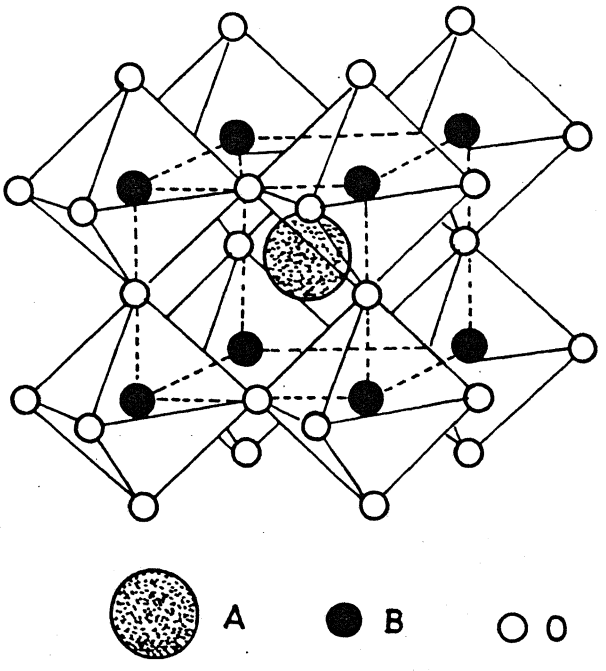

Figure 1.1 : A simple Cubic Perovskite Structure.

1.1 Why are some oxides metallic and the rest are not?

The question " Why some transition metal oxides are metallic and the rest are not? " has been puzzling the condensed matter physicists working on these oxides for a long time. In the beginning some efforts were made to answer this question using simple band theory. According to this theory the transition metal oxides in which the d-levels are partially filled should be metallic. But in 1937, de Boer and Verwey[2] (during a conference in Bristol) pointed out the inadequacy of this model to explain the insulating behavior of NiO. In NiO nickel is in 2+ state and has 8 d electrons; d-band is expected to be partially filled and hence NiO should be a metal. But it is well known that NiO is an insulator. Later on simple band theory considerations were found to fail in explaining the behavior of several other transition metal compounds also[3].

In 1949 Mott[4] pointed out the need to go beyond the single particle model and to take the coulomb correlations between electrons into account for explaining the properties of transition metal compounds. A major breakthrough in this field occurred in 1964 when Hubbard[5] introduced a model in which the interaction between electrons is included. This model takes into account the interaction between the electrons when they are on the same atom. For large interatomic separation this model leads to the splitting of d-band in to two bands, a full band and an empty band. These are known as the lower and upper Hubbard bands. These bands are separated by an energy "U" known as the coulomb correlation interaction energy. Depending upon the relative magnitudes of "U" and the hybridization between the bands, Hubbard model predicts metallic or insulating states for the transition metal oxides. Hubbard model works to some extent for the compounds of the early transition metals, but it fails to explain the behavior of Co, Ni and Cu compounds[6,7]. This model takes into account only the d-orbitals of the transition metal, however recent spectroscopic measurements[8-10] have shown that there is appreciable amount of hybridization between oxygen p and metal d orbitals. So, a model in which only transition metal d orbitals are taken into account and the ligand p orbitals are totally neglected has only limited applicability.

In 1985 Zaanen, Sawatzky and Allen proposed a model known as ZSA model[11] which takes into account both oxygen p orbitals as well as transition metal d orbitals. ZSA model has been quite successful in explaining the properties of several transition metal oxides

and it provides a unified basis for the metallic/insulating behavior of the transition metal oxides. According to this model the metallic or insulating properties of the TM oxides are determined by the relative positions of the fully occupied oxygen (O^{2-}) 2p states, the lowest unoccupied transition metal orbital (upper Hubbard band) and the highest filled transition metal orbital (lower Hubbard band). According to the relative positions of these levels the following four situations, as shown in figure 1.2, are possible

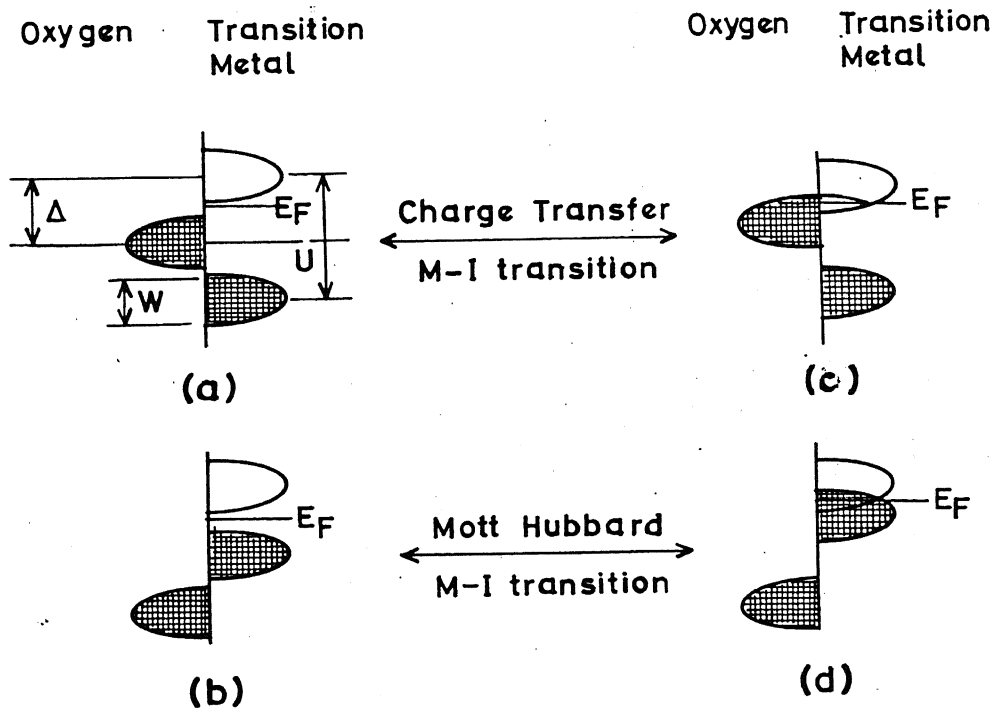

Figure 1.2 : Schematic illustration of energy levels for (a) Charge Transfer Insulator (b) Mott-Hubbard Insulator (c) Low Δ metal and (d) Low U metal.

In the first case the Fermi level lies in the forbidden region between oxygen 2p band and upper hubbard band; the material is an insulator known as a charge transfer insulator. In the second case Fermi level lies in the forbidden region between lower and upper Hubbard bands; material is again an insulator known as a Mott-Hubbard insulator. In the third case, oxygen 2p band and upper Hubbard band overlap and the Fermi level lies in the allowed region; material is a metal known as low Δ metal. In the fourth case lower and upper Hubbard bands overlap and the Fermi level lies in the allowed region; material is a metal known as low U metal.

Depending upon the relative values of Δ, U and W a material can be a metal or an insulator. Also any change in the relative values of Δ, U and W may cause a transition from metallic state to the insulating state and vice versa. So according to ZSA model transition metal oxides can undergo two kinds of M-I transition namely charge transfer M-I transition (when the charge transfer gap between the oxygen 2p and upper Hubbard band closes) and Mott-Hubbard M-I transition (when the coulomb correlation gap between the lower and upper Hubbard bands closes).

1.2 Anderson Transition

In addition to the above M-I transitions there is another mechanism which can drive a metal into the insulating side. This transition arises when some kind of disorder is introduced in the system. The disorder driven M-I transition is called Anderson transition[12,13]. In a disordered conductor electrons move in a random potential as shown in figure 1.3(a).

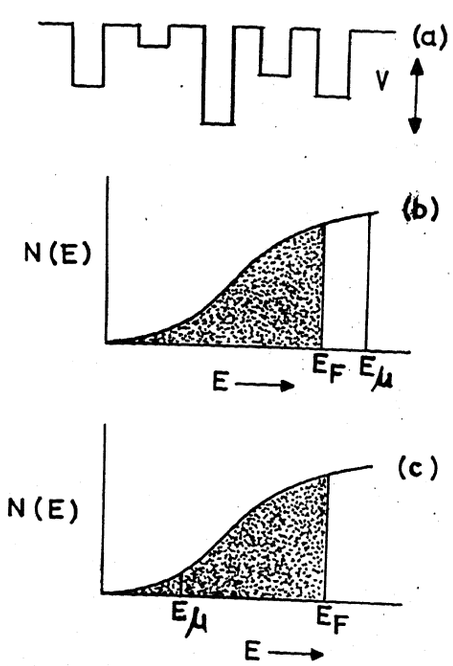

Figure 1.3 : (a) Random potential energy due to disorder (b) schematic diagram of the density of states vs. energy in an Anderson localized insulator (c) density of states vs. energy in a disordered metallic system.

The width of potential distribution (V) is a measure of the randomness of the potential. When the disorder and hence the randomness in potential is large (V $\gtrsim$ band width) all the states at the Fermi level gets localized (see figure 1.3(b)). If the disorder is small only the states at the band edges are localized (see figure 1.3(c)). The critical energy, which separates the extended states from the localized states, is known as the mobility edge, E_μ[14]. As long as $E_\mu < E_F$ the system remains metallic. However this disordered metallic phase[15,16] is quite different in its behavior from clean metals.

1.3 Disordered Metallic Systems

Condensed matter physics has been devoted largely to the study of crystalline materials. Periodicity of the crystal allows the electronic wave functions to be classified as Bloch waves[17]. However there are very few systems which can be classified as perfect crystals. Almost all the systems have some disorder in them. Degree of disorder varies from system to system. On the one hand we have weakly disordered systems with a few impurities or interstitials in an otherwise crystalline host. On the other hand we have highly disordered systems like alloys, glasses, heavily doped semiconductors etc.

Because of the disorder the electronic waves are scattered from impurities. In the weak disorder limit the mean free path for elastic scattering of electrons (l) is much larger than the wavelength of electron (λ) i.e. $k_F l \gg 1$ where $k_F = 2\pi/\lambda$ is the Fermi wave vector. In this case electron travels ballistically between two scattering events and the electrical transport properties are usually described by the Boltzmann transport equation. Within the framework of the Boltzmann transport theory supported by appropriate models the resistivity of a metal at low temperature has the form[17]:

$$\rho(T) = \rho(0) + AT^n \qquad (1.1)$$

with $2<n<5$ and $A>0$.

In the last few years it has been realized that the real physics of disordered material can not be understood by evading the issue and forcing them into the mold of ordered systems[16]. It has been found both experimentally as well as theoretically, that even in the weak disorder limit, some aspects of the Boltzmann transport theory are wrong[16]. For instance in several disordered systems it has been found that the electrical resistivity follows eq. (1.1) with $A<0$ and $n \approx 0.5$. Few other phenomena, which could not be understood within the framework of Boltzmann transport theory, are large negative magnetoresistance and zero bias anomaly in the tunneling conductance[18-20].

Failure of Boltzmann transport theory to explain the above features promoted the discovery of new concepts and theories for disordered systems namely the theories of weak localization and electron-electron interactions collectively known as quantum correction theory.

1.3.1 Weak Localization

In disordered metallic systems the phenomenon of weak localization[21] is observed. It arises because of the interference of electron waves as they get scattered from defects. The origin of weak localization has been very well described by Bergmann[21] and it can be explained with the help of figure 1.4.

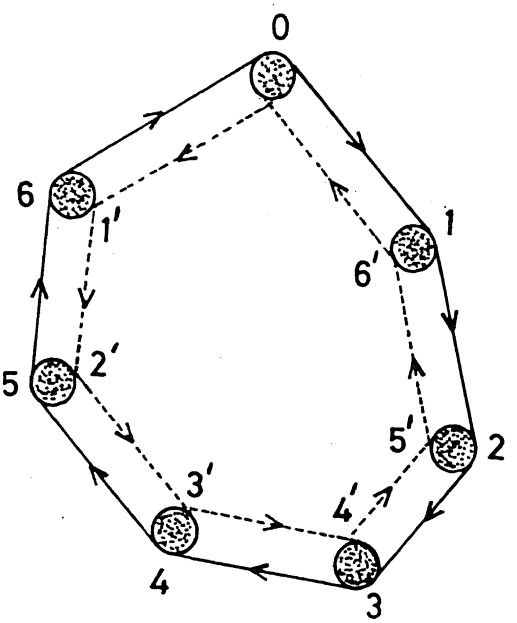

Figure 1.4 : Illustration of the mechanism of weak localization.

In this figure solid circles represent the defects and arrows on lines represent the direction of movement of electron. Let us consider an electron which starts initially from point O, undergoes elastic collisions from various defects (numbered 1, 2, 3 etc.) and finally comes back to the point O. Let the amplitude for this process be A. Now suppose instead of travelling the path O→1→2...6→O electron travels the time reversed path O→1'→2'…6'→O. Both these processes will have the same amplitude(A) if the time reversal symmetry is not broken during the process which will be the case if there are no inelastic collisions. If the electron gets inelastically scattered during its journey, the phase coherence between the two paths will be lost. In this

case the probability for the electron to return to its starting point will be $|A|^2+|A|^2=2|A|^2$. However if the electron is not inelastically scattered during its journey, the two partial electron waves will interfere constructively. In this case their amplitudes will add giving rise to probability $|2A|^2= 4|A|^2$ for the electron to return to its starting point. In other words electron has a tendency to stay where it is. This phenomenon is called weak localization.

Weak localization and electrical resistivity:

Because of the weak localization low temperature electrical conductivity follows the relation:

$$\sigma(T) = \sigma(0) + AT^{\frac{p}{2}} \qquad (1.2)$$

Here p is the exponent, which appears in the temperature dependence of the inelastic scattering lifetime of electrons also i.e. $\tau_{in} \propto T^{-p}$; p ≈ 1.5-3 and A>0.

Effect of Magnetic field:

When a magnetic field is applied the time reversal symmetry between the two paths of the electron breaks down. The electron waves travelling along the two otherwise equivalent paths acquire a phase difference, which is proportional to the area enclosed by the path as well as to the strength of the magnetic field. This destroys the constructive interference between the two electron waves and hence opposes the process of weak localization. As the strength of the magnetic field is increased, the weak localization tendency diminishes and consequently the conductivity of the system increases.

1.3.2 Electron-Electron Interaction

When the disorder is large the electrons undergo intense scattering from the impurities and hence their motion becomes diffusive. Now because of the reduced mobility the electron screening cloud can not follow a scattered electron as easily as in a clean metal. Due to reduced screening the phenomenon of enhanced electron-electron (e-e) interaction arises[15,16].

Electron-electron interaction and electrical resistivity: Because of the enhanced e-e interactions the electrical conductivity varies at low temperatures as[15].

$$\sigma(T) = \sigma(0) + m_\sigma T^{\frac{1}{2}} \tag{1.3}$$

Where

$$m_\sigma = 0.915\left(\frac{e^2}{2\pi^2 h}\right)\left(\frac{k_B}{\hbar D}\right)^{1/2}\left[\frac{2}{3} - \frac{3}{4}\tilde{F}_\sigma\right] \tag{1.4}$$

F_σ is a constant and depends on another constant F by the relation

$$\tilde{F}_\sigma = -\frac{32}{F}\left[1 + \frac{3F}{4} - \left(1 + \frac{F}{2}\right)^{3/2}\right] \tag{1.5}$$

F is known as the interaction constant and depends on the screening length and other details of the static screened coulomb potential between the electrons. Within the Thomas-Fermi approximation[22] F is related to the inverse screening length (x) by the relation

$$F = \left(\frac{x}{2k_F}\right)^2 \ln\left[1 + \left(\frac{2k_F}{x}\right)^2\right] \tag{1.6}$$

and x is related to the density of states at the Fermi level $N(E_F)$ by

$$x = \left[\frac{e^2 N(E_F)}{\varepsilon_0}\right]^{1/2} \tag{1.7}$$

Electron-electron interaction and the density of states :

Electron-electron interactions modify not only the transport properties but also the thermodynamic properties and the single particle density of states[15,16]. According to Altshuler and Aronov[15] single particle density of states shows a dip at the Fermi level. See figure 1.5.

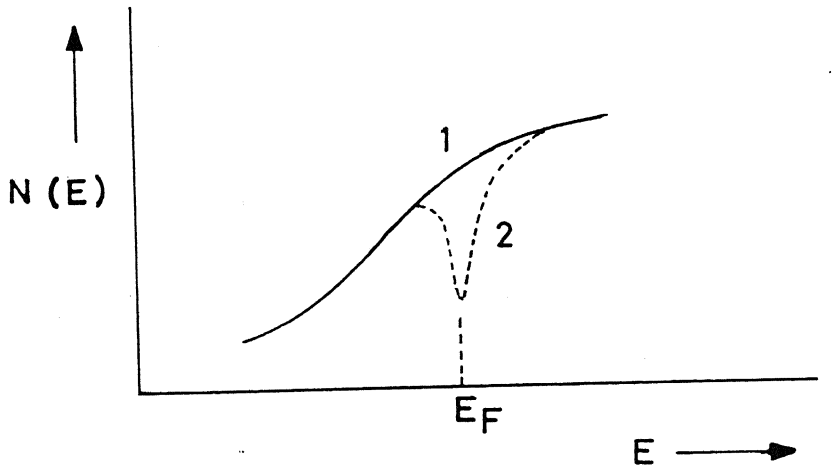

Figure 1.5 : Single particle density of states (1) in a noninteracting electronic system (2) in an interacting electronic system.

In a three dimensional interacting electronic systems the density of states (at T=0K) varies as

$$N(E) = N(0) + \delta N(E) \qquad (1.8)$$

Here $\delta N(E)$ is the correction to the density of states due to e-e interactions and it varies as:

$$\delta N(E) = N(0)\left(\frac{|E|}{\Delta}\right)^{1/2} \qquad (1.9)$$

$N(0)$ and Δ are constants and energy E is measured from the Fermi level.

At nonzero temperature the correction to the density of states goes as

$$\delta N(E) \propto \left[1 + \frac{1}{24}\left(\frac{\pi k_B T}{E}\right)^2\right] |E|^{1/2} \qquad (1.10)$$

1.4 Disorder in transition metal perovskite oxides

Most of the normal metallic transition metal oxides[23-24] have a high electron density (10^{22}/cm^3) but a rather low electrical conductivity (σ_{300K} ~ 10^3-10^4 S/cm). The low conductivity and high electron density indicates a low electron diffusivity, D (~ $\sigma / e^2 N(E_F)$=10^{-1}-10^{-2} cm^2/s). This shows that some disorder is always present in these oxides.

In a perovskite oxide ABO_3, disorder may arise in several ways. It can be created by the substitution of A and B by other atoms (by doping) or by creating oxygen deficiency. As a matter of fact in almost all the oxides some of these defects are always present. The degree of disorder in these oxides can be varied quite smoothly by changing the concentration of dopants or by changing the oxygen nonstoichiometry.

1.5 Nickelates

During last one decade there has been considerable interest in the study of the nickelates of the type $RNiO_3$ (R: rare earths)[25-31]. These oxides have been known for a long time[32], but after the discovery of high temperature superconductivity and giant magnetoresistance(GMR) in similarly structured oxides they gained a renewed interest. Although the nickelates do not show any of these fascinating phenomena, they provide a unique opportunity to understand various processes involved in the electrical transport in perovskite transition metal oxides.

First member of this series, $LaNiO_3$, is the most studied material[33-35]. It is a metal. The nominal electronic structure of Ni^{3+} is $t_{2g}^6 e_g^1$. The t_{2g} levels are filled and the conduction band is formed by the hybridization of the nickel e_g orbitals and oxygen 2p orbitals. Physical properties of $LaNiO_3$ have been widely reported in the literature[33-35]. All the reports show a large residual resistivity ($\rho(0)$~ 0.5 mΩ-cm). This large value of $\rho(0)$ implies an intrinsic disorder in the system. Also it has been found that when Ni is replaced by other atoms like Fe or Co, electrical resistivity shows a minimum at low temperature[33-35]. This minimum was attributed to the enhanced e-e interaction in the system due to disorder.

Other members of this series are either insulators or undergo an M-I transition. But there are very few studies on these samples, mainly because of the difficulties in the synthesis. Normally the nickel compounds with valencies higher than two are unstable. Their synthesis, if possible, therefore takes place either at a high temperature and high oxygen pressure or by low temperature chemical methods. Due to the extreme conditions required for synthesis not many studies of these samples could be done till 1989 when Vassiliou *et al.*[36] prepared $NdNiO_3$ by a novel low temperature sol-gel decomposition process. After this $NdNiO_3$ attracted a lot of attention and became the most widely studied sample of the series after $LaNiO_3$.

There are some differences between the samples prepared by these two methods i.e. the high temperature and high oxygen pressure method[31] and the low temperature sol-gel method[34]. While the samples prepared by the first method are stoichiometric, those prepared by the second method are oxygen deficient. Electrical resistivity measurements have been reported on the samples prepared by both the methods (see figure 1.6).

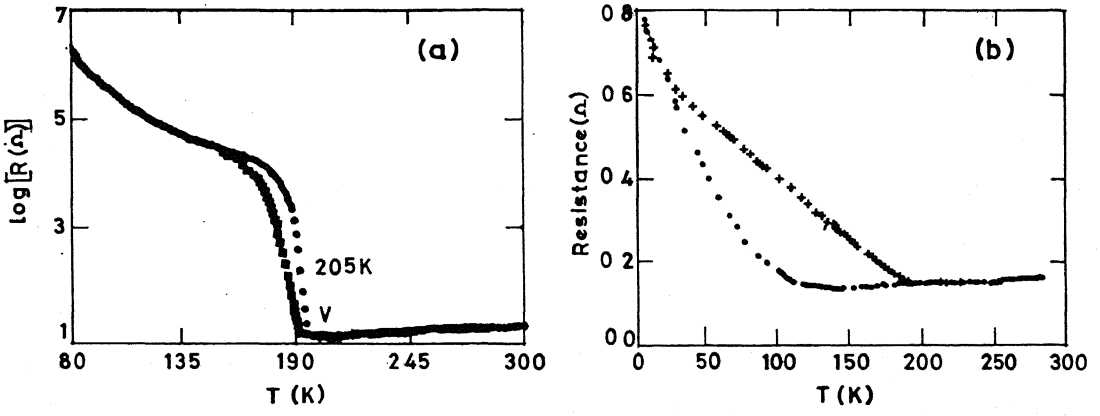

Figure 1.6 : (a) Resistivity vs. temperature for stoichiometric $NdNiO_3$ (after Granados *et al.*[30] (b) resistance vs. temperature for sol-gel prepared nonstoichiometric $NdNiO_{3-\delta}$ (after Vassiliou *et al.*[36]).

Stoichiometric $NdNiO_3$ shows a positive temperature coefficient of resistivity (TCR) above $\approx$ 200 K, below this temperature TCR is negative and the resistivity shows a sharp rise. A rise of 5-6 orders in resistivity is observed over a temperature interval of 10 K near the transition. At lower temperature resistivity tends to a very high value (i.e. conductivity tends to zero), a characteristic of insulators. Torrance *et al.*[29] explained this behavior using ZSA model[11]. According to the picture proposed by them $NdNiO_3$ is a charge transfer insulator at low temperature, but as the temperature increases because of the thermal energy, bands get broadened and finally at around 200 K they start overlapping resulting in the metallic state. As can be seen from figure 1.6 the high temperature behavior of sol-gel prepared nonstoichiometric $NdNiO_{3-\delta}$ is quite similar to that of stoichiometric $NdNiO_3$, but the low temperature behavior is different. In this case the resistivity increases only by a factor of 4-5 in going from 200 K to 4.2 K. Furthermore resistivity appears to remain finite (or extrapolated zero temperature conductivity is nonzero) even at T=0 K. We know that for an insulator the electrical conductivity at T=0 K should be zero so in the true sense $NdNiO_{3-\delta}$ can not be termed as an insulator. However in the literature the behavior of $NdNiO_{3-\delta}$ has been interpreted using ZSA model on similar lines as for $NdNiO_3$[25,26,36].

1.6 Manganates

Rare earth manganates $R_{1-x}A_xMnO_3$ (R: La, Pr, Nd,..; A: Ca, Sr, Ba, Pb) have been known and studied for more than a half century[37-41]. $LaMnO_3$ is the most widely studied member of this family. It is an antiferromagnetic charge transfer insulator. It was found by Van Santen *et al.*[38] in 1950 that when La is partially replaced by divalent atoms (like Ca, Sr, Ba) the material shows some very interesting properties. They observed a beautiful correlation between the electrical and magnetic properties of these materials. In 1969 Searle and Wang[41] reported a large magnetoresistance in the single crystals of $La_{1-x}Pb_xMnO_3$. After this these materials were almost forgotten for more than two decades. Interest in these materials was renewed by the discovery of giant magnetoresistance in thin films of $La_{2/3}Ba_{1/3}MnO_3$[42] and $La_{0.72}Ca_{0.25}MnO_z$[43] in 1993. Thereafter this material has created a lot of excitement in condensed matter physics[44-53].

The physicists are interested in these materials not only because of their potential for technological applications, but also because of the fundamental physics of the unusual metal-insulator transition observed in these materials. The typical composition where GMR effect is most prominent is $La_{1-x}A_xMnO_3$ with x=0.3. This compound is characterized by a ferromagnetic-paramagnetic transition at T_c and a resistivity peak at T_p, $T_p \approx T_c$. Above T_c the material behaves as a paramagnetic insulator while below T_c it behaves as a ferromagnetic metal.

The underlying physics of this system has been traditionally explained in terms of the double exchange model of Zener[54] in which the Hund's coupling is considered to be the most important factor.

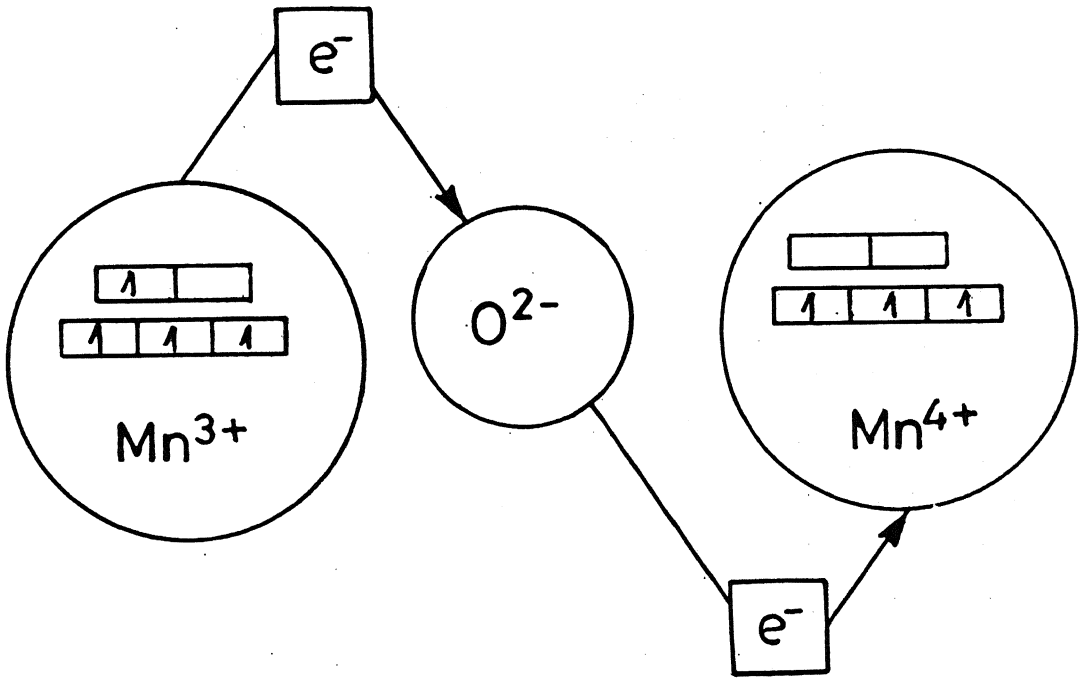

Fig 1.7: Schematic illustration of double exchange interaction between Mn^{3+} and Mn^{4+}.

In this compound Mn exhibits variable valence and exists in Mn^{3+} as well as in Mn^{4+} state. Because of the strong Hund's coupling, the electronic configuration of Mn^{3+} and Mn^{4+} are $t_{2g}^3 e_g^1$ and $t_{2g}^3 e_g^0$ respectively. Oxygen exists in O^{2-} state and hence has a closed cell. According to Zener the e_g electron jumps from Mn^{3+} to O^{2-} and at the same time one

electron jumps from O^{2-} to Mn^{4+}. This double hopping event requires that both hopping electrons have the same spin. Since in both the ions Hund's coupling is quite strong (i.e. all the electrons in the ion have a tendency to align parallel), the hopping event requires both Mn ions to have parallel moments. In this way D.E. mechanism connects the ferromagnetism (parallel alignment of Mn moments) and metallic behavior (hopping of carriers) in the system.

Other members of the series $La_{1-x}A_xMnO_3$ with $x \neq 0.3$ also show very interesting physics. In a classic paper Urushiborra *et al.*[45] have studied the electrical and magnetic properties of $La_{1-x}Sr_xMnO_3$ ($0 \leq x \leq 0.6$) single crystals and deduced a phase diagram in the plane of the temperature vs. x (see figure 1.8).

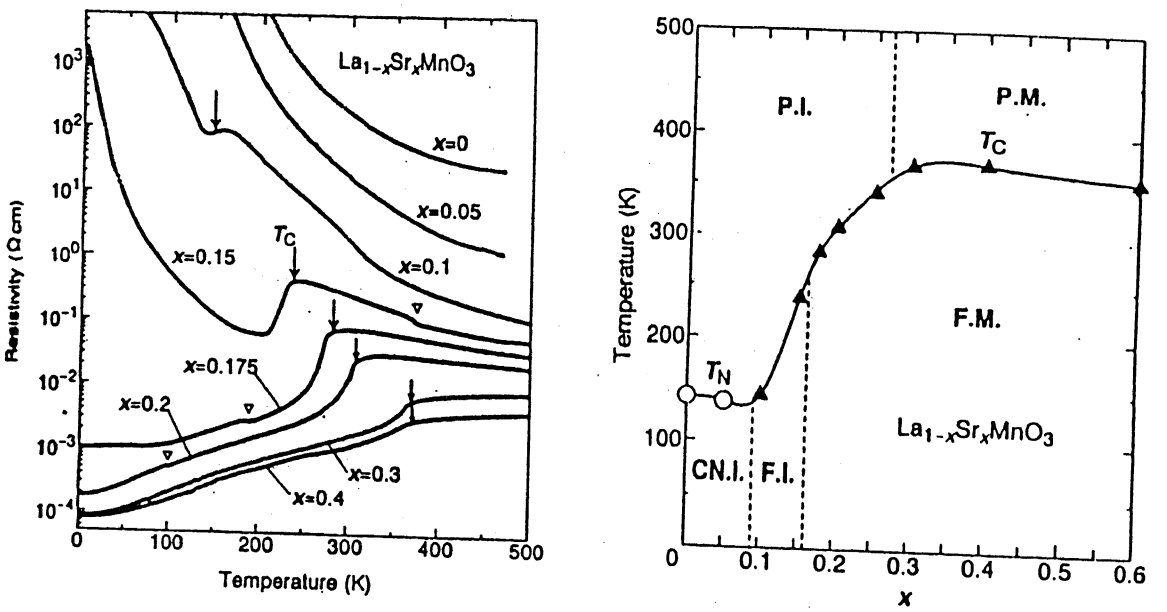

Figure 1.8 : (a) Temperature dependence of resistivity for $La_{1-x}Sr_xMnO_3$ crystals. Arrows show the critical temperature for the ferromagnetic phase transition. Anomalies indicated by triangles are due to the structural transition. (b) Electronic phase diagram of $La_{1-x}Sr_xMnO_3$. Open circles and filled triangles are the Neel (T_N) and Curie (T_c) temperatures, respectively. The abbreviations mean paramagnetic insulator(PI), paramagnetic metal(PM), spin-canted insulator(CNI), ferromagnetic insulator(FI) and ferromagnetic metal (FM). (after Urushibara *et al.* [45])

As can be seen from this figure, below the magnetic transition temperature, the system consists of three phases; a spin canted antiferromagnetic insulator for $x<0.1$, a ferromagnetic insulator for $0.1\leq x \leq 0.15$, a ferromagnetic metal for $x>0.15$. Above the magnetic transition temperature (T_N or T_c) the system is either a paramagnetic insulator ($x \leq 0.3$) or a paramagnetic metal ($x>0.3$). Among all these phases the most interesting one is FI phase, because double exchange theory predicts only the metallic ferromagnetic phase at low temperature. This phase is attributed[45] to arise because of the Anderson localization of conduction electrons due to random potentials. The localized carriers, which can not contribute to the macroscopic electrical transport, may mediate ferromagnetic interaction between the neighboring local spins to cause the ferromagnetic phase in a bond percolative manner[45].

Anderson localization[12,13] is encountered due to disorder in the system, which causes a randomization of the potential seen by the conduction electron. In the present system disorder might be arising because of the random impurity potential. As a matter of fact these random impurity potentials should be present in the metallic phase also. In the metallic regime these random fluctuations in the potential may affect the low temperature electrical transport and the density of the states quite significantly.

1.7 Present study and Motivation

In the past few years our understanding of electrical conduction in disordered metallic systems has advanced significantly[15,16]. The effect of disorder on the electrical transport and thermodynamic properties has been found to be extremely important, causing significant modifications to the conductivity and the density of states. A lot of theoretical as well as experimental efforts have gone in to understand the behavior of disordered materials. However most of these studies were confined to amorphous metals and doped semiconductors. There are very few reports about the effect of disorder on the electrical transport in oxide materials[23,33,34]. In this thesis an effort has been made to understand the electrical transport in some transition metal perovskite oxides. Here mainly the following issues have been addressed:

(1) Effect of disorder on the electrical transport in $LaNiO_{3-\delta}$

The parent compound $LaNiO_3$ is a well-studied sample[33,34] and it has been reported to have a high electron density ($\approx 10^{22}$ /cm^3) but a low conductivity (10^3-10^4 S/cm). The combination of a low conductivity and a high electron density indicates a low electron diffusivity(D) and a sizable amount of disorder. So this transition metal oxide looks ideal for a study of the effect of disorder on a metallic system. Furthermore, it is possible to exert fine control over the strength of the disorder by controlling the oxygen deficiency δ. Another interesting feature of this system is that the thermopower of the parent compound $LaNiO_3$ varies almost linearly with temperature. A linear temperature dependence suggests that the thermopower of the system is mainly due to the diffusion of electrons, and hence any interaction among the electrons due to disorder may be reflected in the thermopower of the system also.

(2) Electrical transport in sol-gel prepared $NdNiO_{3-\delta}$

As mentioned earlier in section 1.5, the low temperature behavior of the electrical resistivity of nonstoichiometric $NdNiO_{3-\delta}$ is quite different from that of stoichiometric $NdNiO_3$; the extrapolated zero temperature conductivity $\sigma(0)$ of stoichiometric $NdNiO_3$ tends to zero while that of $NdNiO_{3-\delta}$ attains a nonzero value. However, in literature, the behavior of $NdNiO_{3-\delta}$ is described on the same lines as for the stoichiometric $NdNiO_3$ (see section 1.5). But we are not convinced of this description and feel that a more precise analysis of the resistivity data of $NdNiO_{3-\delta}$ is needed. Also we find it interesting to do a systematic study of the effect of oxygen stoichiometry on the electrical transport behavior of the system.

(3) Study of $La_{1-x}Nd_xNiO_{3-\delta}$ and $NdNi_{1-x}Fe_xO_{3-\delta}$ solid solutions

In a perovskite oxide ABO_3, disorder can be introduced in several ways; it can be created by introducing oxygen nonstoichiometry as well as by substitutions at A and B sites. After studying the effect of oxygen nonstoichiometry we found it interesting to see how does the system behaves when the substitutions are made at the Nd and Ni sites.

(4) Electrical transport in Manganates

During the last 5-6 years a lot of work has been done on the perovskite manganate $La_{0.7}A_{0.3}MnO_3$ (A: Ca, Sr, Ba). Most of these studies are aimed at understanding the behavior of the system near T_c, where GMR effect is most prominent. Little work has gone in to understand the low temperature behavior of these oxides. Although the low temperature ($T<T_c$) electrical resistivity ρ shows metallic behavior (the temperature coefficient of resistivity, TCR, is positive), the magnitude of ρ is rather high even at T well below T_c. Sometimes, these ρ values are larger than or comparable to the Mott's maximum metallic resistivity for the system, which is of the order of 10 mΩ-cm. For typical metallic carrier densities this low conductivity implies a low diffusivity (D) for the carriers. Under such conditions the material is expected to behave as a highly disordered, interacting, electronic system. Here we have done a detailed analysis of low temperature electrical resistivity and electron tunneling conductance data to explore the disordered nature of these materials.

Most of the previous studies on manganates were done by replacing La by other rare earths. There are very few studies where doping is done at the Mn site. We feel that the partial replacement of Mn, which plays a key role in the conduction process, by other transition metals, may give important information about the nature of the system. For this purpose Fe was doped in $La_{0.7}Sr_{0.3}MnO_3$ and precise measurements of electrical resistivity and electron tunneling conductance were performed.

1.8 The effect of polycrystallinity

During this thesis work all the measurements were made on highly packed sintered pellets. The density of these samples was better than 90% of its theoretical value but still some effect of the grain boundaries may be present in the system. As a matter of fact the disorder in the system may owe its origin not only to the oxygen vacancies and dopants but also to the grain boundaries.

All of our studies were made over a group of samples. All the members of a particular group have the same packing density. So the effect of disorder due to grain

boundaries is expected to be more or less the same in all the samples while that due to other factors change systematically across the series. In all the systems investigated here, a systematic change in the properties is observed as we move through the series. This allows us to delineate the behavior of the system that is mainly determined by the disorder in the system.

Here it will be in order to mention that to date (to the best of our knowledge) there is no report about the preparation of the single crystals of $RNiO_3$, however the single crystals of manganates have been prepared by several groups.

1.9 Data analysis

Analysis of the data was done by fitting them to various possible models using a non-linear least squares fit program. Fitting was performed by minimizing the quantity $\chi^2 = \sum_{i=1}^{N}\left[\frac{Y_i(data) - Y_i(fit)}{Y_i(error)}\right]^2$, where $Y_i(data)$ is the experimentally determined quantity, $Y_i(fit)$ is the fit value and $Y_i(error)$ is the error estimate (standard deviation) for the i'th data point. N is the number of data points. $Y_i(error)$ was determined by collecting a large number (typically 25) of Y values at a particular temperature and taking their standard deviation. For a good fit χ^2 should be of the order of N i.e. $\chi^2 \approx N$.

1.10 Thesis layout

This thesis contains eight chapters.

Chapter 2 contains the details about the sample preparation, design and construction of cryostats, techniques and methodologies used in measurements.

Chapter 3 is about $LaNiO_{3-\delta}$ ($0 \leq \delta \leq 0.14$) samples. This chapter contains the electrical resistivity (2.5 K $\leq$ T $\leq$ 300 K), thermopower (5 K $\leq$ T $\leq$ 300 K) and electron tunneling conductance (at T=1.2 K) data of various samples.

Chapter 4 is about $NdNiO_{3-\delta}$ ($0.08 \leq \delta \leq 0.22$) samples. This chapter deals mainly with the resistivity data ($1.2\ K \leq T \leq 300\ K$). A careful analysis of the data has been done and results are compared with earlier reports.

Chapter 5 is about $La_{1-x}Nd_xNiO_{3-\delta}$ ($0.0 \leq x \leq 1.0$) samples. In this chapter a detailed investigation of structure, electrical resistivity ($2.5\ K \leq T \leq 300\ K$), thermopower ($5\ K \leq T \leq 300\ K$), magnetoresistance ($0 < B \leq 4.5T$; $4.2\ K \leq T \leq 40\ K$) and electron tunneling conductance (at T=1.2 K) has been presented.

Chapter 6 is about $NdNi_{1-x}Fe_xNiO_{3-\delta}$ ($0.0 \leq x \leq 0.4$). This chapter contains the electrical resistivity ($2.5\ K \leq T \leq 300\ K$), thermopower ($5\ K \leq T \leq 300\ K$), magnetoresistance ($0 < B \leq 4.5T$, $4.2\ K \leq T \leq 40\ K$) and electron tunneling conductance (at T=1.2 K) of various samples.

Chapter 7 is about manganates. First part of this chapter contains a thorough quantitative analysis of low temperature electrical resistivity and electron tunneling conductance data of $La_{0.7}A_{0.3}MnO_3$ (A: Ca, Sr, Ba) samples. In the second part of this chapter the effect of Fe doping at the Mn site has been studied.

Chapter 8 presents the main conclusions of the thesis.

References:

[1] C. N. R. Rao and B. Raveau, Transition metal oxides (Wiley, New York, 1998).

[2] J. H. de Boer and E. J. W. Verwey, Proc. Phys. Soc. A **49,** 59 (1937).

[3] J. B. Torrance, P. Lacorre, C. Asavaroengchai and R. Metzger, J. Solid State Chem. **81**, 208 (1991).

[4] N. F. Mott, Proc. Phys. Soc. A **62**, 416 (1949).

[5] J. Hubbard, Proc. R. Soc. A, **277**, 237 (1964).

[6] S. Hüefner, Solid State Commun. **49**, 1177(1984).

[7] N. F. Mott, Metal-Insulator transitions (Taylor and Francis, London, 1974).

[8] M. Medarde, A. Fontaine, J. L. García-Muñoz, J. Rodríguez-Carvajal, M. de Santis, M. Sacchi, G. Rossi and P. Lacorre, Phys. Rev. B **46**, 14975 (1992).

[9] J. García, J. Blasco and M. G. Proietti, Phys. Rev. B **52**,15823 (1995).

[10] T. Mizokawa, A. Fujimori, T. Arima, Y. Tokura, N. Mori and J. Akimitsu , Phys. Rev. B **52**, 13865 (1995).

[11] J. Zaanen, G. A. Sawatzky and J. W. Allen, Phys. Rev. Lett. **55**, 418 (1985).

[12] P. W. Anderson, Phys. Rev B **109**, 1492 (1958).

[13] N. F. Mott and E. A. Davis, Electronic processes in non-crystalline materials (Clarendon, Oxford, 1979).

[14] N. F. Mott, Adv. Phys. **16**, 49 (1967).

[15] B. L. Altshuler and A. G. Aronov, in A. L. Efros and M. Plollak eds., Electron-electron interactions in disordered systems (North Holland, Amsterdam, 1985).

[16] P. A. Lee and T. V. Ramakrishnan, Rev. Mod. Phys. **57**, 287 (1985).

[17] N. W. Ashcroft and N. D. Mermin, Solid State Physics (Halt-Saunders, Tokyo, 1976).

[18] G. Bergmann, Z. Phys. B, **48**, 5 (1982).

[19] J. B. Bieri, A. Fert, G. Creuzet and J. C. Ousset, Solid State commun. **49**, 849 (1984).

[20] B. L. Altshuler and A. G. Aronov, Solid State Commun. **30**, 115 (1979).

[21] G. Bergmann, Phys. Rep. **101**, 1 (1984).

[27] X. Q. Xu, J. L. Peng, Z. Y. Li, H. L. Ju and R. L. Greene, Phys. Rev. B **48**, 1112 (1993).

[28] P. C. Canfield, J. D. Thompson, S-W. Cheong and L. W. Rupp, Phys. Rev. B **47**, 12357 (1993).

[29] J. B. Torrance, P. Lacorre, A. I. Nazzal, E. J. Ansaldo and Ch. Niedermayer, Phys. Rev. B **45**, 8209 (1992).

[30] X. Granados, J. Fontcuberta, X. Obradors, Ll. Mañosa, J. B. Torrance, Phys. Rev. B, **48**, 11666 (1993).

[31] X. Granados, J. Fontcuberta, X. Obradors, J. B. Torrance, Phys. Rev. B, **46**, 15683 (1992).

[32] G. Demazeau, A. Marbeuf, M. Pouchard and P. Hagenmuller, J. Solid State Chemistry **3**, 582 (1971).

[33] K. P. Rajeev, G. V. Shivashankar and A. K. Raychaudhuri, Solid State Communications **79**, 591 (1991).

[34] K. P. Rajeev and A. K. Raychaudhuri, Phys. Rev. B **46**, 1309 (1992).

[35] A. Chainani, D. D. Sharma, I. Das and E. V. Sampathkumaran, J. Phys.: Condens. Matter **8**, L631 (1996).

[36] J. K. Vassiliou, M. Hornbostel, R. Ziebarth and F. J. Disalvo, J. Solid State Chemistry **81**, 208 (1989).

[37] G. H. Jonker and J. H. Van Santen, Physica **16**, 337 (1950).

[38] J. H. Van Santen and G. H. Jonker, Physica **16**, 599 (1950).

[39] E. O. Wollan and W. C. Koehler, Phys. Rev. **100**, 545 (1955).

[40] J. B. Goodenough, A. Wold, R. J. Arnott and N. Manyuk, Phys. Rev. **124**, 373 (1961).

[41] C. W. Searle and S. T. Wang, Can. J. Phys. **48**, 2023 (1970).

[42] R. von Helmolt, J. Wecker, B. Holzapfel, L. Schultz and K. Samwer, Phys. Rev. Lett. **71**, 2331 (1993).

[43] K. Chahara, T. Ohno, M. Kasai and Y. Kozmo, Appl. Phys. Lett. **63**, 1990 (1993).

[44] A. Asamitsu, Y. Moritomo,, Y. Tomioka, T. Arima and Y. Tokura, Nature **373**, 407 (1995).

[45] A. Urushibara, Y. Moritomo, T. Arima, A. Asamitsu, G. Kido and Y. Tokura, Phys. Rev. B **51**, 14103 (1995).

[46] A. J. Millis, P. B. Littlewood and B.I. Shraiman, Phys. Rev. Lett. **74**, 5144 (1995).

[47] J. M. D. Coey, M. Viret, L. Ranno and K. Ounadjela, Phys. Rev. Lett. **75**, 3910 (1995).

[48] S. E. Lofland, S. M. Bhagat, H. L. Ju, G. C. Xiong, T. Venkatesan and R. L. Greene, Phys. Rev. B **52**, 15058 (1995).

[49] R. Mahendiran, S. K. Tiwary, A. K. Raychaudhuri, T. V. Ramakrishnan, R. Mahesh, N. Rangavittal and C. N. R. Rao, Phys. Rev. B **53**, 3348 (1996).

[50] A. P. Ramirez, P. Schiffer, S-W. Cheong, C. H. Chen, W. Bao, T. T. M. Palstra, P. L. Gammel, D. J. Bishop and B. Zegarski, Phys. Rev. Lett. **76**, 3188 (1996).

[51] Soo Hyun Park, Yoon-Hee Jeong, Ki-Bong Lee, S. J. Kwon, Phys. Rev B **56**, 67 (1997).

[52] H. Y. Hwang, P. Dai, S-W. Cheong, G. Aeppli, D. A. Tennant and H. A. Mook, Phys. Rev. Lett. **80**, 1316 (1998).

[53] P. Wagner, I. Gordon, A. Vantomme, D. Dierickx, M. J. VanBael, V. V. Moshchalkov and Y. Bruynseraede, EuroPhysics Letters **41**, 49 (1998).

[54] C. Zener, Phys. Rev. **82**, 403 (1951).

Chapter 2

Experimental

This chapter presents the details of the sample preparation and characterization, design and construction of cryostats and sample holders, various techniques and methods used in the measurements.

2.1 Sample Preparation

This thesis deals with two different classes of transition metal oxides, namely nickelates and manganates. Different methodologies were used to prepare these samples. A brief description of these methods is given below:

2.1.1 Preparation of Nickelates of the type $RNiO_3$

In $RNiO_3$, nickel exists in Ni^{3+} state. But the Ni compounds with valencies higher than two are usually unstable. Their preparation, if possible, therefore takes place either in the presence of a high oxygen pressure[1,2] or by low temperature chemical methods[3]. We do not have access to high oxygen pressure so we decided to prepare these samples by a low temperature citrate precursor decomposition method[3,4].

In this method appropriate amounts of metal nitrate solutions were mixed with citric acid. The resulting solution was heated to obtain a green colored gel. The gel was fired to give a fine powdered precursor. This powder was pressed into rectangular pellets and these pellets were sintered under appropriate conditions. More details about the preparation of specific samples are given in the respective chapters.

2.1.2 Preparation of Manganates

Manganates were prepared by the usual solid state method. This method consists of thoroughly grinding the powders of oxides, carbonates, oxalates or other compounds containing the relevant metals; pelletizing and then heating the mixture at the desired temperature. More details about the preparation of specific samples are given in chapter 7.

2.2 Characterization

All the samples studied during this thesis work were carefully characterized using x-ray diffraction and iodometric titration. X-ray diffraction gives information about the phase purity, crystal structure and lattice parameters while iodometric titration is useful for knowing the oxygen stoichiometry of the sample.

2.2.1 X-ray diffraction

X-ray diffraction patterns were recorded using a Rich-Seifert x-ray diffractometer(model Isodebyeflex 2002) and Ni filtered Cu K_α radiation. The x-ray tube operates at 20 mA/30 kV. The powdered samples were packed into a circular cavity (diameter = 1cm) in a perspex sample holder. The sample holder is mounted in a platform such that the beam of radiation falls properly on the sample. The diffracted beam is received by a scintillation counter detector at an angle 2θ from the incident beam. The specimen and detector are rotated synchronously to maintain the focusing condition and to scan the reflecting planes to record the 2θ vs. intensity curves.

2.2.2 Iodometric titration

Physical properties of oxides depend quite sensitively on their oxygen stoichiometry. So it is always desirable to estimate the exact oxygen concentration in the material. Iodometric titration is the most reliable and widely used method for determining the oxygen stoichiometry. Basic idea behind this method is that when an oxide is treated with a large excess of iodide ion (I^-) in an acidic medium, it gets reduced. This is followed by the liberation of an equivalent amount of iodine. The amount of liberated iodine can be determined by titrating it with a standard solution of sodium thiosulphate(reducing agent) and from this the estimates of the oxygen content in the sample can be made[5]. Details of this titration are described below :

100 ml of distilled water is taken in a conical flask and 15 ml of conc. Hcl is added to it followed by the mixing of approximately 0.5 gm of sodium bicarbonate ($NaHCO_3$). Solution is shaken for some time and then approximately 5 gm of KI is dissolved in it. Now

the sample (≈ 0.2 gm) is dissolved in this solution and the volume of the solution is made up to 250 ml using distilled water. The solution is heated gently to around 45 ^{0} C. Sample reacts with KI to liberate iodine. Because of the liberated iodine the color of the solution becomes yellow. Now this solution is treated with 0.1N solution of sodium thiosulphate. As the titration proceeds the color of the solution fades and at the end point the color disappears completely. But this color change at the end point is not very sharp and hence makes the determination of the end point difficult. The test of end point is made much more sensitive by adding few drops of freshly prepared sodium starch glycolate in the solution just before the end point. Starch reacts with iodine in the presence of iodide to form an intensely blue colored complex. At the end point the blue color of solution disappears very sharply.

2.3 Design and Construction of cryostats

An apparatus in which low temperature experiments are performed is known as a cryostat. During the course of this thesis work several cryostats were designed and constructed. Brief descriptions of some of them are given below.

2.3.1 A Dipper cryostat for Storage Dewars

Cryostats designed for insertion into storage dewars are known as dipper cryostats. They are often used for fast low temperature measurements. During this thesis work a dipper cryostat for 60 Litre helium dewars of 2 in. neck size was constructed. This cryostat is very similar to that constructed by Swartz[6] in 1986.

Conventional He^4 cryostats are usually permanently mounted in experimental dewars, need frequent transfer of liquid helium and take long cooling-down (and warming-up) time. This makes liquid helium experiments quite expensive and time consuming. Our dipper cryostat does away with many of these shortcomings. It has fast cool-down and warm-up times, consumes very little liquid helium and has excellent temperature stability. It is a multipurpose cryostat and it can be used for various kinds of measurements like electrical resistivity, thermopower, specific heat etc..

2.3.1(A) Cryostat Design and Construction:

A schematic diagram of the cryostat is shown in figure 2.1. The central part of this cryostat is the vacuum can made of brass. Length of this can is 8", outer diameter is 1.9" and wall thickness is 0.1". This can be immersed in liquid helium in a storage dewar of 2" neck diameter. Liquid helium provides cooling down to 4.2K. Temperatures below 4.2K are achieved by pumping on a He^4 pot. The body of He^4 pot is made by drilling a hole on an OFHC solid copper rod, the top of this pot is made separately from a thin copper plate. At the center of the top plate a thin hole is made for He^4 feedthrough capillary. A thin capillary connects the He^4 pot to the outside of the vacuum can. This capillary is used for continuously filling the He^4 pot. The impedance of this capillary can be adjusted by inserting copper wires of different diameters in it. When the continuous filling of helium is not required the capillary can be closed by soldering a copper wire at the outer end of the capillary. At the bottom of the pot threading is made so that the sample holder can be attached to the pot using a threaded brass rod. This brass rod acts as a thermal link between the sample holder and the pot. Different kinds of sample holders are used for different measurements. The heater and temperature sensor are mounted on the sample holder. Two thermal anchoring posts are made at the top flange of the vacuum can. All the wires are properly anchored to these posts before connecting them to the sample holders.

Vacuum can is sealed with the help of indium O'ring. All the wires enter inside the vacuum can through a S.S tube (vacuum can pumpout tube). This tube goes to a copper "T". One arm of this "T" goes to a 20 Pin electrical feedthrough and the other arm goes to a quarter inch vacuum valve. Pumping of Helium pot is done through another S.S tube (Helium pumpout tube). This tube goes directly to another quarter inch vacuum valve. The vacuum can pumpout tube and Helium pumpout tube are held parallel to each other with the help of a split perspex block. These tubes slide through a specially designed flange which is kept at the top of the 60L storage dewar. This flange is a modified version of a triclover flange[6]; a half inch thick brass block has been silver soldered to the top of the flange. The thicker flange makes sliding of tubes smooth. To seal the tubes at desired heights we have made a special split tube seal cap. It consists of a 0.25 inch thick brass plate. It can be screwed to the top of the flange so that it squeezes an O'ring between each tube and flange.

By tightening the tube seal cap, the tubes can be locked at any position. We have kept some additional O'rings in both the tubes, old O'rings can be replaced any time by just separating the two ends of the split tube seal cap and bringing down new O'rings after cutting out the old ones.

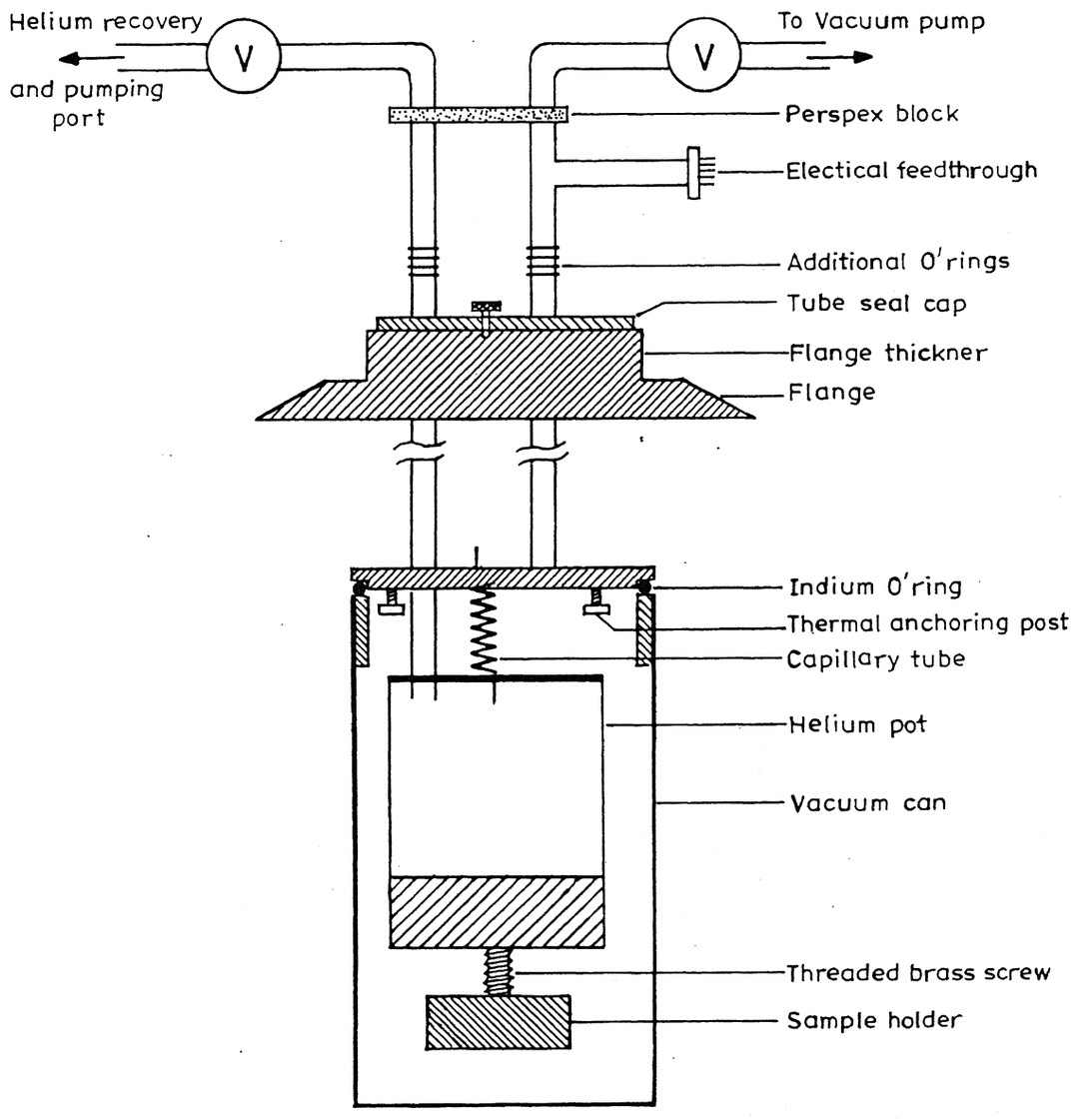

Figure 2.1 : Schematic diagram of dipper cryostat.

2.3.1(B) Sample holders: Different kinds of measurements can be performed in the dipper cryostat by attaching different sample holders at the bottom of He^4 pot. Schematic designs of the sample holders for the electrical resistivity and thermopower measurements are shown below.

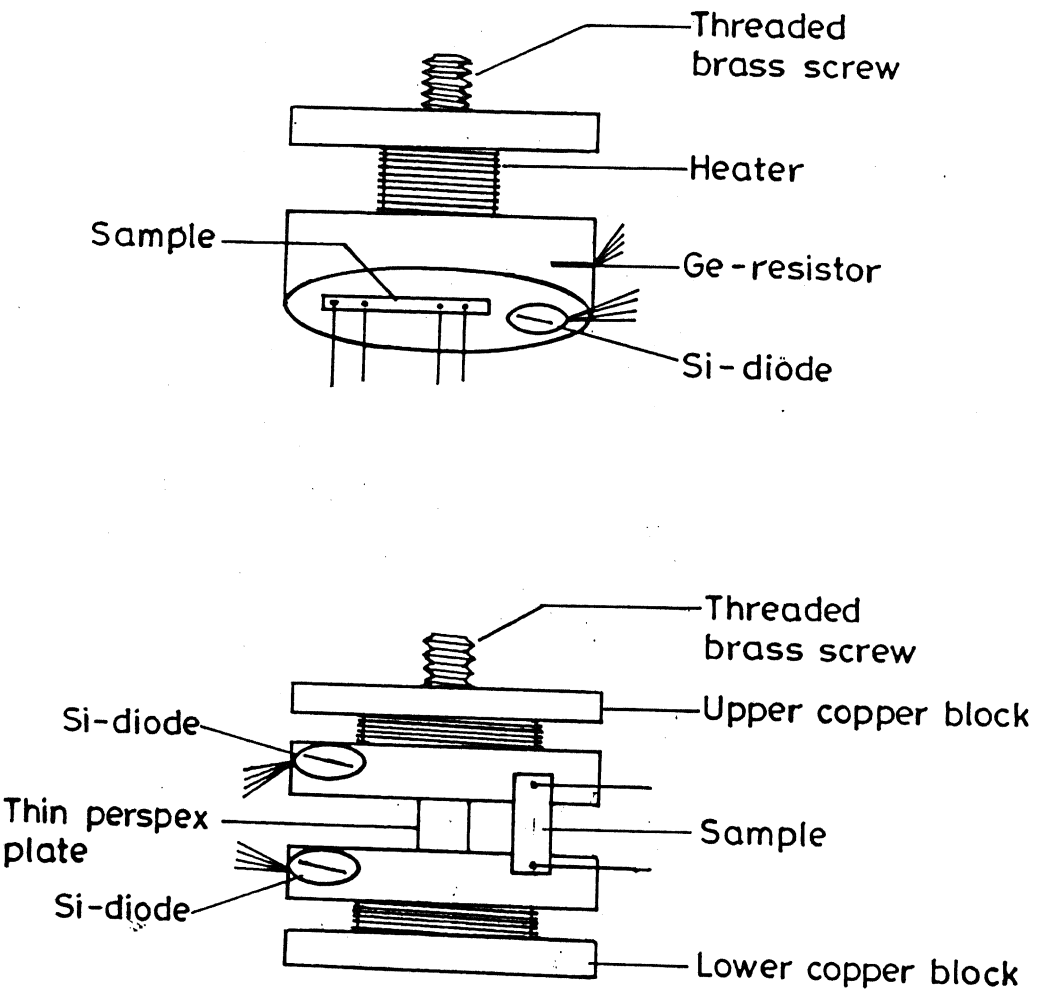

Figure 2.3 : Sample holder for thermopower measurement.

2.3.1(C) Operation:

This cryostat can operate in two modes, namely single shot mode and continuous fill mode. In single shot mode, He^4 feed through capillary is closed while in continuous fill mode capillary is kept open. If the temperature below 4.2K is continuously required for a very long time the continuous mode is used; otherwise most of the time single shot mode is preferred.

Single Shot Mode: First of all the sample is mounted in the sample holder and the vacuum can is closed using a new indium O'ring. Now the vacuum can is pumped using a rotary pump. Pumping of 30-40 minutes brings down the pressure to about 10 μ of Hg. After this He^4 pot is evacuated and pure He^4 gas is filled in it at a pressure slightly higher than the atmospheric pressure. Now the cryostat is ready for cooling down. Cooling from RT to 100 K can be done in two different methods. In the first method the cryostat is inserted into a liquid Nitrogen flask. In the second method the cryostat is inserted into the He^4 container itself but in such a way that it does not touch the liquid; cold helium gas cools the cryostat. Most of the time we preferred the second method. Cooling from 300 K to 100 K takes around 3 hours, if faster cooling is required a little bit of dry helium gas can be introduced into the vacuum can. Once the cryostat has cooled down to 100 K, it is dipped in liquid helium. After the cryostat has attained the temperature of 4.2 K, pure helium gas is introduced at a pressure of ~ 2-3 bar in the He^4 pot through the helium pump-out tube. When helium gas enters the pot, the temperature of the pot goes up momentarily. After some time helium starts condensing in the pot. It takes around 35-40 minutes before He^4 pot gets filled completely. As soon as the pot gets fully filled, helium gas stops going in as indicated by the pressure gauge on the helium supply cylinder. To get temperature below 4.2 K the He^4 pot is pumped using a rotary pump. Below 4.2 K, the temperature control is achieved manually by controlling the pumping speed with the valve. Volume of He^4 pot is about 6cc and it can be pumped continuously for around 2 hours before the can is empty. When temperature above 4.2 K is required pumping is stopped and a little amount of dry helium gas is inserted in the pot. Between 4.2 K and 10 K temperature is controlled by a LakeShore temperature controller. For getting temperatures above 10 K the He^4 pot is completely evacuated, now the temperature controller can raise the temperature up to 100

K. Above 100 K the cryostat is raised in the dewar so that the bottom of the cryostat is above the liquid level. Another way to operate above 100 K is to take out the cryostat from the helium dewar and put it in a flask containing liquid nitrogen.

Continuous Fill Mode: In this mode capillary is kept open. In this situation there is a danger that if any gas (other than helium) is present in the capillary, it will freeze at low temperature and block the capillary. To avoid this the He^4 pot is pressurized with dry helium gas so that any gas other than helium is removed from the pot and capillary. Now the cryostat is inserted in the storage dewar in such a way that the vacuum can remains at the top of the dewar. Once the cryostat is inside the dewar there is no need to further pressurize the pot because inside the dewar there is no other gas than the extremely pure helium gas. Cryostat is kept in this position for about 3-4 hours, cold helium gas cools down the cryostat to about 100K. Now the cryostat is lowered in steps of 2 inches in every 15 minutes until the bottom of the vacuum can touches the bottom of the dewar. Once the whole system has cooled down to 4.2K, He^4 pot is pumped. Liquid helium enters through the capillary in He^4 pot and expands. Since capillary tube always supplies helium to the pot, the operation of cryostat at higher temperature (>40K) is difficult. Because of this problem we preferred one shot mode most of the time, continuous mode is used only in those experiments where temperature below 4.2K is required for a very long time.

2.3.1(D) Limitations of dipper cryostat:

While there are several advantages in dipper cryostat, there are certain limitations too. Firstly, the experimental space is limited. Secondly, its operation requires raising and lowering operations quite frequently and hence needs a lot of attention from the operator.

2.3.2 Conventional He^4 cryostat for glass dewar

A conventional He^4 cryostat with glass dewar was also frequently used for electrical resistivity measurements. Some parts of this cryostat were already existing in our laboratory, remaining things were constructed and the cryostat was brought to the working condition during this thesis work only. The advantage of this cryostat over the dipper cryostat is that it can go to lower temperature (1.2 K) and the data is more stable. A schematic diagram of this cryostat is shown below.

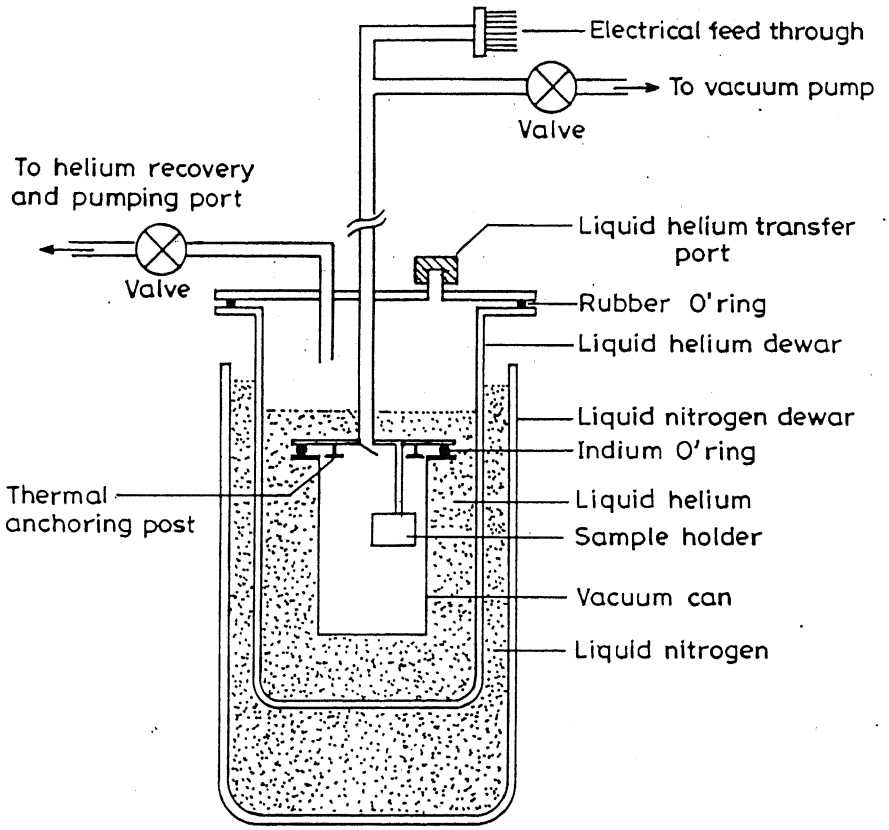

Fig 2.4 : A Schematic diagram of He^4 cryostat.

2.3.3 A device for quick determination of Curie Temperature

In our day to day laboratory work we encounter several systems which undergo ferromagnetic-paramagnetic phase transition. Very often we want to know the transition temperature (T_c) of these materials. For this purpose we constructed a very simple device [7] which can determine T_c easily and accurately.

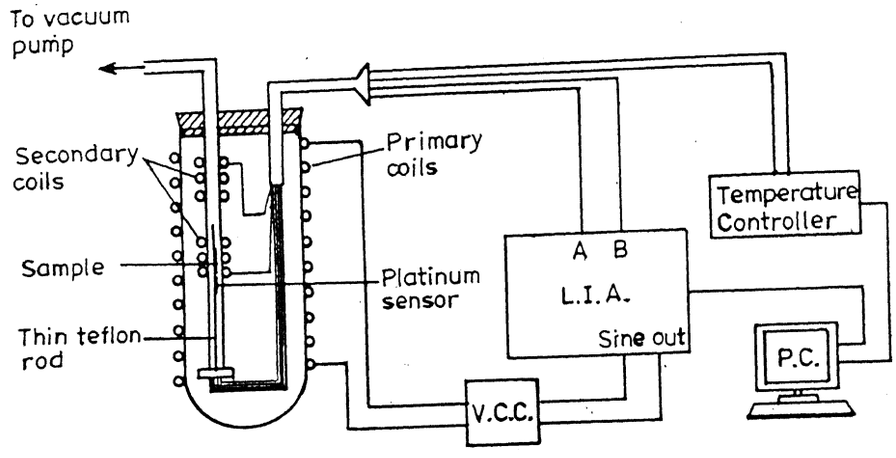

Fig 2.5 : A Schematic diagram of Curie temperature device

In this device two matched secondary coils, having the same cross sectional area and the same number of turns (but wound in opposite sense) and connected in series, are placed in an uniform alternating magnetic field produced by a long solenoid (primary coil). Since the secondary coils are almost identical, the net emf developed across the pair is zero. Now if the sample is placed in one of these coils, there will be an unbalanced emf across the pair. This emf is proportional to the susceptibility of the sample. Whenever there is a ferro-para transition, there is a drastic change in the susceptibility and hence in the net emf across the pair of the coils.

With the help of a thin teflon rod, sample is introduced in one of the coils. The temperature of the sample is measured by a calibrated platinum sensor, kept in contact with the sample. Temperature of the sample is lowered by immersing the setup in a liquid nitrogen dewar. Liquid nitrogen dewar can slowly be raised or lowered so as to change the sample temperature. The reference oscillator of a lock-in amplifier (Stanford Research Systems,model:SR830 DSP) provides ac source signal for the primary coil. The net emf

developed across the pair of secondary coils is monitored by the A-B mode of the lock-in amplifier.

2.3.4 Construction of a specific heat setup

In the course of this work a calorimeter have been designed and constructed to measure the specific heat of solid samples. A brief discussion of this setup is given in appendix-I.

2.4 Measurement Techniques

2.4.1 Electrical resistivity

A four-probe low frequency ac technique was employed to measure the electrical resistivity of the samples (see figure 2.6). A Lock-in amplifier (Stanford Research Systems, model SR830), a voltage to current converter (home made; driven by Lock-in sine out) and a temperature controller (LakeShore Cryotronics, DRC-82C) were used for the measurement. The current and voltage leads were attached to the sample with silver paint after cleaning the sample surface mechanically. It was ensured that the current does not cause any heating of the sample during measurement. The absolute accuracy of resistivity is $\approx$ 5 % mainly due to uncertainties in the geometrical factors; however, the resolution was better than 1-5 parts in 10^5.

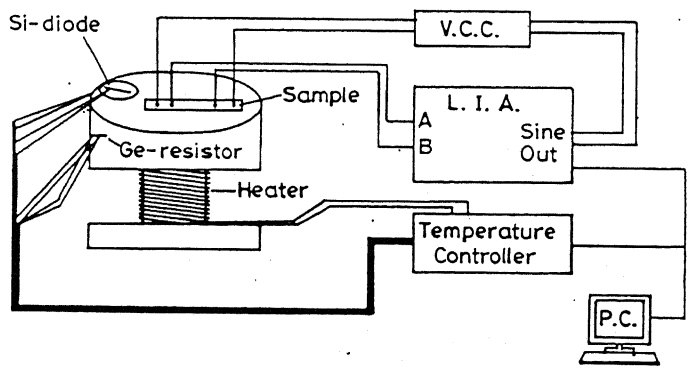

Figure 2.6: Arrangement for the electrical resistivity measurement.

2.4.2 Thermopower

The thermopower is an important tool for studying the nature of charge carriers and various processes that occur close to the Fermi surface. It is defined as the voltage developed across the two ends of the sample when a unit temperature gradient is applied between them[8]. There are two basic techniques to measure the thermopower of materials, the integral technique and the differential one. In the integral technique the sample is normally in the form of a long wire, one end of the sample is kept at a fixed temperature and the temperature of the other end is continuously raised. In the differential technique the sample could be in the form of a short wire or even a pellet. The differential technique of the thermopower measurement may further be divided in two categories: (a) ac technique and (b) dc technique. In the ac technique a slowly alternating temperature gradient is applied between the two ends of the sample while in the dc technique a fixed temperature gradient is applied.

During this thesis work the thermopower measurements were done by dc differential technique with copper as the other arm of the thermocouple (see figure 2.7). A temperature difference (ΔT) of 1-2K was applied across the two ends of the sample and the voltage difference (ΔV) developed across the sample was measured using a Keithley nanovoltmeter (model 182). The ratio $\Delta V/\Delta T$ gives the thermopower of the sample with respect to copper. The absolute thermopower was obtained by adding to this quantity the absolute thermopower of copper, which was obtained from reported data[8]. The performance of the setup was checked by measuring the thermopower of platinum and comparing it with the already reported data[8] (see figure 2.8).

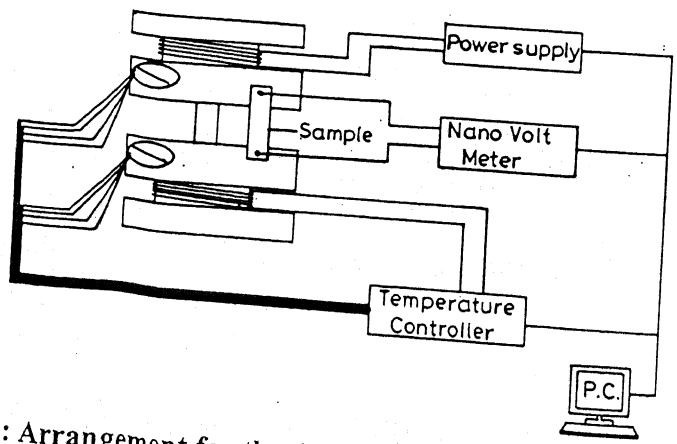

Figure 2.7 : Arrangement for the thermopower measurement.

Synopsis

TITLE: Electron Interaction Effects in some Correlated Transition Metal Perovskite Oxides Through Transport and Tunneling Experiments.

Name of Student:	ASHUTOSH TIWARI
Roll No:	9310962
Degree for which submitted:	Ph. D.
Department:	Physics
Thesis supervisor	Dr. K. P. Rajeev
Month and Year of submission:	April 1999

Transition metal oxides constitute one of the most interesting classes of solids, exhibiting a wide range of phenomena. The range of transport properties exhibited by these oxides is vast. Some of them are metallic, some are insulating and some of them undergo a metal-insulator transition as a function of temperature, pressure or composition. Some of the interesting M-I transitions which are observed in transition metal oxides are Mott-Hubbard, Charge transfer and Anderson M-I transitions.

Anderson transition arises when disorder is introduced in a metallic system. Because of the disorder electrons move in a random potential. Localization of electronic states can occur in this situation and if the potential is random enough the metal becomes an insulator . However if the disorder is not sufficient to cause M-I transition, the system remains metallic. In this case only the states at the band edges are localized and those at the Fermi level remain extended. In these disordered metallic systems the interesting phenomena of e-e interactions and weak localization are observed.

Disordered metallic systems close to M-I transition have been explored actively by condensed matter physicists in recent times. Most of the previous studies of disordered systems were confined to amorphous metals and doped semiconductors but recently oxides have also attracted considerable attention for such studies. In oxides disorder can be introduced by substitution of one or more of the constituents or by creating oxygen nonstoichiometry in the system.

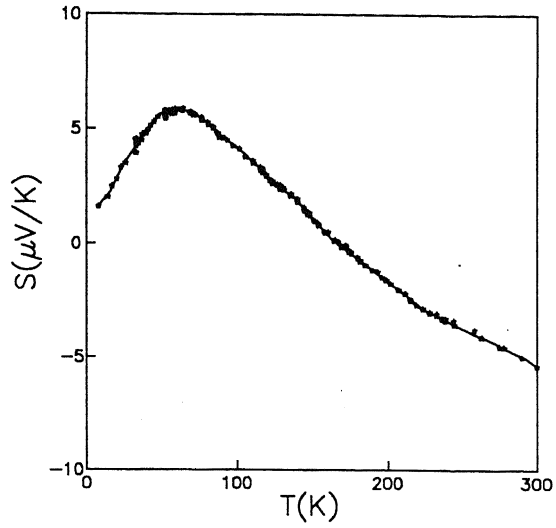

Figure 2.8 : Thermopower of platinum measured using our thermopower setup. Symbols represent the present experimental data and solid line represents previously reported data[8].

2.4.3 Tunneling conductance*

The tunneling measurements were carried out on tunnel junctions formed by pressing a small Pb (counter-electrode) piece against the sample. The tunnel barrier is formed by the native oxide surface on Pb. A programmable current source (Keithley Model 220) and a nanovoltmeter (Keithley Model 182) were used to obtain the I-V characteristics of the junction. The differential conductance (dI/dV) was obtained numerically. All the measurements were performed at 1.2 K by dipping the samples in a pumped He^4 bath in a glass dewar.

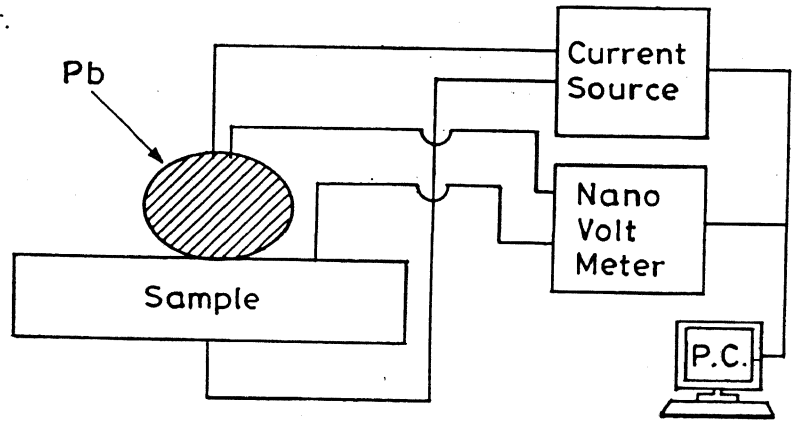

Figure 2.9: Arrangement for the electron tunneling conductance measurement.

* More details about the Electron tunneling spectroscopy are given in Appendix-II.

2.4.4 Magnetoresistance

The magnetoresistance measurements were done by a standard four-probe dc method using a 45 kG superconducting magnet. The temperature of the sample was measured using a calibrated carbon glass resistance. The resistance was measured as a function of magnetic field strength. $(R_B-R_0)/R_0$ gives the magnetoresistance of the sample.

2.5 Automation and data acquisition

All the measurements were automated during this thesis work and the data acquisition was done using a GPIB card with a PC. Computer programs used for data acquisition were developed during the course of this thesis work.

2.6 Miscellaneous

Vibrating sample magnetometer with a 95 kG superconducting magnet was used to measure the High field Magnetization of $NdNiO_{2.88}$ in the temperature range 4.2-200K[9].

A Faraday balance was installed during this thesis work and it was used to measure the room temperature magnetization of some of the samples[10] in magnetic fields of 0-6 kG. The field gradients at different fields were calibrated using $HgCo(SCN)_4$.

The Mössbauer spectra* of $NdNi_{1-x}Fe_xO_{3-\delta}$ samples[10] were recorded at room temperature using a ^{57}Co source deposited on a rhodium matrix. The spectra were analyzed using the Mössbauer analysis software PC-MOS supplied by CMTE Electronik, Germany.

* See appendix –III.

References:

[1] G. Demazeau, A. Marbeuf, M. Pouchard and P. Hagenmuller, J. Solid State Chem. **3**, 582 (1971).

[2] P. Lacorre, J. B. Torrance, J. Pannetier, A. I. Nazzal, P. W. Wang and T. C. Huang, J. Solid State Chem. **91**, 225 (1991).

[3] J. K. Vassiliou, M. Hornsbostel, R. Ziebarth and F. J. Disalvo, J. Solid State Chem. **81**, 208 (1989).

[4] Ashutosh Tiwari, K.P. Rajeev, R. N. Panda and N. S. Gajbhiye (Proceedings of the DAE Solid State Physics Symposium), Solid State Physics (India), **38C**, 252 (1995).

[5] A. I. Vogel, A text-book of quantitative inorganic analysis (Longmans, Great Britain 1960).

[6] E. T. Swartz, Rev. Sci. Instrum. **57**, 2848 (1986).

[7] Ashutosh Tiwari and K. P. Rajeev (Proceedings of the DAE Solid State Physics Symposium), Solid State Physics (India) **39C** , 414 (1996).

[8] J. S. Dugdale, The electrical properties of metals and alloys (Adward Arnold, London, 1977).

[9]Ashutosh Tiwari and K.P.Rajeev, Modern Physics Letteres B **11** , 1161 (1997).

[10] Ashutosh Tiwari, Journal of Alloys and Compounds **274** ,42 (1998).

Chapter 3

Electrical transport in $LaNiO_{3-\delta}$

3.1 Introduction

During the last few decades a lot of effort have gone into understanding the fundamental physics involved in disordered metallic systems[1]. Disorder has been found to affect the electrical transport and thermodynamic properties of metals quite remarkably. It causes significant corrections to the conductivity and the density of states: a minimum in the temperature dependence of resistivity and a strong anomaly in the density of states[2] at the Fermi level are frequently observed. Altshuler and Aronov[3,4] showed that in these systems many-body e-e interactions are important. Taking into consideration e-e interactions, they predicted[3] a $T^{1/2}$ temperature dependence for the low temperature correction to the electrical conductivity and a square root anomaly in the density of states at E_F for three dimensional systems. According to them[4], the modification to the density of states goes as $\delta N(E) \propto | E - E_F |^{1/2}$. Later, McMillan[5], considering both localization and e-e interaction effects, predicted a similar expression for the density of states:

$$N(E) = N(0)\left[1+\left(\frac{|E-E_F|}{\Delta}\right)^{0.5}\right] \qquad 3.1$$

here Δ is a constant, named as the correlation gap [5].

Previously, most of the studies of disordered systems were confined to amorphous metals and doped semiconductors[6], but recently oxides have also attracted considerable attention for such studies[7-10]. In this chapter an effort has been made to investigate the effect of disorder due to oxygen deficiency on the electrical resistivity ρ(T), tunneling conductance G(V) and thermopower S(T) of a three dimensional transition metal perovskite

This chapter is mainly based on the published work by A. Tiwari and K. P. Rajeev, J. Phys.: Condens. Matter **11**, 3291 (1999).

oxide system. For this study we found $LaNiO_{3-\delta}$ system to be the most suitable, for the following reasons: (i) The parent compound $LaNiO_3$ [9,10] has a high electron density ($\approx 10^{22}$ cm^{-3}) but a low conductivity ($\approx 10^3$-10^4 S cm^{-1}). Low conductivity and high electron density indicates a low electron diffusivity (D) and a sizeable amount of disorder. This transition metal oxide seems ideal for a study of the effect of disorder on a metallic system. (ii) It is possible to have a fine control over the strength of disorder by controlling the oxygen deficiency δ. The nature of disorder in this case would be mainly oxygen vacancies in the lattice. This would randomize the potential 'seen' by the conduction electrons. (iii) The thermopower of the parent sample $LaNiO_3$ varies almost linearly with temperature; a linear temperature dependence suggests that the thermopower of the system mainly arises from the diffusion of electrons, and hence any interaction among the electrons due to disorder may be reflected in the thermopower of the system also [11].

With the above objectives in mind we have carried out precise measurements of the electrical resistivity, tunneling conductance and thermopower of $LaNiO_{3-\delta}$ (δ = 0-0.14).

3.2 Experimental

All the samples investigated in this work were prepared by the sol-gel method. Stoichiometric amounts of La_2O_3 and $Ni(NO_3)_2.6H_2O$ were dissolved in nitric acid, and citric acid was added to this solution so as to maintain the ratio of La:Ni:citric acid as 1:1:2.05. The molarity of this solution was maintained at 0.1 M and the solution was refluxed at 360 K for 24 hours. The solution was gently warmed to get a fluffy gel; this gel was fired at 925 K for 12 hours. The sample thus prepared was pressed to form four rectangular pellets and the pellets were sintered under different conditions to vary the oxygen stoichiometry of the sample. The oxygen concentration for all the samples were determined by iodometry. The crystal structures and lattice parameters for all the samples were determined by x-ray diffraction (see figure 3.1).

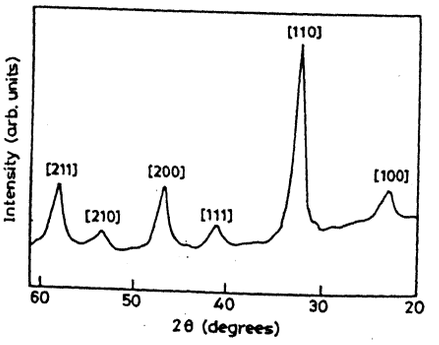

Figure 3.1 : X-ray diffraction pattern of $LaNiO_3$ taken with Cu K_α radiation.

The electrical resistivity measurements were done by a four probe low frequency ac technique (1 kHz) in the temperature range of 2.5-300 K. A Lock-in amplifier (Stanford Research Systems: SR830), a voltage to current converter (home made, driven by the lock-in sine out) and a temperature controller (LakeShore Cryotronics: DRC-82C) were used. A measuring current of 2-5 mA was used. It was ensured that the current did not cause any self heating. The absolute accuracy of resistivity is about 10 percent (large mainly due to uncertainties in the geometrical factor) however, the resolution was much better at 1-5 parts in 10^5. The tunneling measurements were carried out on tunnel junctions made with Pb counter-electrode. The absolute thermopower measurements were performed over the temperature range of 5-300 K. The homemade apparatus employs a standard dc differential technique with copper as the other arm of the thermocouple. A temperature difference (ΔT) of 1-2K was maintained across the two ends of the sample and the voltage difference (ΔV), thus developed was measured using a Kiethley nanovoltmeter (model 182). $\Delta V/\Delta T$ gives the thermopower of the sample with respect to copper. The absolute thermopower of copper was added to this quantity to get the absolute thermopower of the sample.

3.3 Results

X-ray diffraction pattern of all the samples show single-phase systems. All the samples are found to be cubic, with almost similar lattice parameters (see table 3.1).

Table 3.1 : Sintering conditions, oxygen nonstoichiometries (δ) and lattice parameters (a) for various $LaNiO_{3-\delta}$ samples.

Sintering atmosphere	Duration (days)	Sintering Temp.(K)	δ	a (Å)
O_2	7	1100	0.00	3.850
O_2+air	7	1100	0.06	3.851
Air	7	1100	0.11	3.853
N_2	7	1050	0.14	3.855

The electrical resistivity data for $LaNiO_{3-\delta}$ samples from 2.5 K to 300 K are shown in figure 3.2. $LaNiO_3$ shows a positive temperature coefficient of resistivity (TCR) through out the whole temperature range while the oxygen deficient samples exhibit a minimum in the resistivity at low temperature (T_{min}). At higher temperature all the samples show linear variation with temperature, indicating that electron-phonon scattering determines the temperature dependence at high temeperature in these samples.

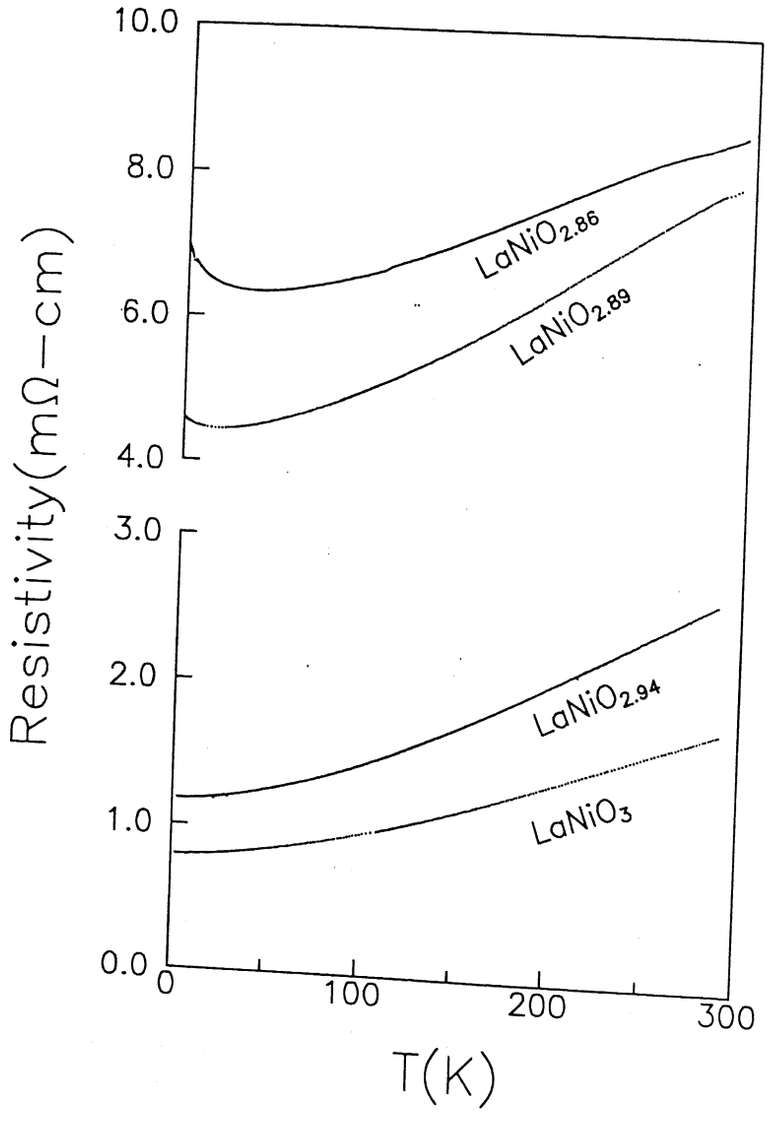

Figure 3.2 : Electrical resistivity of $LaNiO_{3-\delta}$ (δ=0.00, 0.06, 0.11, 0.14) from 2.5K to 300K.

In figure 3.3 the differential tunneling conductance data G(V) (=dI/dV) of various samples at 1.2 K are shown. We have chosen Pb as the counter-electrode and performed the measurements at 1.2 K where Pb is in the superconducting state. This was chosen because the observation of the superconductivity gap is a strong evidence for the quality of the tunnel junction and ensures that the tunnel injection is indeed the mechanism of charge transfer. For all the junctions we have observed a well defined dip in conductance for $|V| < \Delta_{Pb}$. In the inset of figure 3.3 we have shown the superconductivity gap of Pb as observed in the case of $LaNiO_3$.

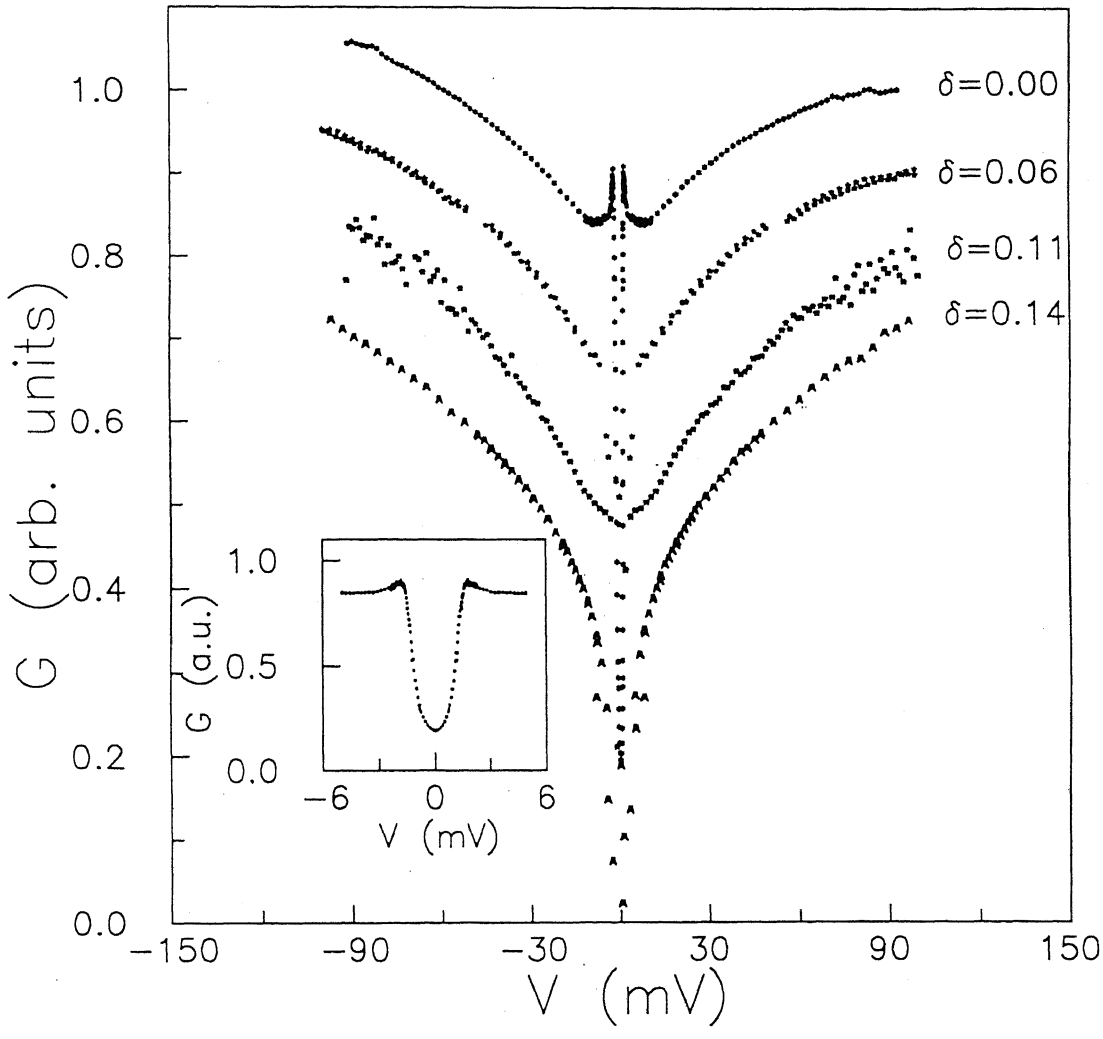

Figure 3.3 : Tunneling conductance (G) vs. the bias voltage for $LaNiO_{3-\delta}$ (δ=0.00, 0.06, 0.11, 0.14) at 1.2 K. The data have been normalized to unity at 100 mV and shifted vertically for clarity. Information about the absolute values is given in table 3.2. The inset shows the low-bias (|V|< 10 mV) experimental data for $LaNiO_3$, reflecting the signature of the superconductivity gap of Pb.

Thermopower data for $LaNiO_{3-\delta}$ samples from 5 K to 300 K are shown in figure 3.4. $LaNiO_3$ has a negative thermopower with almost linear thermal variation, while the thermopower of oxygen-deficient samples show a sign reversal from negative to positive and a distinct maximum at low temperature.

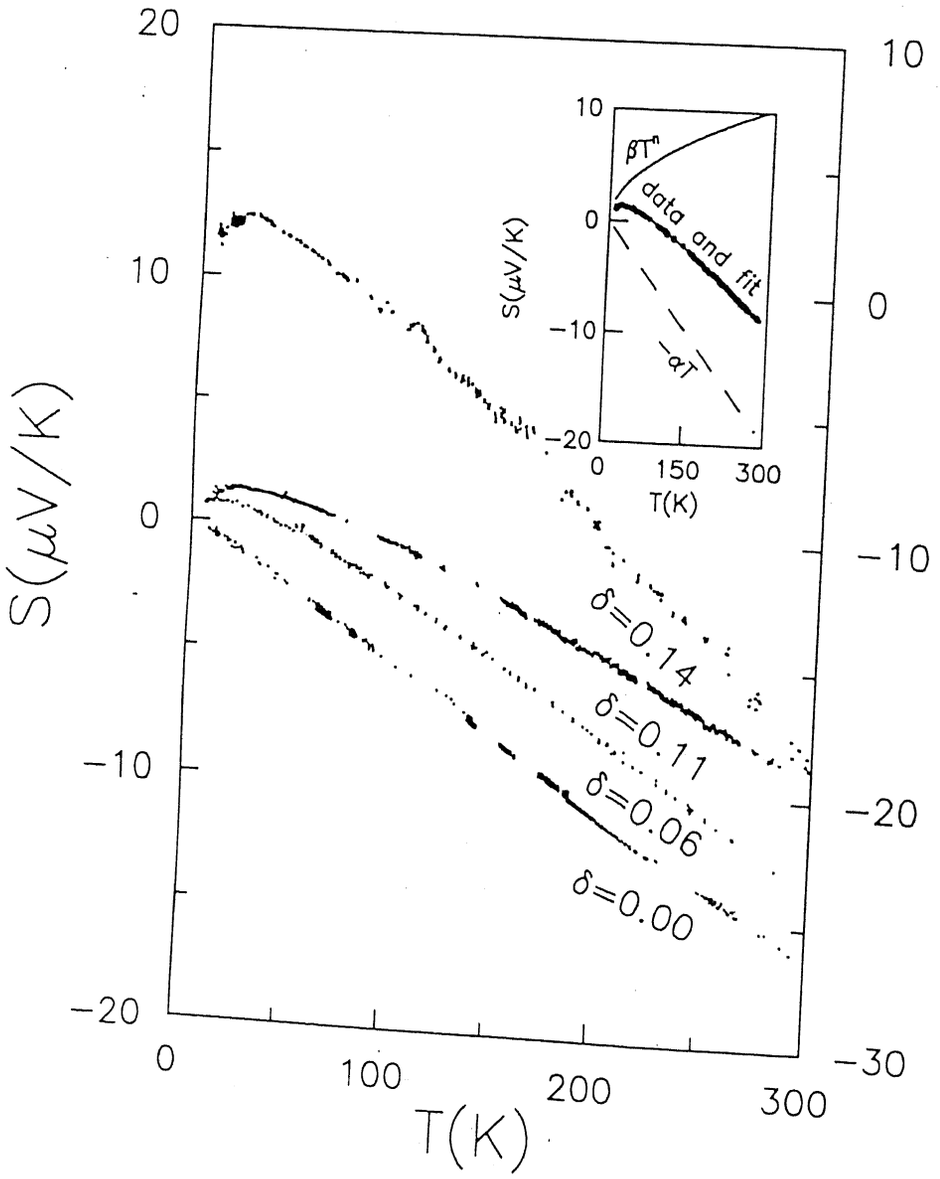

Figure 3.4 : Thermopower of $LaNiO_{3-\delta}$ (δ=0.00, 0.06, 0.11, 0.14) from 5 K to 300 K. For δ=0.00, 0.06 and 0.11, the y-scale is on the left hand side, while for δ=0.14, it is on the right hand side. The inset shows the fit for $LaNiO_{2.89}$ to $S = -\alpha T + \beta T^n$.

3.4 Discussion

3.4.1 Electrical Resistivity

The variation of resistivity with temperature for $LaNiO_3$ is very similar to that for good metals except for its large magnitude. At higher temperature, ρ(T) varies linearly with temperature and at lower temperatures it approaches a residual value following the relation $\rho(T) = \rho(0) + C \cdot T^2$. Here it is to be noted that, although $LaNiO_3$ has a high electron density, its electrical conductivity is very low ($\approx 2\times10^4$ S cm^{-1}). This implies a low electron diffusivity.

For oxygen-deficient samples, distinct resistivity minima are observed. In metals the low temperature minima may arise for the following reasons: (i) because of the Kondo effect[13] and (ii) because of the weak localization and e-e interactions, collectively known as the quantum correction effects[1]. The Kondo effect is encountered in nonmagnetic systems containing small amounts of magnetic impurity. Kondo systems show a giant thermopower, at low temperature. Since none of our samples exhibit giant thermopower the possibility of a Kondo effect is ruled out. Weak localization and e-e interactions effects are seen in disordered metallic systems. In the case of disordered metals, because of the interference of partial electron waves, weak localization effects are observed. Weak localization and e-e interaction effects have been discussed in some detail in chapter 1. The correction to the conductivity in the case of weak localization goes as $\delta\sigma_{WL} \propto T^{p/2}$ with p≈1.5-3. In the case of strongly disordered metals, the electrons undergo intense elastic scattering from the impurities. This makes their motion diffusive and hence reduces their ability to screen out the electric field of other electrons. Reduced screening causes an enhanced Coulomb interaction among the electrons[1]. The correction to the conductivity due to the enhanced interaction goes as $\delta\sigma_{e-e} \propto \sqrt{T}$. Quantum correction effects affect the electrical conductivity at low temperatures; at higher temperatures the usual inelastic contributions become significant[14]. Because of the inelastic scattering, the electrical conductivity has an additional contribution of the kind $\delta\sigma_{inel} = -cT^p$.

To get some idea about the real mechanisms involved, we fitted our low temperature (2.5-20 K) conductivity data to an empirical relation of the kind $\sigma(T) = \sigma(0) + bT^m - cT^n$. The details of fit are given in table 3.2. It can be seen from this table that for all the samples the value of m lies very close to 1/2, thus suggesting that e-e interactions might be mainly determining the low temperature behavior of system.

Table 3.2 : Parameters used in fitting the low temperature (2.5 K < T < 20 K) conductivity data for $LaNiO_{3-\delta}$ to the empirical relation $\sigma(T) = \sigma(0) + bT^m - cT^n$. Number of data points used for fitting, N≈200.

δ	$\sigma(0)$ (S/cm)	b (S/cm-K^m)	c (S/cm-K^n)	m	n	χ^2
0.00	1262.07(1)	–	0.0377(1)	–	1.993(1)	242
0.06	841.61(2)	3.976(8)	0.0649(4)	0.51(2)	2.026(2)	285
0.11	209.18(4)	5.586(9)	0.141(2)	0.49(1)	1.367(3)	291
0.14	132.71(3)	7.075(3)	0.244(3)	0.49(1)	1.188(2)	317

3.4.2 Tunneling Spectroscopy

Tunneling conductance *G(V)* is a direct measure of the single-particle electronic density of states *N(E)* at energy $E = q_e \cdot V + E_F$. In highly disordered metallic systems, electron-electron interactions give rise to a correction to the density of states *N(E)* at $E=E_F$ (see eq.(3.1)). According to Altshuler and Aronov[1], in three dimensional disordered systems this correction to the density of states goes as $\delta N(E) \propto | E - E_F |^{1/2}$ causing a cusp in the tunneling conductance at V=0 such that $G(V) = G(0)\left[1+\left(\frac{|V|}{\Delta}\right)^{0.5}\right]$. Here G(0) is the zero bias conductance and Δ is a constant. Interestingly, all the samples under investigation are found to obey the above relation very well. In table 3.3 we have shown the values of χ^2 and the parameters used in fitting our data to the above equation.

Table 3.3 Parameters used in fitting the tunneling conductance data for $LaNiO_{3-\delta}$ to $G(V)=G(0)[1+(|V|/\Delta)^{0.5}]$. Data in the range 10 mV< V < 100 mV were used for fitting. Number of data points used for fitting, N≈100.

δ	G(0) (S)	Δ (meV)	χ^2
0.00	0.8473(9)	649(9)	173
0.06	0.1203(2)	267(2)	139
0.11	0.0410(1)	128(2)	164
0.14	0.00273(2)	116(3)	180

Shown in figure 3.5 are the values of Δ as a function of the extrapolated zero temperature conductivity $\sigma(0)$. Altshuler and Aronov[1] showed that Δ should vary as $\sigma(0)^3$ while McMillan's model[5] predicts an exponent of 2. Our experimental data is found to follow an empirical relation, $\Delta = u + v \cdot \sigma(0)^q$ (u=114.5 meV, v=0.741×10^{-7} meV S^{-1} cm^q , q=3.2), which is very close to the prediction of Altshuler and Aronov[1].

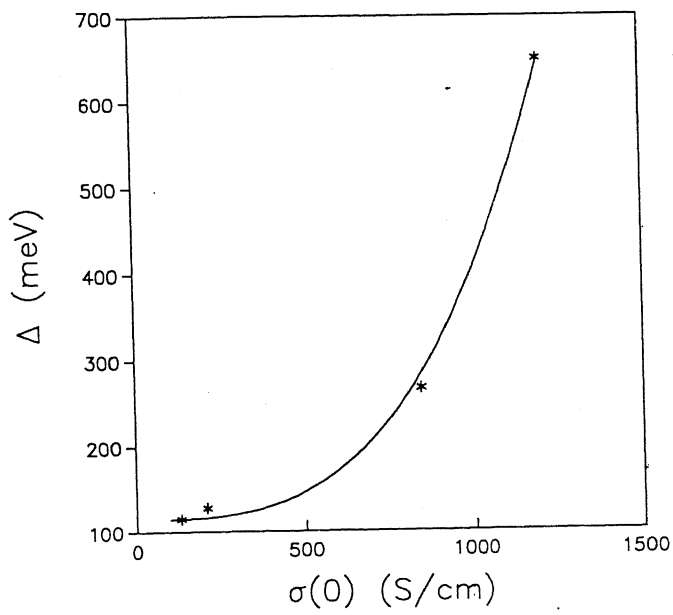

Figure 3.5: The variation of Δ with $\sigma(0)$. The solid curve represents the best fit to $\Delta = u + v \cdot \sigma(0)^q$.

3.4.3 Thermopower

The thermopower of $LaNiO_3$ varies linearly with temperature in good agreement with the free- electron expression for the thermopower:

$$S = -\frac{\pi^2}{6}\frac{k_B^2 T}{eE_F} \qquad (3.2)$$

Using this expression for the δ=0 sample, we found E_F = 0.24 eV, which agrees well with the already reported value [9] of E_F =0.21 eV. A linear temperature dependence of thermopower means that the main contribution comes from the diffusion component. As the value of δ increases, some very interesting features appear in the thermopower of the system. It is negative at room temperature and as we go down in temperature at a characteristic temperature T_0 it changes sign from negative to positive. Below T_0 its magnitude further increases to a maximum and then starts falling. Also we observed that the value of T_0 changes with δ: T_0 =42K, 75K and 71K for δ= 0.06, 0.11 and 0.14 respectively. We found that S fits best to the relation $S = -\alpha T + \beta T^n$ with n ≈1/2 (see table 3.4).

Table 3.4 : Parameters used in fitting the thermopower data (5 K < T < 300 K) to the empirical relation $S = -\alpha T + \beta T^n$. Number of data points used for fitting, N≈300.

δ	a (μV/K^2)	β (μV/K^{n+1})	n	χ^2
0.00	0.0541(9)	-	-	495
0.06	0.0739(9)	0.48(1)	0.50(1)	400
0.11	0.084(3)	0.505(8)	0.59(1)	347
0.14	0.136(4)	0.91(3)	0.56(1)	470

For several other materials also an additional contribution to thermopower along with the diffusion component is observed and this is usually attributed to phonon drag. Since all of our samples have similar crystal structure and almost identical molecular

weights, their Debye temperatures will also be the same, and hence the phonon drag thermopower is expected to be the same for all the samples. But in our case a systematic variation in the strength of T^n term with δ is observed. These observations suggest that the phonon drag mechanism can not account for the observed thermopower. Since the presence of enhanced interaction among the charge carriers due to disorder is unambiguously established from the electrical conductivity and the tunneling conductance data, we feel that the thermopower may also be showing the effects of enhanced electron-electron interactions in this system. However, in the absence of any theoretical predictions[11] we can not make any further progress on this front.

3.5 Conclusion

In this study we have observed the evolution of enhanced electron-electron interaction effects in a three dimensional perovskite oxide system $LaNiO_{3-\delta}$. Stoichiometric $LaNiO_3$ behaves as a normal metal although with a very small electron diffusivity; as oxygen deficiency is introduced into the system the material becomes more disordered and the electron-electron interactions become quite significant and starts affecting the electrical transport. Observed changes in the electrical conductivity and tunneling conductance agree very well with the theoretical predictions for e-e interactions. A systematic variation in the thermopower of the system with δ is also observed.

At the end of this chapter we want to mention that although the electrical resistivity and electron tunneling conductance data show the presence of dominant e-e interactions, the simultaneous presence of weak localization effect can not be ruled out at this stage. Some more discussion on the possibility of weak localization effect is made in chapter 5 where we present the magnetoresistance data of $La_{1-x}Nd_xNiO_3$ samples.

References:

[1] P. A. Lee and T. V. Ramakrishnan, Rev. Mod. Phys. **57**, 287 (1985); B. L. Altshuler and A. G. Aronov, in A. L. Efros and M. Plollak eds., Electron-electron interactions in disordered systems (North Holland, Amsterdam, 1985).

[2] G. Hertel, D. J. Bishop, E. G. Spencer, J. M. Rowell and R. C. Dynes Phys. Rev. Lett. **50**, 743 (1993).

[3] B. L. Altshuler and A. G. Aronov, Sov. Phys. JETP **50**, 968 (1979).

[4] B. L. Altshuler and A. G. Aronov, Solid State Commun. **30**, 115 (1979).

[5] W. L. McMillan, Phys. Rev. B **24** , 2739 (1981).

[6] J. S. Dugdale, The Electrical Properties of Disordered Metals (Cambridge University Press, Cambridge, 1995); K. D. D. Rathnayaka, K. Rhie, B. D. Hennings, D. G. Naugle, J. Phys.: Condens. Matter **5**, 7251(1993).

[7] P. P. Edwards, T. V. Ramakrishnan and C. N. R. Rao, J. Phys. Chem. **99**, 5228 (1995).

[8] M. A. Dubson and D. Holcomb, Phys. Rev. B **32**, 1955(1985).

[9] A. Tiwari and K. P. Rajeev, Solid State Commun. **109**, 119 (1999); K. P. Rajeev, G. V. Shivashankar and A. K. Raychaudhuri, Solid State Communication **79,** 1112 (1991).

[10] K. P. Rajeev and A. K. Raychaudhuri , Phys. Rev. B **46**, 1309 (1992).

[11] There are several experimental reports[1,6] about the electrical resistivity, magnetoresistance, tunneling conductance and specific heat of the interacting electronic systems, but still not much attention has been paid to find the effect of electronic interactions on the thermoelectric power of the system. Furthermore except for the work of

Ting *et al.*[12] which deals with the thermopower of a disordered two dimensional electronic system, there is no theoretical prediction about the thermopower of the interacting electron systems to the best of our knowledge.

[12] C. S. Ting, A. Houghton and J. R. Senna, Phys. Rev. B **25**, 1439 (1982).

[13] J. Kondo, Prog. Theor. Phys. **32**, 37 (1964).

[14] N. W. Aschroft and N. D. Mermin, Solid State Physics (Halt Saunders:Tokyo,1976).

Chapter 4

Electrical transport in $NdNiO_{3-\delta}$

4.1 Introduction

Next to $LaNiO_3$, $NdNiO_3$ is the most widely studied member of $RNiO_3$ (R: rare earth) series. It was prepared for the first time by Demazeau *et al.*[1] who prepared it under a high temperature and a high oxygen pressure. Later on, Vassiliou *et al.*[2] prepared $NdNiO_{3-\delta}$ by a low temperature sol-gel method. The samples prepared under high oxygen pressure have been found to be almost stoichiometric[3,4] while the sol-gel prepared samples are oxygen deficient[5].

Electrical resistivity measurements have been reported on samples prepared by both methods[2,5-8] and there is a general consensus that the material is metallic at high temperature (roughly T > 200 K), insulating at low temperature and there is a metal-insulator (M-I) transistion in between (see section 1.5 of chapter 1 for more details). We do not question this interpretation in the case of samples prepared by the high temperature, high oxygen pressure method. But a close look at the previously reported low temperature electrical resistivity data (see figure 1.6 of chapter 1) of nonstoichiometric $NdNiO_{3-\delta}$ shows that the electrical conductivity of the material tends to a nonzero value as $T \rightarrow 0K$. This suggests that even at low temperature $NdNiO_{3-\delta}$ can not be called an insulator. Here it would be in order to clarify what we mean by the terms metal or insulator at this juncture. A metal is something which has a non-zero electrical conductivity at the absolute zero of temperature. An insulator's electrical conductivity at 0K is strictly zero. This is just a recognition of the fact that a metal has extended states at the Fermi level while an insulator has no extended states at the Fermi level. However, in most of the previous reports[2,6], the behavior of $NdNiO_{3-\delta}$ is described on the same lines as for the stoichiometric $NdNiO_3$.

This chapter is mainly based on the following two published Papers: (i) A. Tiwari and K. P. Rajeev , Modern Physics Letters B **11**, 1161 (1997) and (ii) A. Tiwari and K. P. Rajeev, Solid State Commun. **109**, 119 (1999).

One of the most important parameters that affects the physical properties of oxides is the oxygen stoichiometry. Any change in it may cause significant changes in the transport mechanism too. A model which describes the behavior of a stoichiometric sample may fail when oxygen nonstoichiometry is created in the system. So we feel that it is not proper to presume that the same mechanism which controls the electrical conduction in stoichiometric $NdNiO_3$ is operative in $NdNiO_{3-\delta}$ too. Rather one should study the behavior of $NdNiO_{3-\delta}$ independently. In this chapter we have made an attempt to understand the electrical conduction in nonstoichiometric $NdNiO_{3-\delta}$.

4.2 Experimental

$NdNiO_{3-\delta}$ samples were prepared by the sol-gel method described by Vassiliou *et al.*[2]. Stoichiometric amounts of Nd_2O_3 and $Ni(NO_3)_2.6H_2O$ were dissolved in nitric acid and citric acid was added to this solution so that the ratio of Nd:Ni:citric acid was 1:1:2.05. The molarity of this solution was maintained at 0.1 M and the solution was refluxed at 360 K for 24 hours. The solution was gently warmed to produce a fluffy gel, which was fired at 925 K for 12 hours. The resulting powder was pressed into five rectangular pellets and these pellets were sintered at 800 ° C under different atmospheres to vary the oxygen contents of the sample (see table 4.1). The oxygen stoichiometries of the samples were determined by iodometry. The crystal structure and lattice parameters of all the samples were determined by x-ray diffraction. A four-probe low frequency ac technique was employed to measure the electrical resistivity of the sample in the temperature range 1.2-300 K. The thermopower and high field magnetization measurements on some of the samples were performed.

4.3 Results and Discussion

The x-ray diffraction patterns of the samples show them to be single-phase. All the samples were found to have orthorhombic crystal structure. The lattice parameters are summarized in table 4.1. The oxygen stoichiometries of the samples were found to depend very sensitively on the sintering atmosphere. The sample sintered in oxygen for seven days is

found to have the maximum oxygen concentration (=0.08) while the sample sintered in N_2 has the minimum oxygen concentration (δ=0.22).

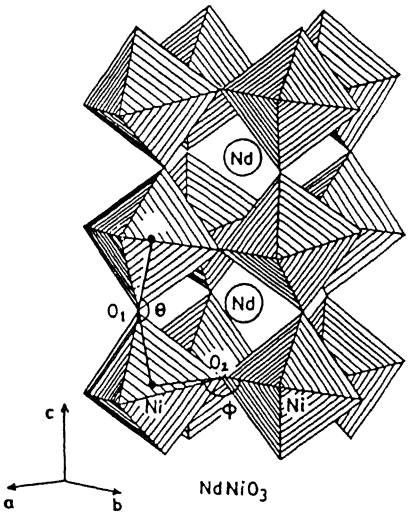

Figure 4.1: Structure of $NdNiO_{3-\delta}$, showing NiO_6 octahedra. Because of the orthorhombic distortion the Ni-O-Ni bond angles are less than 180^0.

The crystallographic unit cell of $NdNiO_3$ can be visualized as corner-sharing octahedra forming a three dimensional perovskite structure (see figure 4.1). At the common apex of two adjacent octahedra sits an oxygen ion making up an Ni-O-Ni bond. A rough estimates of Ni-O-Ni bond angles is made using the method of Hayashi *et al.*[10]. The Ni-O-Ni bond angles are less than 180^0 and they decrease as δ increases, see table(4.1).

Table 4.1: Sinterring conditions, δ, lattice parameters and Ni-O-Ni bond angles for various $NdNiO_{3-\delta}$.

Sinterring atmosphere	δ	Lattice parameters			Ni-O-In bond angles*	
		a (Å)	b (Å)	c (Å)	θ (deg.)	ϕ (deg.)
7d. in O_2	0.08	5.423	5.431	7.556	157.82	159.86
2d. in air+5d. in O_2	0.12	5.392	5.430	7.604	155.55	158.47
4d. in air+ 3d. in O_2	0.15	5.390	5.429	7.611	155.49	157.40
7d. in air	0.20	5.387	5.428	7.620	155.37	156.36
7d. in N_2	0.22	5.383	5.426	7.628	155.26	155.51

* See endnote with ref[10] for more details.

4.3.1 Electrical Resistivity

The electrical resistivity data of $NdNiO_{3-\delta}$ from 1.2 to 300 K are shown in figure 4.2.

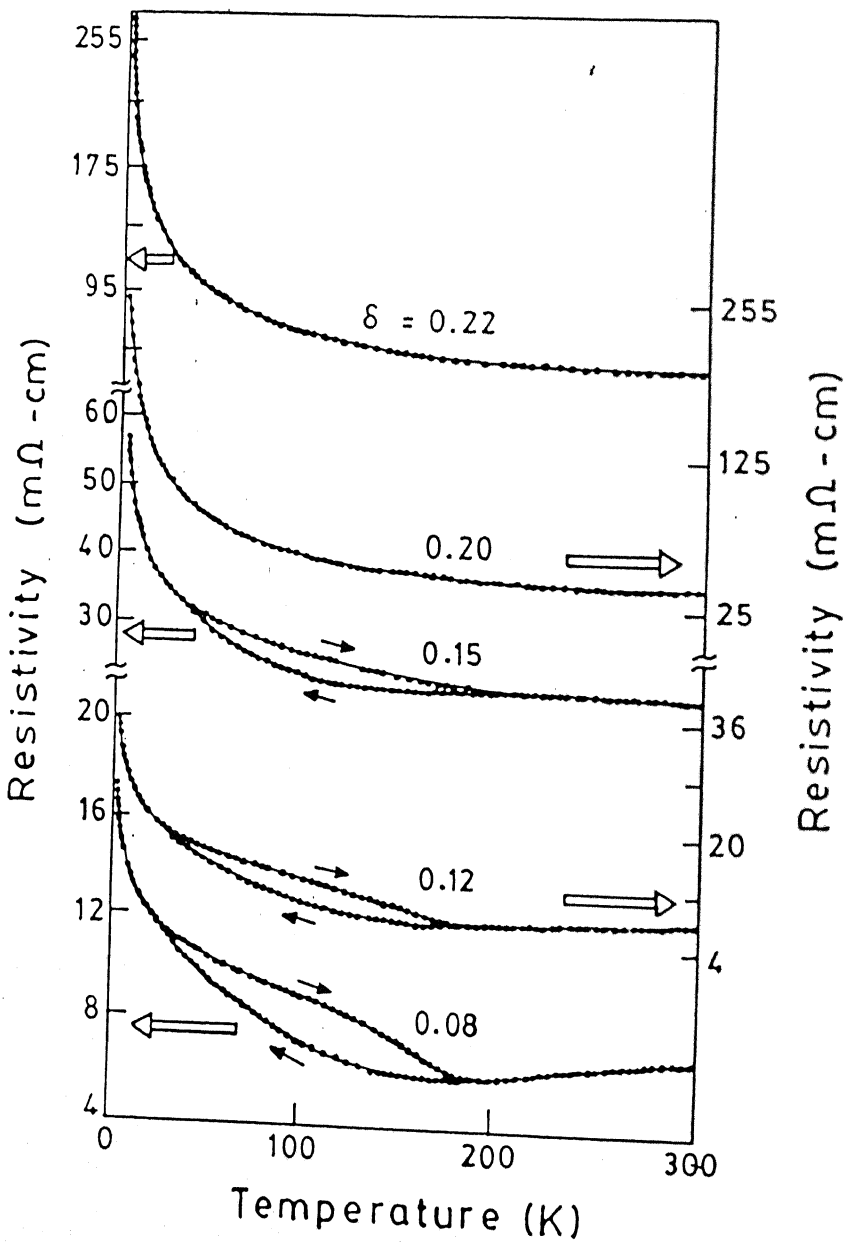

Figure 4.2 : Electrical resistivity of $NdNiO_{3-\delta}$ for various δ. Thin arrows represent whether the data was taken during cooling or heating. Not all the points are shown for clarity.

At low temperatures all the samples show a negative temperature coefficient of resistivity (TCR). Above T ≈ 200K the situation is different for different samples. For δ=0.08 and 0.12, the resistivity increases almost linearly with temperature in the temperature range 200-300K. For δ=0.15, it remains almost constant while for δ=0.15 and 0.22 it continues to decrease with increase in temperature. Another interesting feature of this system that is most unusual is the hysteresis shown by some of the samples below ≈ 200K. On heating from a low temperature upwards the resistivity is higher than that observed on cooling by as much as 30%. The hysteresis becomes small as T goes below 30 K and is negligibly small (< 0.1%) for T < 20 K. In figure 4.3 we have shown the relative hysteresis $[(\rho_{heating}-\rho_{cooling})/\rho_{cooling}]$ for various samples. It can be seen from this figure, that, the relative hysteresis depends strongly on δ (oxygen deficiency). When δ decreases from 0.22 relative hysteresis first increases, reaches a maximum at δ=0.12 and then starts decreasing.

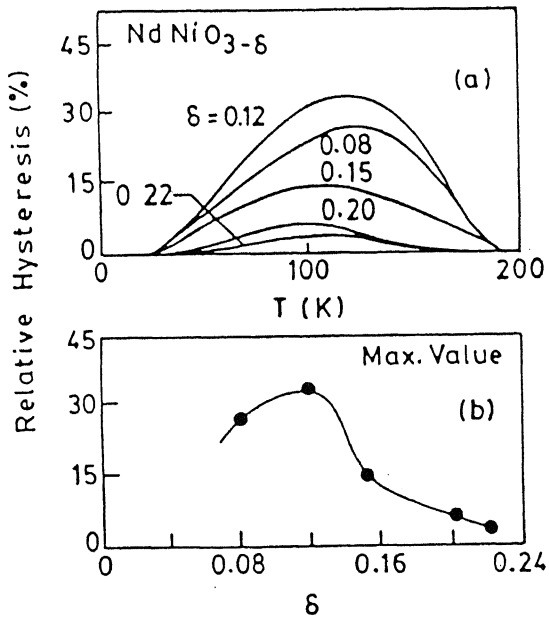

Figure 4.3 : (a) Relative hysteresis $[(\rho_H-\rho_C)/\rho_C]$ vs. temperature for various δ, (b) Max. relative hysteresis as a function of δ. When δ decreases relative hysteresis first increases and then starts decreasing. Experimental data points are shown by solid circles. The line shown is a guide to the eye.

At low temperatures all the samples show negative TCR and thus appear to be insulating. But appearances can be deceptive. A positive TCR definitely means that the material is a metal but a negative TCR does not necessarily indicate an insulator (for an insulator it is essential that as T→0K the electrical conductivity, σ→0). Even in the case of metals there are several effects which may give a negative TCR.

To find out whether the material is metallic or insulating and what are the real mechanisms affecting the electrical transport we fitted our low temperature electrical conductivity data to following expressions*:

Model 1. Activated transport[11]; here the conductivity is given by:

$$\sigma = \sigma_{\infty} \exp[-T_0/T] \qquad (4.1)$$

where σ_{∞} and T_0 are constants.

Model 2. Variable range hopping (VRH)[11,12]; in this case

$$\sigma = AT^{-\frac{1}{2}} \exp[-(T_0/T)^{0.25}] \qquad (4.2)$$

where A and T_0 are constants.

Model 3. Conduction in disordered metallic systems [13]; in this case the low temperature electrical conductivity follows the relation:

$$\sigma = \sigma(0) + bT^m - cT^n \qquad (4.3)$$

where σ_0, b, c, m and n are constants. More details about this expression can be found in section 3.4.1 of chapter 3.

The details of the fits are given in table 4.2. It can be seen from this table that the values of χ^2 are quite high for the first two models while it is close to N for the last model. So the description of $NdNiO_{3-\delta}$ as an insulator at low temperature is not true. All the above analysis and a nonzero value of σ_0 suggests that the material is metallic even at low temperature. We have shown the raw data and fit to various expressions for one of the samples ($NdNiO_{2.88}$) in figure 4.3. The large deviation of the experimental

*In the most of the previous reports authors fitted their data to the first two expressions only.

Table 4.2: Parameters used in fitting the low temperature (1.2 K < T < 16 K) conductivity data of $NdNiO_{3-\delta}$ to eqs.(4.1)-(4.3). Number of data points used for fitting, N≈200.

δ	Equ.4.1	Equ.4.2	Equ.4.3
0.08	χ^2= 11037	χ^2=10985	χ^2=248
	σ=80(2)S/cm	A=2546(30) S/cm	$\sigma(0)$=39.21(3) S/cm
	T_0=0.86(1)K	T_0=301(5) K	b=14.02 (1) S/cm-K^m
			c=0.363((3) S/cm-K^n
			m=0.46(1)
			n=1.201(2)
0.12	χ^2=36443	χ^2=29627	χ^2=281
	σ=40.6(1) S/cm	A=1205(13) S/cm	$\sigma(0)$=14.61(4) S/cm
	T_0=0.78(1)K	T_0=284(4) K	b= 9.27(3) S/cm-K^m
			c=0.092(2) S/cm-K^n
			m=0.44(1)
			n=1.399(1)
0.15	χ^2=105929	χ^2=55645	χ^2=347
	σ=25(1) S/cm	A=973(15) S/cm	$\sigma(0)$=7.56(1) S/cm
	T_0=1.26 (2)K	T_0=474(9) K	b= 5.97(3)S/cm-K^m
			c= 0.037(1)S/cm-K^n
			m=0.41(1)
			n=1.321(1)
0.20	χ^2 =163361	χ^2=55987	χ^2=303
	σ=8.09(3) S/cm	A=479(6) S/cm	$\sigma(0)$=1.517(2) S/cm
	T_0=2.42(3) K	T_0=1018(15) K	b= 1.501(6) S/cm-K^m
			c=0.0018(1) S/cm-K^n
			m= 0.50(3)
			n= 1.648(9)
0.22	χ^2=75625	χ^2=29025	χ^2=245
	σ=7.26(4) S/cm	A=406(5) S/cm	σ(0=1.399(7) S/cm
	T_0=2.09(3) K	T_0= 898(9) K	b= 1.374(4) S/cm-K^m
			c= 0.0026(4) S/cm-K^n
			m=0.52(1)
			n=1.750(2)

data from the insulating expressions and the good fit to the empirical expression is obvious from the figure. The situation becomes more interesting when we notice that the values of m are quite similar to those observed in highly disordered metals[13-15].

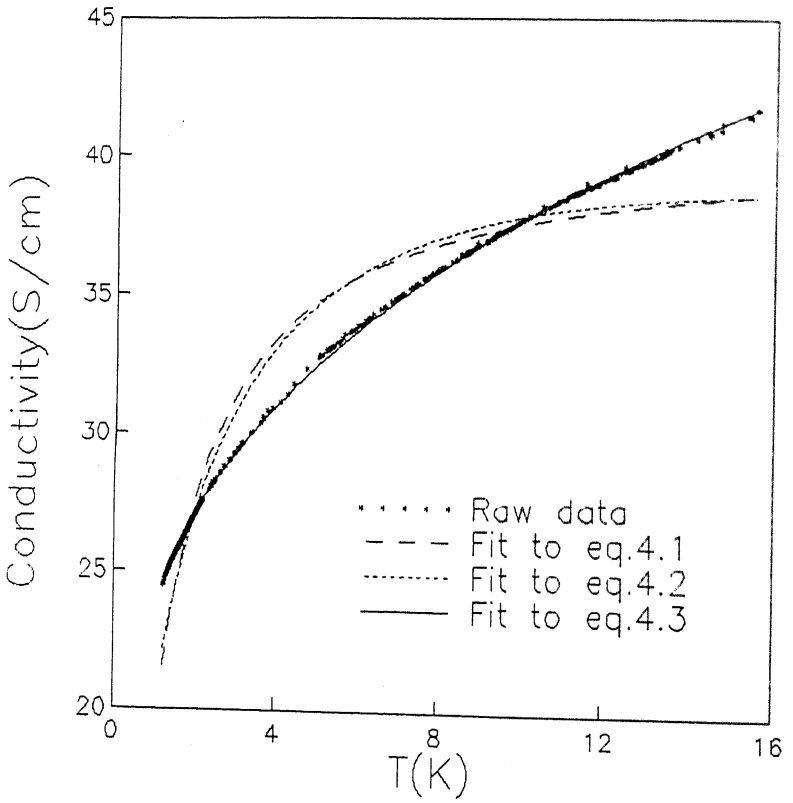

Figure 4.4: Low temperature (1.2 K < T < 16 K) conductivity data of $NdNiO_{2.88}$ and fits to eqs. (4.1)-(4.3).

Now we come to the hysteretic behavior of electrical resistivity. Hysteresis is usually observed at first order phase transitions. Some of the important materials which undergo first order M-I transition are VO_2, Ti_2O_3, V_2O_3 etc.[16]. But in all these cases the M-I transition is accompanied by a structural transition that changes the symmetry of the low temperature insulating state. For example in V_2O_3 system a 3.5% change in volume and a change in lattice symmetry from monoclinic to trigonal is observed. But a neutron diffraction experiment[17] on high oxygen pressure prepared samples show that in $NdNiO_3$ the transition is not accompanied by any change in lattice symmetry. Only a slight expansion (while cooling) in lattice volume occurs ($\approx$ 0.2 %) at $\approx$ 190 K and moreover this change is not sharp but occurs over a temperature range of about 10 K. This small change in

lattice volume is in sharp contrast with the much larger ones found in the former materials and hence is unlikely to cause the observed large hysteresis in resistivity. The origin of hysteresis in $NdNiO_3$ samples is probably more complex and hence it needs more investigation.

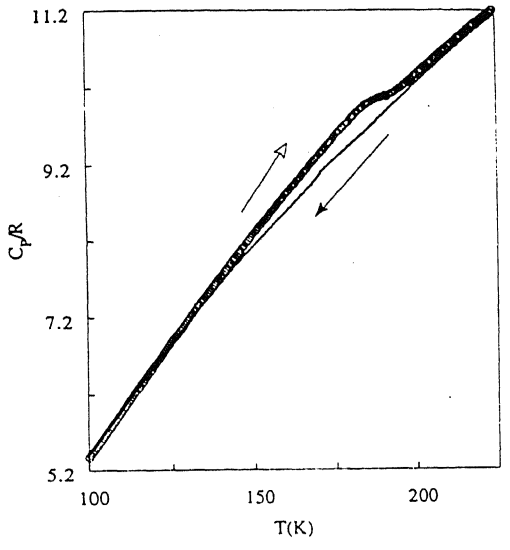

Figure 4.5: Specific heat vs. temperature for $NdNiO_{3-\delta}$. After Blasco *et al.*[18].

Although no neutron diffraction data is available for the sol-gel prepared $NdNiO_{3-\delta}$ samples, in a specific heat measurement[18] it has been found that the specific heat of the sample does not show any sharp discontinuity at the transition but only a small hump of magnitude ≈ 2%, spread over ≈ 10K; it also shows hysteresis (see figure 4.5). We know that if any sample undergoes a first order transition its specific heat should blow up at the transition point due to latent heat so it is clear that if we go by the data of Blasco *et al.*[18], the transition is not of first order and hence the observed hysteresis has some other origin. The fact that the specific heat, a thermodynamic quantity, itself is hysteretic indicates that the system is not in thermodynamic equilibrium.*

Now we present a plausible picture that can account for the hysteresis and the low temperature behavior of the electrical conductivity. In this picture when the temperature of the material decreases, at a transition point, a part of the material becomes insulating. As the temperature further decreases the conc. of the insulating phase increases and that of the metallic phase decreases. The insulating and metallic phases are thoroughly mixed. We observed that during the cooling cycle if the sample is maintained at some temperature the resistivity of the sample starts increasing with time (see figure 4.6). This suggests that in the intermediate temperature range the metallic phase is metastable and has a tendency to

* One wonders whether this could be a case of glass transition.

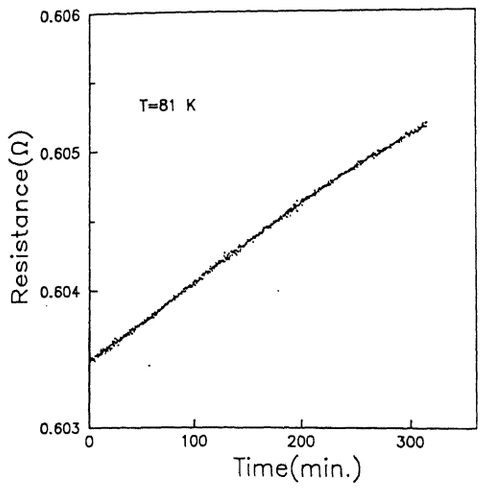

Figure 4.6 : Time dependence of resistance for $NdNiO_{2.88}$ when the sample was maintained at 81K during the cooling cycle.

go to the insulating side. The coexistence of a metallic phase and an the insulating phase with temperature and history dependent relative concentrations is probably the cause of hysteresis. The fact that at T=0K the samples have nonzero electrical conductivity implies that the fraction of metallic phase is always more than the percolation threshold. Also since below 30K there is almost no hysteresis we believe that in this temperature range the relative concentrations of metallic and insulating phases are temperature independent. So at low temperature we have a mixture of a metallic phase and an insulating phase, with the concentration of the metallic phase more than the percolation threshold. The sample behaves effectively as a metal but the insulating phase, which is thoroughly mixed with the metallic phase on a microscopic scale, causes sufficient disorder in the metal. But we point out here that the picture has to be substantiated and more work is needed to clear up the mystery completely.

4.3.2 Thermopower

Thermopower data of $NdNiO_{2.92}$ in the temperature range 5-300K are shown in figure 4.7. The thermopower is small and negative and has a linear thermal variation above ≈ 180 K. At 180 K a shoulder is observed and below this temperature it decreases in magnitude with decreasing temperature. Between 50K and 180K, thermopower shows a large thermal hysteresis. A finite and linearly varying thermopower again indicates the overall metallic behavior of the sample even at low temperature.

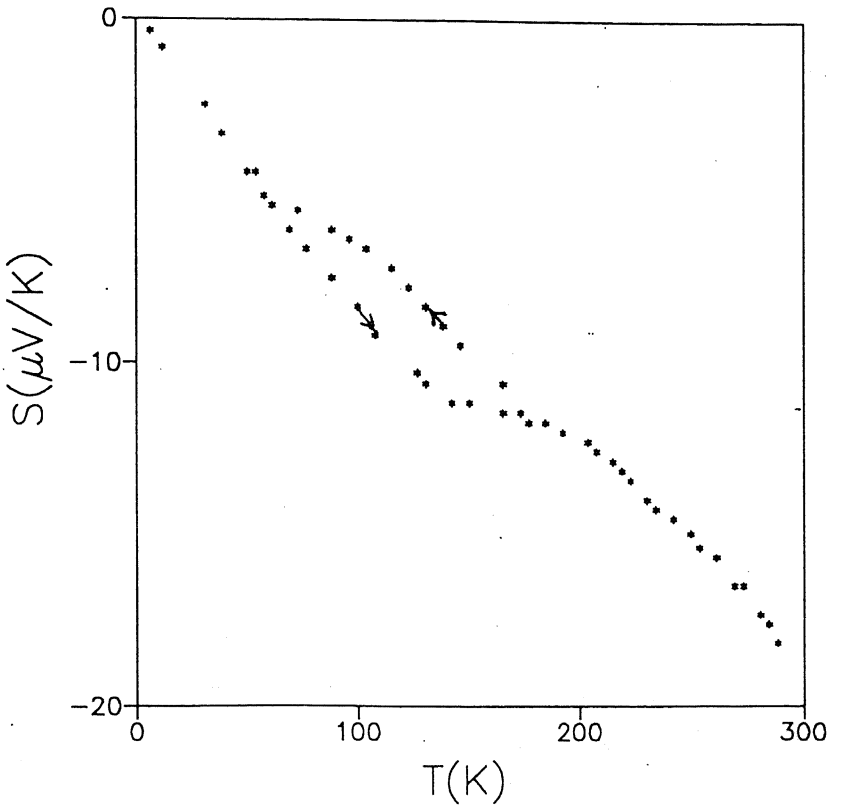

Figure 4.7 Thermopower vs. temperature for $NdNiO_{2.92}$.

4.3.3 Magnetization

Figure 4.8 shows the magnetic susceptibility of $NdNiO_{2.88}$ in the temperature range 4.2-185K. Inset of this figure shows the variation of magnetization (M) with field (H). Any possible interpretation of the temperature dependence of magnetic susceptibility is complicated by the fact that J=9/2 ground state of Nd^{3+} ions undergoes crystal field splitting. Because of this crystal field splitting a Schottky anomaly in the specific heat of $NdNiO_3$ is also found. In specific heat this anomaly occurs at around 10K. This implies that at low temperatures it is not safe to fit the data to Curie-Weiss law. So we confined the temperature range of fitting to well above 10K and fitted our magnetic susceptibility data from 70K to 185K in the equation:

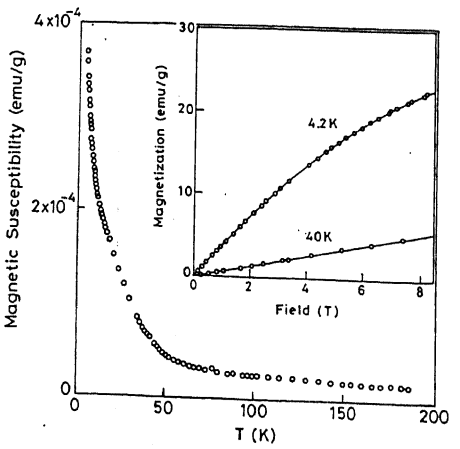

Figure4.8: Magnetic susceptibility vs. temperature for $NdNiO_{2.88}$. The inset shows the variation of magnetization with field at 4.2 K and 40 K.

$$\chi = \chi(0) + \frac{C}{T + T_c}$$

with best fit parameters $\chi(0)$ $=3.279\times10^{-6}$ emu/g, c= 3.362×10^{-3} emu-K/g and T_c= 54 K. Although it is found that the best fit parameters vary slightly depending upon the temperature interval of fit but $\chi(0)$ is always positive. $\chi(0)$ is mainly because of the Pauli paramagnetism of free electrons and its value is very close to that reported earlier[2,6]. Assuming that the core diamagnetism of $NdNiO_{3-\delta}$ is same as that of $LaNiO_3$, the Pauli paramagnetism of $NdNiO_{2.88}$ comes out to be 3.551×10^{-6} emu/g[19].

4.4 Conclusion:

In this study we have observed that even at low temperatures nonstoichiometric $NdNiO_{3-\delta}$ behaves as a metal. At low temperatures (where thermal hysteresis is negligibly small) electrical conductivity follows a sublinear temperature dependence with a nonzero value of extrapolated zero temperature conductivity, $\sigma(0)$. A nonzero value for $\sigma(0)$ indicates metallicity and a sublinear temperature dependence of low temperature electrical conductivity indicates the strongly disordered nature of the system. A small thermopower and a nonzero Pauli contribution to the magnetic susceptibility are also indicative of the overall metallic nature of the system. Some more features reflecting the disordered metallic nature of $NdNiO_{3-\delta}$ will be discussed in the next two chapters.

References:

[1] G. Demazeau, A. Marbeuf, M. Pouchard and P. Hagenmuller, J. Solid State Chem 3, 582 (1971).

[2] J. K. Vassiliou, M. Hornbostel, R. Ziebarth and F. J. Disalvo, J. Solid State Chem. **81**, 208 (1989).

[3] J. L. García-Muñoz, J. Rodríguez-Carvajal, P. Lacorre and J. B. Torrance, Phys. Rev. B **46**, 4414 (1992).

[4] J. A. Alonso, M. J. Martínez-Lope and M. A. Hidalgo, J. Solid State Chem. **116**, 146(1995).

[5] R. Mahesh, K. R. Kannan and C. N. R. Rao, J. Solid State Chem. **114**, 294(1995).

[6] J. Blasco and J. García, J. Phys.: Condens. Matter **6** , 10759 (1994).

[7] J. B. Torrance, P. Lacorre and A. I. Nazzal, E. J. Ansaldo and Ch. Niedermayer, Phys. Rev. B **45**, 8209 (1992).

[8] X. Granados, J. Fontcuberta, X. Obradors, Ll Mañosa and J. B. Torrance, Phys. Rev. B **48**, 11666 (1993).

[9] M. L. Medarde, J. Phys.: Condens. Matter **9**, 1679 (1997).

[10] K. Hayashi, G. Damazeau and M. Pouchard, Revue de chimie minérale **18**, 148 (1981). The Ni-O-Ni bond angles (θ and ϕ) are given by the relations: $\theta = 135 + \sqrt{13.4(\theta_0 - 135)}$ and $\phi = 130.7 + \sqrt{189.9(\phi_0 - 135)}$, where θ_0 and ϕ_0 are related

to lattice parameters (a, b and c) by: $\cos(\theta_0) = [1 - 2a^2 / b^2\}$ and $\cos(\phi_0) = [1 - 2a^2(a^2 + b^2)/b^2c^2]$

[11] N. F. Mott and E. A. Davis, Electronic Processes in non-crystalline materials (Oxford University Press, Oxford, 1979).

[12] D. K. Paul and S. S. Mitra, Phys. Rev. Lett **31**, 1000 (1973)

[13] P. A. Lee and T. V. Ramakrishnan, Rev. of Mod. Physics **57**, 287 (1985).

[14] B. L. Altshuler and A. G. Aronov, in A. L. Efros and M. Plollak eds., Electron-electron interactions in disordered systems (North Holland, Amsterdam, 1985).

[15] A. K. Raychaudhuri, Phys. Rev. B **44**, 8572 (1991).

[16] P. C. Canfield, J. D. Thompson, S-W. Cheong and L. W. Rupp, Phys. Rev. B **47**, 12357 (1993).

[17] P. Lacorre, J. B. Torrance, J Pannetier, A. I. Nazzal, P. W. Wang and T. C. Huang, J. Solid State Chem. **91**, 225 (1991).

[18] J. Blasco, M. Castro and J. García, J. Phys.: Condens. Matter **6**, 5875 (1994).

[19] A. Tiwari and K. P. Rajeev, Modern Physics Letters B **11**, 1161 (1997).

Chapter 5

Electrical transport in $La_{1-x}Nd_xNiO_{3-\delta}$

5.1 Introduction

In the last two chapters the electrical transport properties of $LaNiO_{3-\delta}$ and $NdNiO_{3-\delta}$ have been presented individually. $LaNiO_{3-\delta}$ shows comparatively simple features while the behavior of $NdNiO_{3-\delta}$ is quite involved. However the low temperature electrical conductivity data identify both of these systems to be metallic. It was observed that when disorder is created in $LaNiO_3$ (by creating oxygen deficiency), the e-e interactions become quite significant and start affecting the electrical transport. Disorder can also be introduced by the substitution of one or more of the constituents. In this chapter the effect of substituting La by Nd in $LaNiO_3$ has been studied.

5.2 Experimental

All the samples investigated in this work were prepared by the sol-gel method. The powder sample was pressed into rectangular pellets and these pellets were sintered in flowing oxygen. The oxygen stoichiometries for all the samples were determined by iodometry (see table 5.1). The x-ray diffraction patterns were recorded using a Rich-Seifert x-ray diffractometer (model: Isodebyeflex 2002) and Ni filtered Cu K_α radiation. A four-probe ac (1kHz) technique was employed to measure the electrical resistivity of all the samples in the temperature range of 2.5-300 K. The electron tunneling conductance measurements were carried out at 1.2 K on tunnel junctions made with Pb counter-electrode. The absolute thermopower measurements were done in the temperature range of 5-300 K. The magnetoresistance measurements were performed by a standard four-probe dc method using a 4.5 T superconducting magnet.

5.3 Results and discussion

5.3.1 Crystal structure

X-ray diffraction patterns of $La_{1-x}Nd_xNiO_{3-\delta}$ ($0.0 \leq x \leq 1.0$) are shown in figure 5.1. The reflections in the x-ray diffraction patterns are quite broad, suggesting that the particle size of the samples is small. Due to this broadening, the lines at high angles could not be resolved, and this limited the measurements to a 2θ value of 60^0. Examination of the data suggested $LaNiO_3$ to be cubic with lattice parameter a=3.850 Å. For $x \geq 0.4$ some additional peaks (shown in figure 5.1), characteristic of orthorhombic distortion, appear and the system can be indexed as an orthorhombic system. Values of various lattice parameters are summarized in table 5.1. As a result of iodometric titration it was observed that the sample with x=0.0 is fully stoichiometric (δ=0.0) while the sample with x=1.0 is oxygen deficient (δ=0.08). We found that our samples are actually the solid solutions of $LaNiO_3$ and $NdNiO_{2.92}$, i.e. $(LaNiO_3)_{1-x}(NdNiO_{2.92})_x$.

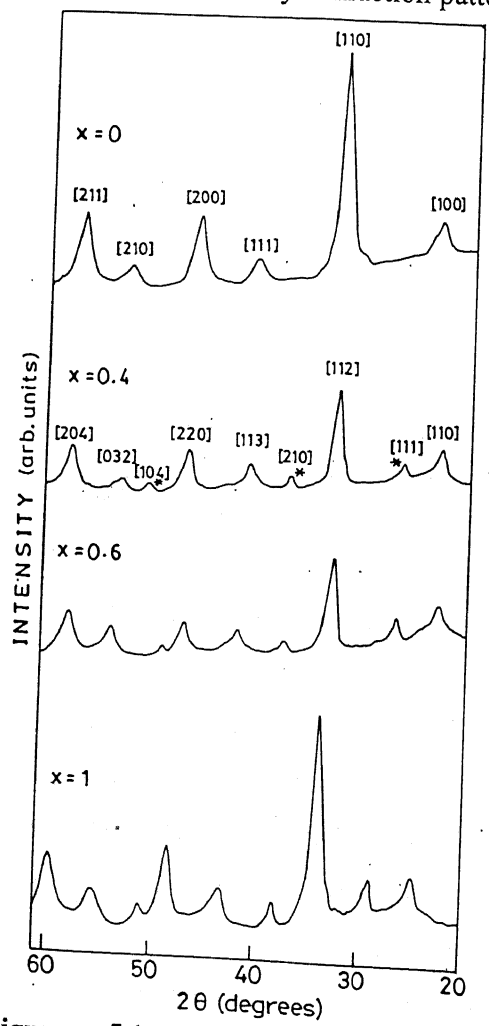

Figure 5.1: X-ray diffraction pattern of $La_{1-x}Nd_xNiO_{3-\delta}$ (x=0.0, 0.4, 0.6 and 1.0).

Table 5.1: Crystal structure. lattice parameters and oxygen contents for various $La_{1-x}Nd_xNiO_{3-\delta}$ samples.

δ	Crystal structure	Lattice parameters			$3-\delta$
		a (Å)	b (Å)	c(Å)	
0.0	Cubic	3.850	-	-	3.00
0.1	Cubic	3.846	-	-	3.00
0.2	Cubic	3.842	-	-	2.98
0.3	Cubic	3.836	-	-	2.98
0.4	Orthorhombic	5.432	5.435	7.645	2.97
0.6	Orthorhombic	5.430	5.435	7.614	2.95
0.8	Orthorhombic	5.427	5.433	7.583	2.94
1.0	Orthorhombic	5.423	5.431	7.556	2.92

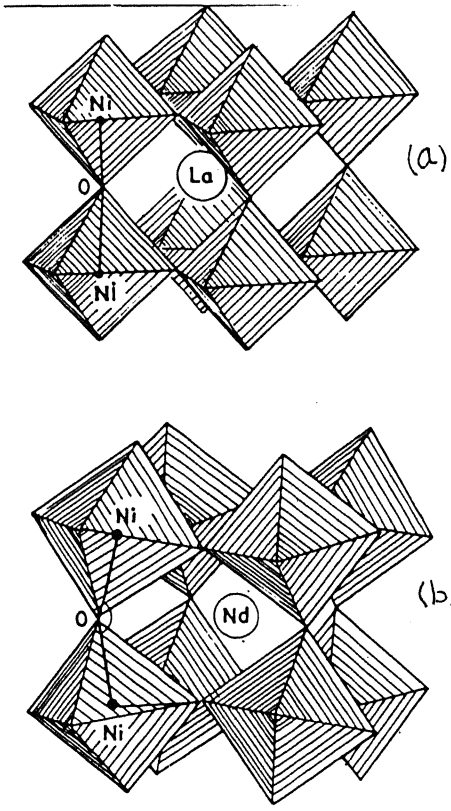

Figure 5.2: Three dimensional network of NiO_6 octahedra in (a) $LaNiO_3$ and in (b) $NdNiO_3$.

The crystallographic unit cell of these materials can be visualized as corner-sharing NiO_6 octahedra forming a three dimensional network. In the case of cubic perovskite ($LaNiO_3$), NiO_6 octahedra are arranged regularly at the nodes of a simple cubic lattice (figure 5.2(a)). In this case Ni-O-Ni angle is 180^0. While in the case of orthorhombic perovskites ($NdNiO_3$), NiO_6 octahedra are tilted (figure 5.2(b)) and the Ni-O-Ni angles are less than 180^0.

5.3.2 Electrical Resistivity

The electrical resistivity data of $La_{1-x}Nd_xNiO_{3-\delta}$ samples from 1.2 K to 300 K are shown in figure 5.3. For the x=0.0 ($LaNiO_3$) sample, the variation of electrical resistivity with temperature is very similar to that for good metals except for its large magnitude. Temperature coefficient of resistivity is positive throughout the whole temperature range. When La is replaced partially by Nd, the high temperature behavior of the system remains unaltered but at low temperature a minimum in electrical resistivity is observed at T_{min}. All the samples with $x \leq 0.6$ show almost similar features except for the fact that as x increases T_{min} moves towards the higher values. On further increasing x, the system starts showing a thermal hysteresis in the electrical resistivity. For x=1.0, the hysteresis becomes quite significant.

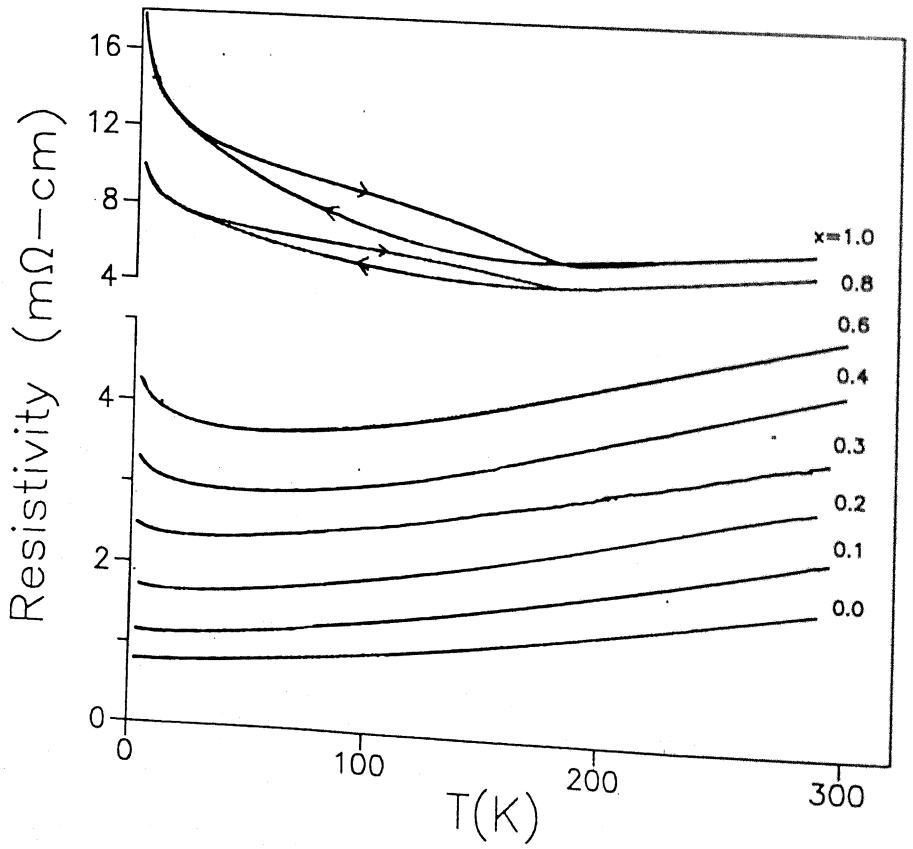

Figure 5.3 : Electrical resistivity vs. temperature for $La_{1-x}Nd_xNiO_{3-\delta}$ ($0.0 \leq x \leq 1.0$).

As discussed before in chapter 3, the low temperature resistivity minima in metals may have following origin (i) Kondo effect[1] (ii) Weak localization and e-e interactions[2,3]. Kondo effect is observed in nonmagnetic systems with a slight magnetic impurity and the Kondo systems show a giant thermopower, at low temperature. No such giant thermopower is observed in any of these samples and hence the possibility of Kondo effect is ruled out.

To uncover the real mechanism involved in the electrical transport we fitted our low temperature (2.5-20 K) conductivity data to an empirical relation of the kind $\sigma = \sigma(0) + bT^m - cT^n$, where $\sigma(0)$, b, c, m, and n are constants. More details about this expression can be found in section 3.4.1 of chapter 3. The details of fit are given in table 5.2.

Table 5.2 : Fit parameters for the low temperature (2.5 K < T < 20 K) conductivity data of $La_{1-x}Nd_xNiO_{3-\delta}$ to empirical relation $\sigma = \sigma(0) + bT^m - cT^n$. Number of data points used for fitting, N ≈200.

x	$\sigma(0)$ (S/cm)	b (S/cm-K^m)	c (S/cm-K^n)	m	n	χ^2
0.0	1262.07(1)	-	0.0377(1)	-	1.993(1)	242
0.1	844.83(9)	12.87(1)	0.1111(8)	0.48(1)	1.817(5)	415
0.2	559.66(8)	11.73(6)	0.08174(6)	0.51(1)	1.771(3)	572
0.3	381.62(5)	13.74(3)	0.1018(9)	0.46(1)	1.611(7)	290
0.4	274.95(9)	17.58(7)	0.1918(7)	0.47(1)	1.452(2)	303
0.6	206.54(8)	17.76(9)	0.1932(4)	0.45(1)	1.418(4)	317
0.8	74.11(7)	17.51(9)	0.269(1)	0.47(1)	1.359(8)	375
1.0	39.22(4)	14.03(1)	0.362(4)	0.46(1)	1.201(2)	290

For all the samples the data fit quite well to the above relation . The value of m lies very close to 1/2, suggesting that the e-e interaction effects are playing an important role in the system. However we want to mention here that since the temperature dependence of weak-localization and e-e interaction effects are quite similar, it will not be proper to conclude from the resistivity data that weak localization effects are totally absent.

5.3.3 Tunneling conductance

In figure 5.4 we show the differential tunneling conductance G(V) (dI/dV) of various samples at 1.2 K .

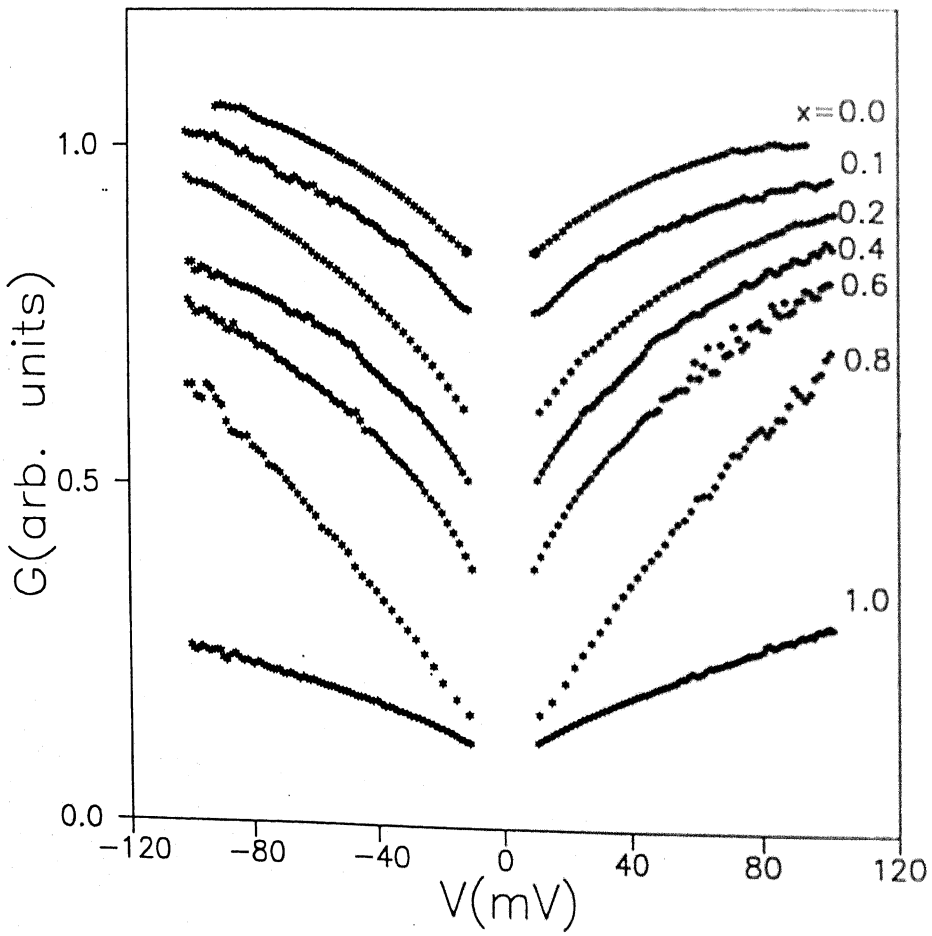

Figure 5.4 : Tunneling conductance vs. bias voltage for $La_{1-x}Nd_xNiO_{3-\delta}$ ($0.0 < x < 1.0$) at 1.2 K. The data have been normalized to unity at 100 mV and shifted vertically for clarity. Information about the absolute values is given in table 5.3.

For all the samples an anomaly in the density of states, with a minimum at the Fermi energy, is observed. The tunneling conductance data follow the relation $G(V) = G_0\left[1 + \left(\frac{|V|}{\Delta}\right)^{0.5}\right]$ as predicted by Altshuler and aronov for disordered metallic systems with dominant e-e interactions[2].

Table 5.3: Parameters used in fitting the tunneling conductance data of $La_{1-x}Nd_xNiO_{3-\delta}$ at 1.2 K to $G(V) = G_0[1 + (|V|/\Delta)^{0.5}]$. Data in the range 10 mV < V < 100 mV were used for fitting. Number of data points used for fitting, N≈100.

x	G_0 (S)	Δ (meV)	χ^2
0.0	0.8473(9)	649(9)	173
0.1	0.6613(2)	587(20)	286
0.2	0.4338(7)	164(4)	320
0.4	0.2634(5)	97(2)	248
0.6	0.1562(5)	42(1)	195
0.8	0.0872(9)	0.5(2)	471
1.0	0.0434(2)	757(17)	394

5.3.4 Magnetoresistance

Magnetoresistance data of $La_{1-x}Nd_xNiO_{3-\delta}$ samples at T=4.2 K are shown in figure 5.5. The magnetoresistance of these samples is negative and its magnitude increases with the field. The inset of figure 5.5 shows the variation of magnetoresistance with temperature at B=4 T. As the temperature increases the magnitude of magnetoresistance decreases for all the samples.

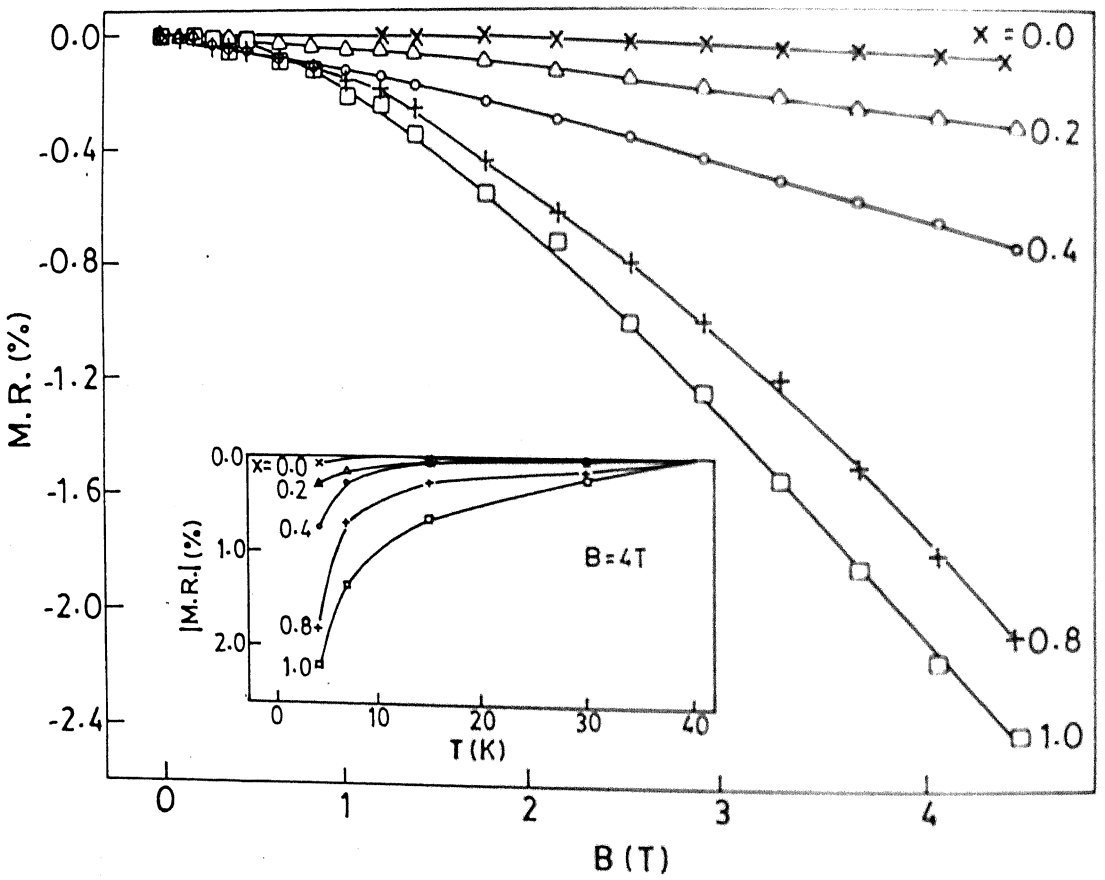

Figure 5.5: Magnetoresistance [R(B)-R(0)]/R(0) vs. B for $La_{1-x}Nd_xNiO_{3-\delta}$ at 4.2K. The inset shows the variation of magnetoresistance with temperature at B=4 T.

The behavior of the magnetoresistance of these samples is very similar to that of disordered electronic systems[2]. Magnetoresistance of all the samples under investigation is negative. This suggests that the weak localization may also be playing a significant role in the system.

5.3.5 Thermopower

The thermopower data of $La_{1-x}Nd_xNiO_{3-\delta}$ samples from 5 K to 300 K are shown in figure 5.6. Thermopower of the parent compound $LaNiO_3$ is negative and varies linearly with temperature. When La is replaced by Nd, some interesting changes are observed in the thermopower data. For smaller doping concentrations, the nature of thermopower remains almost same (as for $LaNiO_3$) except for the fact that now at a characteristic temperature T_0 thermopower changes sign from negative to positive and at a lower temperature a slight peak in thermopower is observed. Similar kind of behavior was observed for $LaNiO_{3-\delta}$ samples also. For higher concentrations of Nd the behavior of the thermopower data becomes quite complicated and it shows appreciable thermal hysteresis.

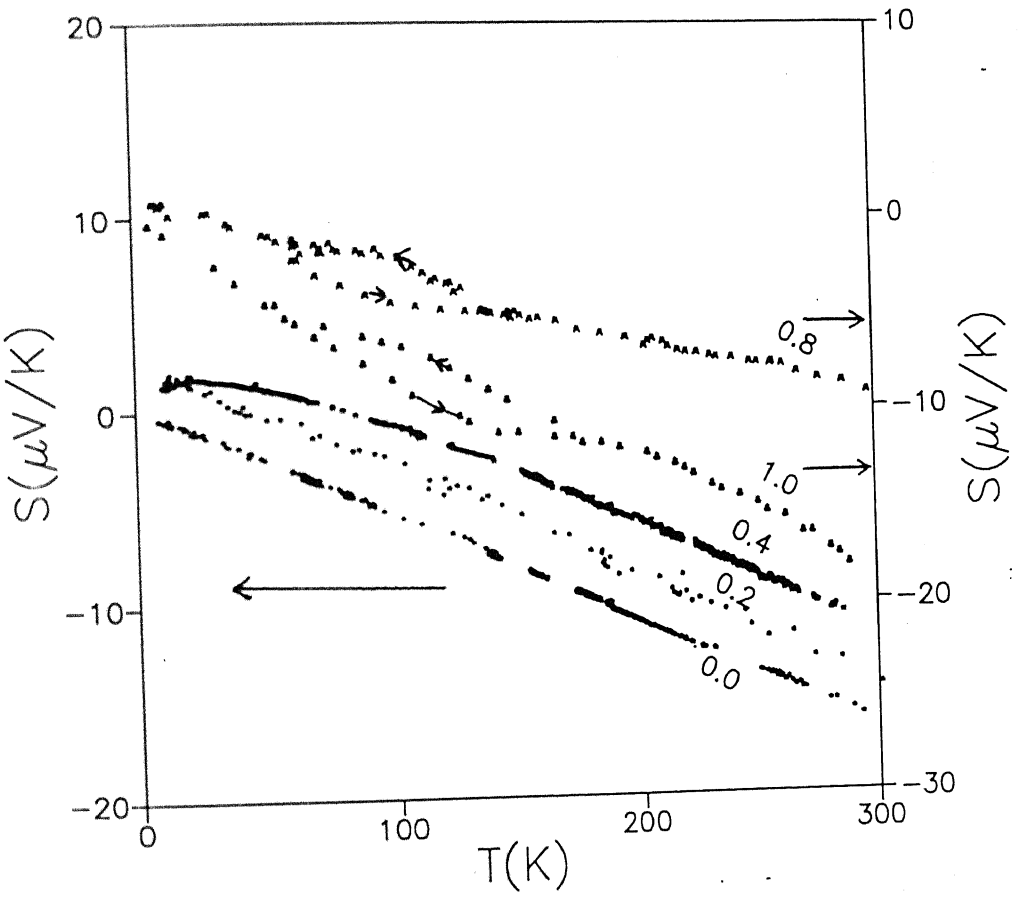

Figure 5.6 : Thermopower of $La_{1-x}Nd_xNiO_{3-\delta}$ (x=0.0, 0.2, 0.4, 0.8, 1.0) from 5 K to 300 K. For x=0.0, 0.2 and 0.4 the y-scale is on the left hand side while for x=0.8 and 1.0 it is on the right hand side.

5.4 Conclusion

In this chapter we have observed clear signatures of enhanced electron-electron interaction and weak localization effects in $La_{1-x}Nd_xNiO_{3-\delta}$ samples. Parent compound $LaNiO_3$ itself behaves as a disordered correlated metal. As the Nd is substituted in place of La the disorder in the system* increases. Electrical resistivity of $La_{1-x}Nd_xNiO_{3-\delta}$ samples show a minimum at low temperature which successively shifts to higher temperature with increasing x. In the low temperature limit the correction to electrical conductivity follows a power law behavior with an exponent ≈ 0.5. Electron tunneling conductance data shows a cusp-like dip in the density of states near the Fermi energy. Both these features are understood to be the consequence of enhanced electron-electron interactions in the system. Magnetoresistance of all these samples is negative and its magnitude increases with x. A negative magnetoresistance suggests the possibility of the simultaneous presence of weak localization effects in the system.

* As the concentration of Nd increases there is a slight decrease in the oxygen stoichiometrry also. So the disorder in the present system will be due to both (i) different scattering potentials of La^{3+} and Nd^{3+} as well as oxygen vacancies.

References

[1] J. Kondo, Prog. Theor. Phys. **32**, 37 (1964).

[2]] B. L. Altshuler and A. G. Aronov, in A. L. Efros and M. Plollak eds., Electron-electron interactions in disordered systems (North Holland, Amsterdam, 1985).

[3] P. A. Lee and T. V. Ramakrishnan, Rev. Mod. Phys. **57**, 287 (1985).

Chapter 6

Metal-insulator transition in $NdNi_{1-x}Fe_x O_3$

6.1 Introduction

In chapter 4 we found that $NdNiO_{3-\delta}$ shows quite unusual characteristics. It beha metal at high temperature as well as at low temperature. At low temperature th appears to be a mixture of two phases, one of which is metallic and the other is in Relative concentration of these two phases is found to be strongly depen temperature; a nonzero value of extrapolated zero temperature conductivity sugge the concentration of the metallic phase is always more than the percolation thresho also observed that the metallic phase is metastable and has a tendency to go to the ins side. The mixed phase nature of the material makes any rigorous analysis of the el resistivity data quite difficult. However some similarities were observed between tl temperature behavior of this material and that of disordered metals.

Substitution of Ni in the lattice of $NdNiO_{3-\delta}$ by other transition metal element provide some more understanding about the system. In this chapter we have studie effect of Fe doping in $NdNiO_{3-\delta}$. Fe was chosen because it is the nearest neighbor of the periodic table. $NdFeO_3$ has the same crystallographic structure as $NdNiO_3$ and is kr to be an antiferromagnetic insulator[1].

6.2 Experimental

$NdNi_{1-x}Fe_xO_{3-\delta}$ samples were prepared by the sol-gel method described in previc chapters. High purity Nd_2O_3, $Ni(NO_3)_2.6H_2O$ and Fe were used as the starting materia The oxygen stoichiometry was determined by iodometric titration. The crystal structure and lattice parameters of all the samples were determined by x-ray diffraction. The

This chapter is mainly based on the published work of A. Tiwari, K. P. Rajeev, T. K. Nath and A. K. Nigam, Solid State Communications **110**, 109 (1999).

Chapter 6

Metal-insulator transition in $NdNi_{1-x}Fe_x O_{3-\delta}$

6.1 Introduction

In chapter 4 we found that $NdNiO_{3-\delta}$ shows quite unusual characteristics. It behaves as a metal at high temperature as well as at low temperature. At low temperature the system appears to be a mixture of two phases, one of which is metallic and the other is insulating. Relative concentration of these two phases is found to be strongly dependent on temperature; a nonzero value of extrapolated zero temperature conductivity suggests that the concentration of the metallic phase is always more than the percolation threshold. It is also observed that the metallic phase is metastable and has a tendency to go to the insulating side. The mixed phase nature of the material makes any rigorous analysis of the electrical resistivity data quite difficult. However some similarities were observed between the low temperature behavior of this material and that of disordered metals.

Substitution of Ni in the lattice of $NdNiO_{3-\delta}$ by other transition metal elements may provide some more understanding about the system. In this chapter we have studied the effect of Fe doping in $NdNiO_{3-\delta}$. Fe was chosen because it is the nearest neighbor of Ni in the periodic table. $NdFeO_3$ has the same crystallographic structure as $NdNiO_3$ and is known to be an antiferromagnetic insulator[1].

6.2 Experimental

$NdNi_{1-x}Fe_xO_{3-\delta}$ samples were prepared by the sol-gel method described in previous chapters. High purity Nd_2O_3, $Ni(NO_3)_2.6H_2O$ and Fe were used as the starting materials. The oxygen stoichiometry was determined by iodometric titration. The crystal structures and lattice parameters of all the samples were determined by x-ray diffraction. The

---

This chapter is mainly based on the published work of A. Tiwari, K. P. Rajeev, T. K. Nath and A. K. Nigam, Solid State Communications 110, 109 (1999).

electrical resistivity measurements were done by a low frequency ac technique. The absolute thermoelectric power measurements were performed in the temperature range of 5-300 K using a homemade thermopower apparatus. The tunneling measurements were carried out on tunnel junctions formed by pressing a small Pb (counter-electrode) ball against the sample. The magnetoresistance measurements were done by a standard four-probe dc method using a 45 kG superconducting magnet.

6.3 Results

The x-ray diffraction pattern of all the samples show single phase systems and the crystal structure is orthorhombic. Iodometric titrations showed that the sample with x=0.0 (i.e. $NdNiO_{3-\delta}$) is highly oxygen deficient with δ=0.08. As the value of x increases the oxygen deficiency (δ) decreases slightly, see table 6.1.

Table 6.1: Lattice parameters and oxygen contents for various $NdNi_{1-x}Fe_xO_{3-\delta}$ samples.

x	Lattice parameters			3-δ
	a (Å)	b (Å)	c (Å))	
0.0	5.423	5.431	7.556	2.92
0.1	5.436	5.452	7.540	2.93
0.2	5.441	5.473	7.546	2.94
0.3	5.449	5.482	7.554	2.95
0.4	5.452	5.492	7.563	2.95

The electrical resistivity data of $NdNi_{1-x}Fe_xO_{3-\delta}$ are shown in figure 6.1. For $NdNiO_{3-\delta}$ the temperature range of measurement was 1.2-300 K and for the samples with x=0.1, 0.2 and 0.3 the resistivity was measured between 2.5 K and 300 K. For x=0.4 the electrical resistivity of the sample was so high that it was not possible to measure it below 130 K using our equipment.

The resistivity of the undoped sample ($NdNiO_{3-\delta}$) has already been described in previous chapters. The most important feature of this data is that even at absolute zero of temperature, the resistivity approaches a nonzero value. When 10 % of Ni is replaced by Fe the material becomes more conducting and the thermal hysteresis in resistivity disappears completely. For 20 % doping of Fe, the material becomes highly resistive and shows negative temperature coefficient of resistivity (TCR) throughout the

entire temperature range. However, the extrapolated zero temperature conductivity is still nonzero. For higher doping of Fe the electrical resistivity blows up at low temperatures.

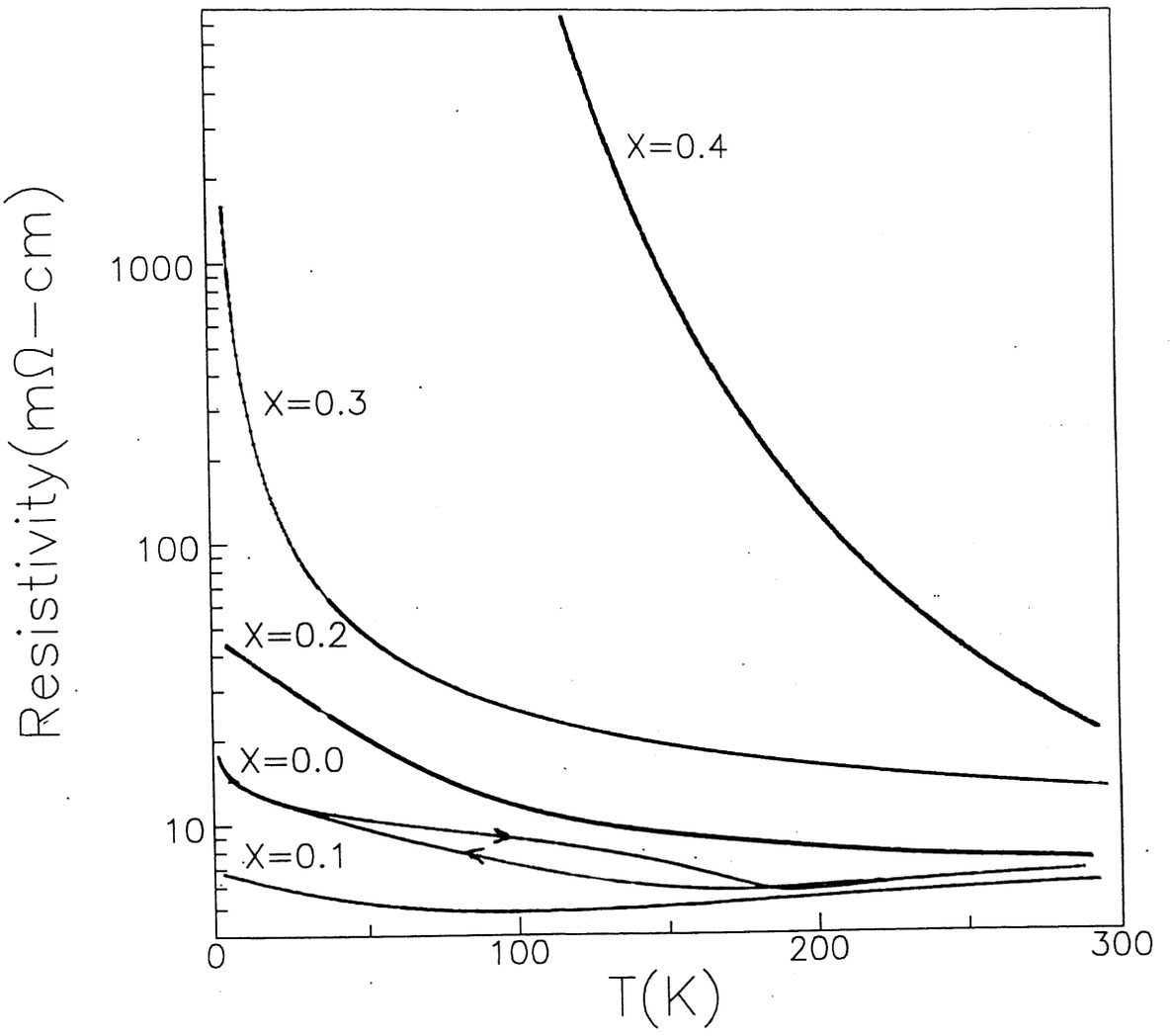

Figure 6.1: Electrical resistivity vs. temperature for $NdNi_{1-x}Fe_xNiO_{3-\delta}$.

The thermopower data of $NdNi_{1-x}Fe_xO_{3-\delta}$ samples are shown in figure 6.2. The thermopower of the undoped sample ($NdNiO_{3-\delta}$) is small, negative and shows a shoulder at around 180 K. Another interesting feature of this data is the large thermal hysteresis between 50 K and 200 K. When 10 % of Ni is replaced by Fe, the shoulder shifts to a much lower temperature (T= 50 K) and also the thermal hysteresis disappears. For x=0.2, the shoulder again shifts to a higher temperature. For x=0.3, the behavior remains more or less the same. For x=0.4, a complete change in the behavior of thermopower is observed; it blows up at lower temperature, a behavior characteristic of insulators with a bandgap[2].

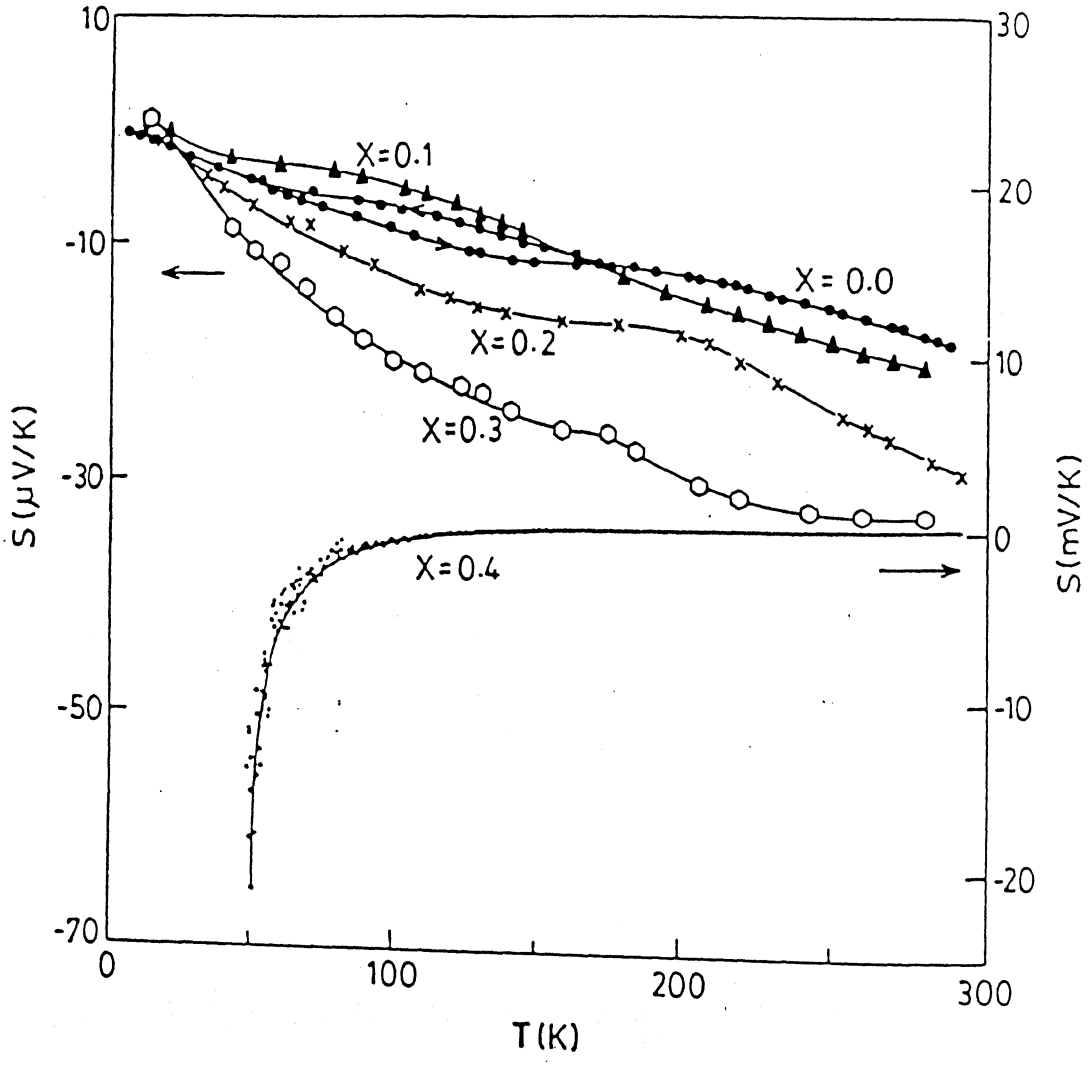

Figure 6.2: Thermopower vs. temperature for $NdNi_{1-x}Fe_xNiO_{3-\delta}$.

In figure 6.3 we have shown the differential tunneling conductance G(V) (=dI/dV) of all the samples at 1.2 K except x=0.4 which becomes highly resistive at 1.2 K.

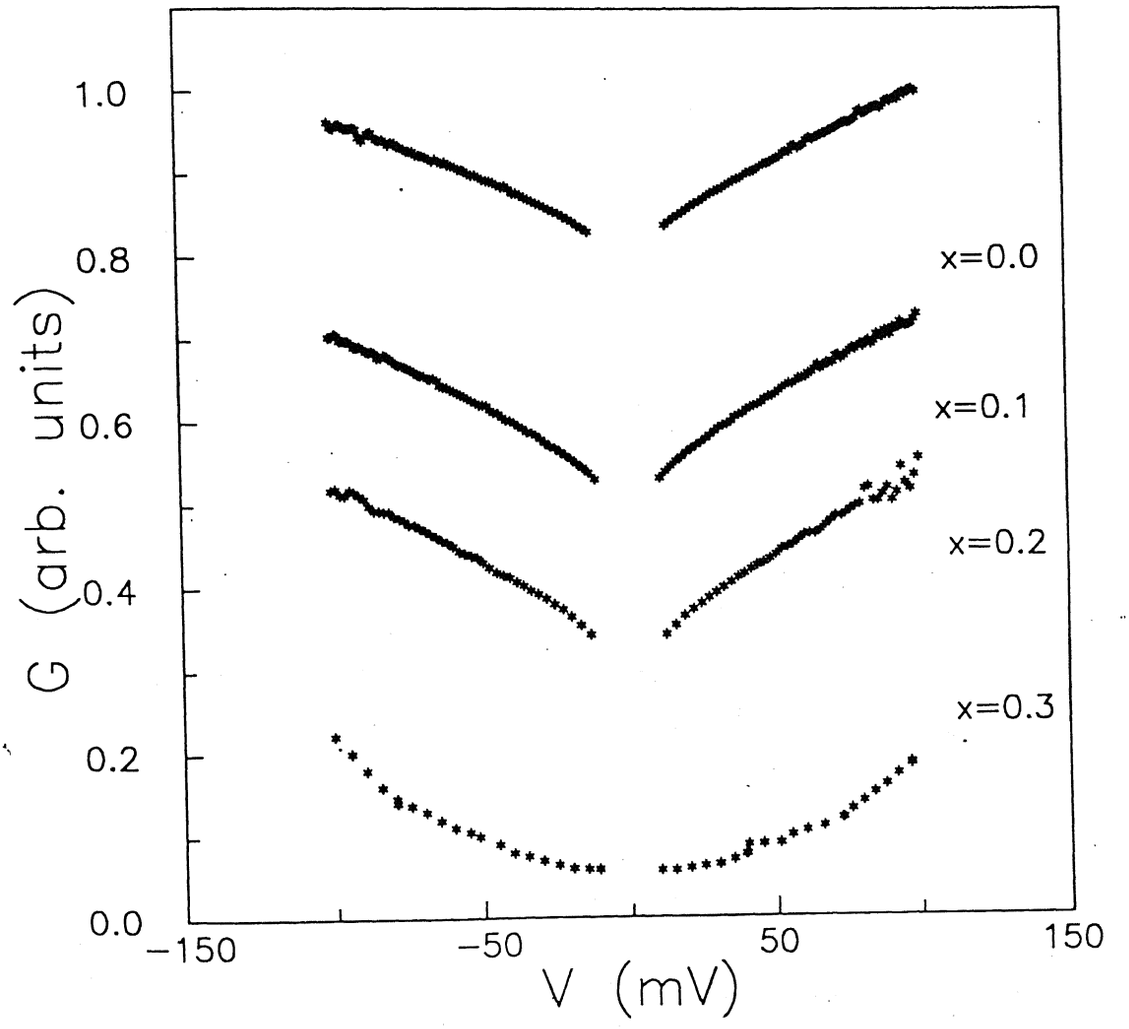

Fig. 6.3: Tunneling conductance vs. bias voltage for $NdNi_{1-x}Fe_xO_{3-\delta}$ at 1.2K. The data were normalized to unity at 100 mV and relatively shifted for clarity.

Magnetoresistance vs. applied field (B) curves for $NdNi_{1-x}Fe_xO_{3-\delta}$ samples at 4.2 K are shown in figure 6.4. The magnetoresistance of all these samples is negative and its magnitude increases with the field. The inset of this figure shows the variation of magnetoresistance with temperature at 40 kG. As the temperature increases the magnitude of the magnetoresistance decreases for all the samples.

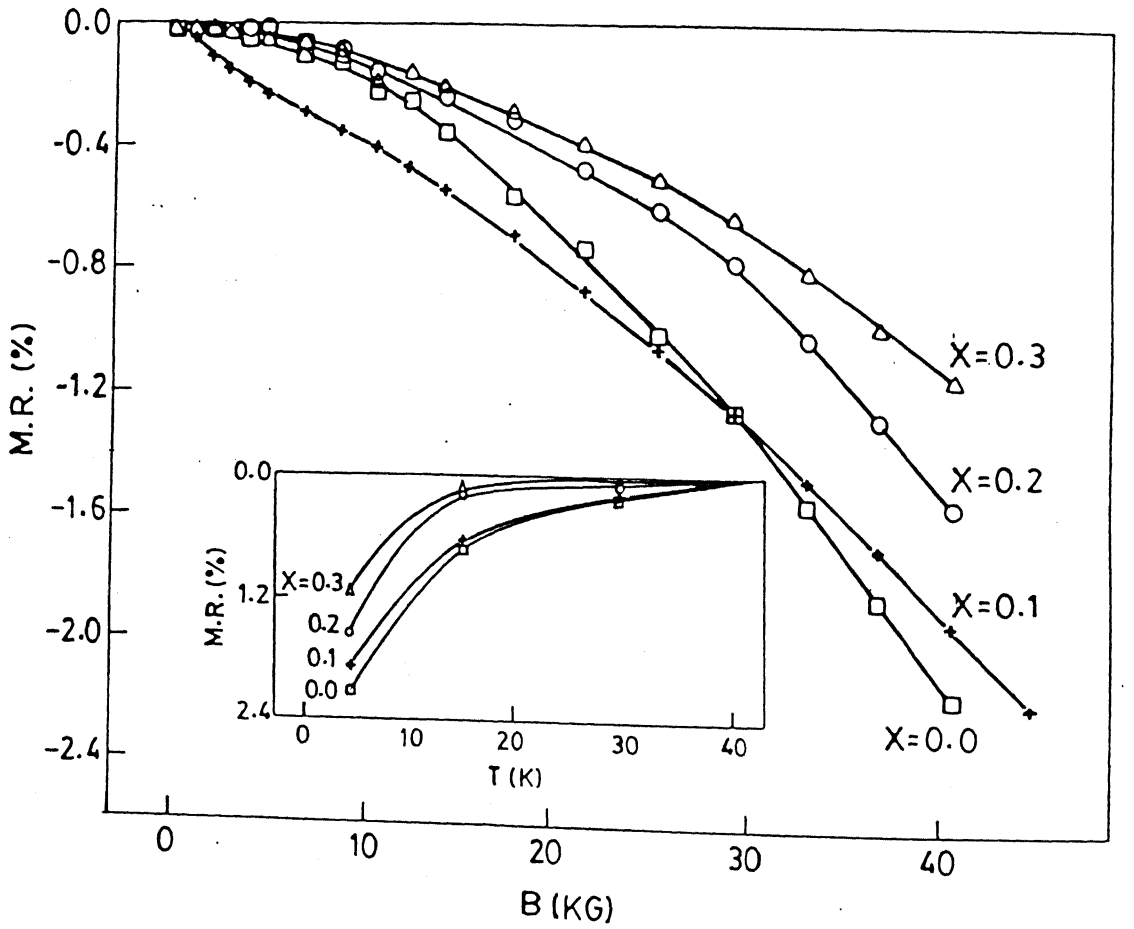

Fig. 6.4: Magnetoresistance [R(B)-R(0)]/R(0) vs B for $NdNi_{1-x}Fe_xO_{3-\delta}$ at 4.2K. The inset shows the variation of magnetoresistance with temperature at B=40 kG.

6.4 Discussion

6.4.1 Electrical resistivity

As in chapter 4 the low temperature electrical resistivity data of $NdNi_{1-x}Fe_xO_{3-\delta}$ (x=0.0-0.3) was fitted to eqs.(4.1)-(4.3) i.e. the expressions for the activated conduction, variable range hopping conduction and the conduction in disordered metals. The details of the fit are given in table 6.2.

Table 6.2: Parameters used in fitting the low temperature conductivity data of $NdNi_{1-x}Fe_xO_{3-\delta}$ to eqs.(4.1)-(4.3. Number of data points used for fitting, N≈200.

x	eq. (4.1) (activated conduc.)	eq. (4.2) (VRH conduc.)	eq.(4.3) (Disordered metal)	Temp. range
0.0	χ^2=11037 σ_∞=80(2) S/cm T_0=0.86(1) K	χ^2=10985 A=2546(30) S/cm T_0=301(5) K	χ^2=248 $\sigma(0)$=39.21(3) S/cm b=14.02(1) S/cm-K^m c=0.363(3) S/cm-K^n m =0.46(1); n =1.201(2)	1.2-16 K
0.1	χ^2=6426 σ_∞=165.7(6) S/cm T_0=0.48(3) K	χ^2=17589 A=4486(114) S/cm T_0=228(10) K	χ^2=315 $\sigma(0)$=144.84(8) S/cm b=1.088(3) S/cm-K^m c=0.0087(2) S/cm-K^n m =1.01(2); n =1.73(1)	2.5-20 K
0.2	χ^2=2700 σ_∞=29.5(2) S/cm T_0=1.42(5) K	χ^2=2684 A=1135(29) S/cm T_0=480(16) K	χ^2=286 $\sigma(0)$=21.05(2) S/cm b=0.263(3) S/cm-K^m c= 0.0016(4) S/cm-K^n m =1.173(6);n=1.336(9)	2.5-20 K
0.3	χ^2=16605 σ_∞=15.9(2) S/cm T_0=18.0(1) K	χ^2=284 A=68890(506) S/cm T_0=70282(238) K	χ^2=50108 $\sigma(0)$=-5.62(9) S/cm b=2.59(7) S/cm-K^m c= -0.106(1)×10^{-10} S/cm-K^n m =0.51(4); n =8.4(8)	2.5-20 K

Samples with $x \leq 0.2$ follow eq.(4.3) with $\sigma(0) > 0$ showing overall metallic behavior. The x=0.3 sample follows eq.(4.2) i.e. the VRH conduction. Owing to the nonavailability of low temperature data we could not perform a similar analysis for x=0.4; however the high temperature data ($130\ K \leq T \leq 300\ K$) fit best to eq.(4.1) i.e. the expression for activated conduction. So as a result of the above analysis we come to the conclusion that the samples with $x \leq 0.2$ are metallic, while those with higher values of x are insulating. The behavior of x=0.1 sample is quite contrary to what one would expect. In the frame of rigid band model, the substitution of Ni by Fe would reduce the carrier density and consequently should cause an increase in the resistivity of the system. From another point of view, following the ionic model of Torrance et.al.[3], substitution of Ni by Fe would open the charge transfer gap making the doped material more insulating. But contrary to both these predictions the resistivity of x=0.1 sample is less than that of the undoped sample. This suggests that the transport mechanism of the system is quite involved. For $x \leq 0.2$ samples the temperature dependence of electrical conductivity is quite similar to that of highly disordered metals. As mentioned before in disordered metallic systems the phenomena of e-e interactions and weak localization may be present[4,5]. In chapters 4 and 5 we got some indications of enhanced e-e interactions in $NdNiO_{3-\delta}$ via the low temperature electrical conductivity and electron tunneling conductance data. The anomalous behavior of the system with x=0.1 suggests that some kind of localization tendency may also be present in the system which gets suppressed due to the spin flip scattering of electrons from Fe^{3+} centers.

6.4.2 Thermopower

The thermopower of all the samples with $x \leq 0.2$ is small, negative and varies almost linearly with temperature, a characteristic of metallic samples. The sample with x=0.3 also displays a more or less linearly temperature dependent thermopower. This is in agreement with the conduction mechanism (VRH) ascribed to this material from the behavior of the resistivity[2]. For x=0.4 the thermopower is large and shows a divergent behavior at low temperatures, a characteristic of insulating samples with an activated conduction mechanism[2].

6.4.3 Tunneling Conductance

As mentioned before the tunneling conductance *G(V)* is a direct measure of the electronic density of states *N(E)* at energy $E=q_eV$ from the Fermi energy. For all the samples with x ≤ 0.2 an anomaly in the density of states, with a minimum at the Fermi energy, has been observed. Furthermore the tunneling conductance obeys the relation $G(V) = G(0)\left[1+\left(\frac{|V|}{\Delta}\right)^n\right]$ with n ≈ 0.6-0.8; this expression is quite similar to that predicted by Altshuler and Aronov[5] for correlated disordered metals except for the observed higher values of n*. A sublinear energy dependence (n < 1) of the tunneling conductance data puts these samples (x ≤ 0.2) into the category of highly disordered metals. For x = 0.3, the tunneling conductance is very small and has a parabolic energy dependence, indicative of the insulating nature of the material .

Table 6.3 : Parameters used in fitting the tunneling conductance data of $NdNi_{1-x}Fe_xO_{3-\delta}$ (x ≤ 0.2) to $G(V) = G_0[1+(|V|/\Delta)^n]$. Data in the range 10 mV < *V* < 100 mV were used for fitting. Number of data points used for fitting, N≈100.

x	G_0 (S)	Δ (meV)	n	χ^2
0.0	0.0451	681(9)	0.61(2)	176
0.1	0.0851	17.89	0.67(3)	211
0.2	0.0204	34.35	0.74(4)	165

* The value of n, predicted by Altshuler and Aronov[5], is 0.5. These predictions are based on a perturbative approach, valid in the weakly disordered metallic regime. In the case of highly disordered metals the perturbative analysis may not be valid. There is no theory which describes the e-e interactions in the entire regime (weakly disordered metal, highly disordered critical regime and insulating regime). However recent experimental results[6] have shown that as the disorder in the system increases the square root dip in the density of states near the Fermi energy deepens and changes to a linear form for highly disordered systems in the critical regime and becomes a quadratic gap just on the insulating site.

6.4.4 Magnetoresistance

The magnetoresistance of all the samples including $NdNiO_{3-\delta}$ is negative. This presumably suggests that the magnetic field counteracts the disorder driven localization tendency of the electrons. The partial suppression of the localization tendency by the spin flip scattering of electrons from Fe^{3+} centers may possibly be the cause of the unexpectedly lower electrical resistivity of the x=0.1 sample compared to that of the x=0.0 sample.

6.5 Conclusion

In this chapter we have found that all the $NdNi_{1-x}Fe_xO_{3-\delta}$ samples with $x \leq 0.2$ behave as disordered metals. However, the energy dependence of the density of states near the Fermi energy indicates that all these samples lie very close to the insulating side of an M-I transition. Enhanced e-e interaction and weak localization effects seem to play a significant role in determining the electronic properties of the system. Any further increase of Fe concentration pushes the system to the insulating side.

References:

[1] J. Blasco and J. García, J. Phys. Chem. Solid **55**, 843 (1994).

[2] N.F. Mott, Metal-Insulator Transitions (Taylor and Francis, London, 1974).

[3] J. B. Torrance, P. Lacorre, A. I. Nazzal, E. J. Ansaldo and Ch. Niedermayer, Phys. Rev. B **45**, 8209(1992).

[4] P. A. Lee and T. V. Ramakrishnan, Rev. Mod. Phys. **57**, 287 (1985).

[5] B. L. Altshuler and A. G. Aronov, in A. L. Efros and M. Pollak (Eds.), Electron-Electron Interactions in Disordered Systems (North Holland, Amsterdam, 1985).

[6] A. K. Raychaudhuri, K. P. Rajeev, H. Srikanth, R. Mahendiran, Physica B **197**, 124 (1994); A. K. Raychaudhuri, Phys. Rev. B, **44**, 8572 (1991).

Chapter 7

Manganates

Recently giant magnetoresistance (GMR) in various perovskite manganates $La_{1-x}A_xMnO_3$ (A: Ca, Sr, Ba), has gained a lot of scientific attention[1-3]. The typical composition where this effect is most prominent is x=0.3. This compound shows a ferromagnetic-paramagnetic transition at T_c and a resistivity peak at T_p, $T_c \approx T_p$. Conventionally, the electrical and magnetic properties of these manganates are explained by the "double exchange" model (DEM)[4] in which the Hund's coupling is considered to be the most important factor. But recently it has been found[5] that, although the DE model explains the behavior of the system qualitatively, it fails to give a quantitative account of the phenomenon (see sections 1.6-1.7 of chapter 1 for more details).

Another peculiar feature of these oxides, not yet addressed widely, is the behavior of electrical resistivity in the metallic state. Even at T well below T_c, the values of ρ are larger than or comparable to the estimated Mott's maximum resistivity for the system. Assuming that all holes introduced by the dopant (A) are mobile carriers, with the dopant concentration x=0.3 and molar volume $V \approx 36$ cm^3, these materials have the charge carrier density of $\approx 0.5\times10^{22}$ carriers/cm^3 which is comparable to that of metals. For typical metallic carrier densities the low conductivity implies a low diffusivity for the carriers. Under such conditions the onset of strong electronic interactions is expected. In an interesting work Lofland *et al.*[6] studied the electrical resistivity of $La_{2/3}Ba_{1/3}MnO_3$ thin films and found it to follow the relation $\rho(T) = A_0 - B_0T + C_0T^2$ for T < 100 K. A negative contribution to low temperature electrical resistivity is quite interesting and similar to that observed in several disordered metallic systems. However, in that report, because of the lack of the precision of data, authors could not do a detailed quantitative analysis and left it for future studies.

This chapter is mainly based on following papers: (i) A. Tiwari and K. P. Rajeev, Solid State Communications **111**, 33 (1999) {in press} (ii)A.Tiwari and K. P. Rajeev, Phys. Rev. B (accepted for publication) and (iii) A. Tiwari and K.P.Rajeev, Journal of Applied Physics (accepted for publication).

Here in the first half of this chapter we have done a careful study of the low temperature electrical resistivity and electron tunneling conductance of $La_{0.7}A_{0.3}MnO_3$ .The second half of this chapter presents a study of the effect of partial replacement of Mn by Fe in $La_{0.7}Sr_{0.3}MnO_3$.

A. Low temperature electrical transport in $La_{0.7}A_{0.3}MnO_3$ (A: Ca, Sr, Ba)

7A.1 Experimental

Samples were prepared by the conventional solid state method. Appropriate amounts of La_2O_3, $CaCO_3$, $SrCO_3$, $BaCO_3$ and MnO_2 were heated at 1250 K for 24 hours. The reacted powder, obtained after heating, was pelletized and heated to 1250 K for 48 hours. The resulting pellet was ground, repelletized and heated at 1300 K for 24 hours in flowing oxygen. The phase purity was checked by x-ray diffraction using a Rich-Seifert x-ray diffractometer. The T_c values were determined by using a Faraday balance and by an ac pickup coil method. A four probe ac (1kHz) technique was employed to measure the electrical resistivity of the samples in the temperature range 2.5-370 K. The tunneling measurements were carried out on tunnel junctions made with a Pb counter-electrode.

7A.2 Results and discussion

The x-ray diffraction pattern of the samples show single phase systems. All the samples crystallize in cubic phase. They show ferromagnetic to paramagnetic transition closely accompanied by a metal-insulator transition. Values of T_c are given in table 7.1.

7A.2.1 Electrical resistivity

Figure 7.1 shows the electrical resistivity of various samples between 2.5 K and 370 K. At the metal-insulator transition temperature T_p ($\approx T_c$) these samples show a peak in the electrical resistivity. Below T_p the samples are metallic. The resistivity of the metallic phase has a close relation with the magnetic properties of the system. As the resistivity of the system increases the ferromagnetic-paramagnetic transition temperature T_c goes down. The

inset of figure 7.1 shows the low temperature (T < 50 K) electrical resistivity of these samples on an enlarged scale. For all the samples a slight upturn in electrical resistivity below ≈ 30 K is observed.

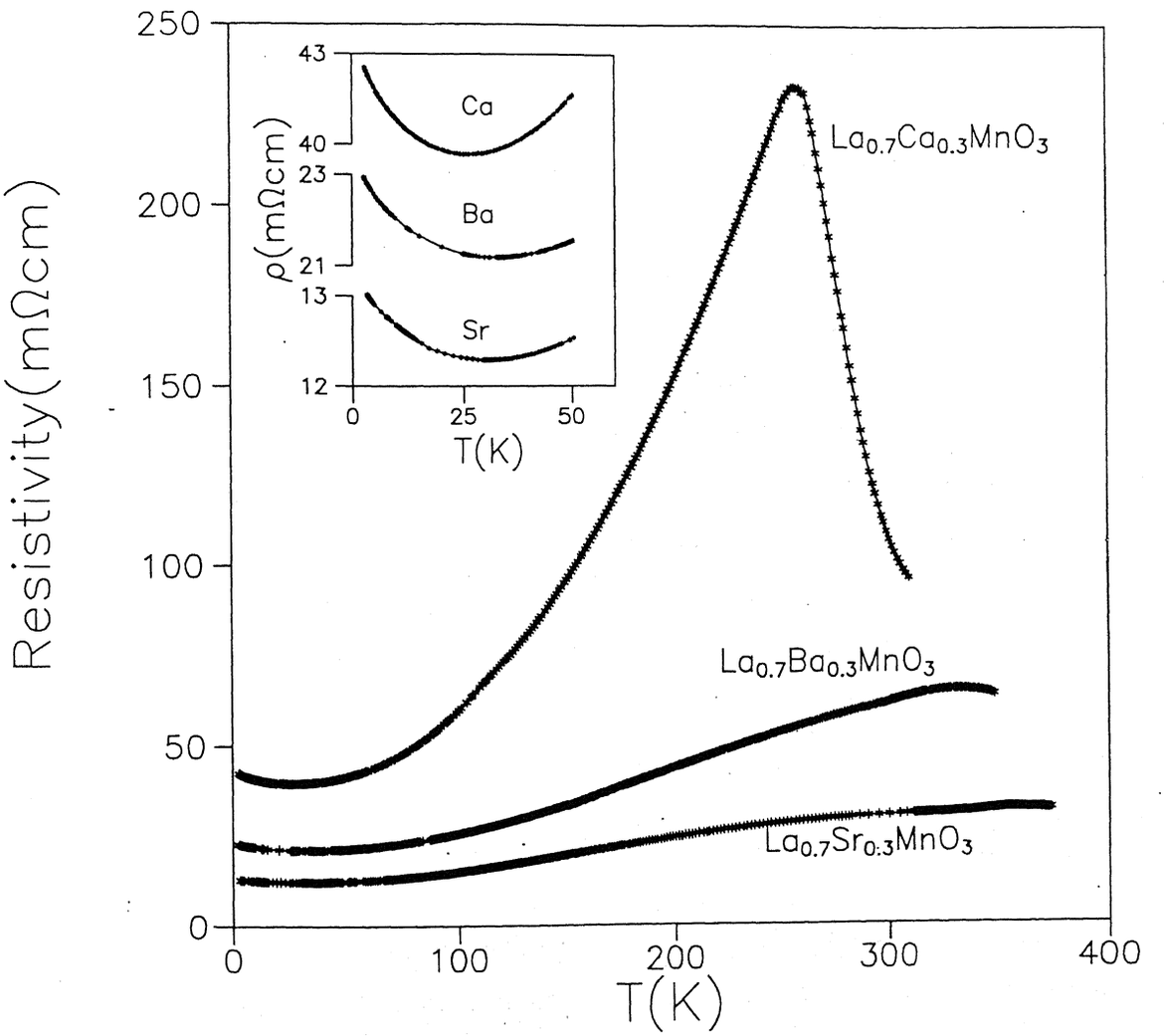

Figure 7.1 : Temperature dependence of the electrical resistivity of $La_{0.7}A_{0.3}MnO_3$ (A: Ca, Sr, Ba). The inset shows the electrical resistivity of the samples below 50 K on an expanded scale.

Table 7.1 : Parameters used in fitting the conductivity data of $La_{0.7}A_{0.3}MnO_3$ (A: Ca, Sr, Ba) to eq.(7.1) between 2.5 K and 15 K and to eq.(7.2) between 2.5 K and 100 K. Number of data points (N) used for fitting were ~300 in the first range and ~ 1000 in the second range.

A	T_c(K)	$\sigma(T) = \sigma_0 + m_\sigma\sqrt{T}$			$\sigma(T) = \sigma_0 + m_\sigma\sqrt{T} - aT^p$				
		σ_0 (S/cm)	m_σ (S/cm-K$^{1/2}$)	χ^2	σ_0 (S/cm)	m_σ (S/cm-K$^{1/2}$)	a (S/cm-K^p)	p	χ^2
Sr	360	74.102(3)	1.540(1)	451	72.912(5)	2.076(9)	0.0065(3)	1.815(9)	1473
Ba	333	41.749(8)	1.168(6)	335	40.651(9)	1.734(4)	0.0143(4)	1.564(8)	1130
Ca	258	22.458(9)	0.648(7)	440	21..76(1)	0.988(9)	0.0069(6)	1.670(8)	1375

As discussed before several times in this thesis, in metallic systems a low temperature resistivity minimum may arise from (1) Kondo effect (2) Weak localization[7,8] (3) enhanced e-e interactions[7,8]. Since all the samples under consideration are ferromagnetic the possibility of Kondo effect is ruled out. Weak localization and e-e interaction effects are seen in disordered metallic systems. Weak localization effect arises due to the interference of partial electron waves. In ferromagnetic metals the strong spontaneous magnetic field destroys the phase coherence of electron waves and hence weak localization will be weak indeed; the possibility of weak localization determining the temperature dependence of resistivity in the present system is hence ruled out. Because of enhanced electron-electron interactions, the electrical conductivity of the metals, at low temperature, goes as [7,8]

$$\sigma(T) = \sigma(0) + m_\sigma\sqrt{T} \qquad (7.1)$$

where m_σ is a constant given by eq.(1.4) of chapter 1.

To check the possibility of e-e interactions we fitted the low temperature (T < 15 K) conductivity data to eq.(7.1). For all the samples, data fit reasonably well to this equation. Details of the fitting parameters along with the values of χ^2 are given in table 7.1. Values of χ^2 close to N indicate the excellent quality of fits.

Now that the low temperature resistivity data have been found to fit very well to the expression of resistivity of a disordered metal with strong e-e interactions, we should

examine whether the fit parameters make sense. The m_σ is related to D by eq.(1.4). This equation involves $\tilde{F}_\sigma$; we do not have any means of exact determination of this number but a gross estimate can be made under the Thomas-Fermi approximation[9,10]. Under this approximation the value of $\tilde{F}_\sigma$ comes out to be $\tilde{F}_\sigma \approx 0.808$[10]. Using this value of $\tilde{F}_\sigma$ in eq.(1.4) the values of D for these samples are found to fall in the range (2.5-14.5×10^{-2} cm^2/s). If we compare these values with the corresponding value for Cu (≈ 2.2× 10^2 cm^2/s) we find that our samples have about 3-4 orders of magnitude less diffusivity than pure metals like copper. Also these values of D are very much similar to those found for highly correlated metals like[11] $YBa_2Cu_3O_{7-\delta}$ (D≈4.4 × 10^{-1} cm^2/s) and [12] $LaNiO_3$ (D ≈ 10^{-2} cm^2/s). Using the values of σ_0 and D in the Einstein formula[7,8] $\sigma_0 = e^2 N(E_F) D$, the values of $N(E_F)$ are found to lie in the range (0.03-0.67×10^{24} $eV^{-1}mole^{-1}$). These values are in fairly good agreement with the reported[13] values of $N(E_F) \approx 1\times10^{24}$ $eV^{-1}mole^{-1}$, keeping in mind the various approximations involved in the process.

In the above analysis of resistivity data we have ignored the contributions coming from the inelastic scattering of electrons. At higher temperatures in addition to e-e interactions, the usual inelastic contributions also become significant. The contribution due to the inelastic scatterting of electrons can be taken into account by adding a term $-aT^p$ in the electrical conductivity expression. So the expresion for the electrical conductivity can be written as:

$$\sigma(T) = \sigma_0 + m_\sigma \sqrt{T} - aT^p \qquad (7.2)$$

Resistivity data of all the samples in the temperature range 2.5 K < T < 100 K fit very well to the above equation. Details of the fit are given in table 7.1. Here we have restricted the upper temperature limit of analysis to 100 K (well below T_c) because near T_c polaronic effects become significant. It can be seen from this table that there is no substantial difference in the values of σ_0 and m_σ obtained by fitting the data to eq.(7.1) and eq.(7.2). So the values of various physical quantities obtained by using the fit parameters to these equations will be almost same and hence most of our conclusions remain unaffected..

To summarize, the electrical resistivity of the system shows the clear signature of strong e-e interactions. As a matter of fact a similar kind of low temperature upturn in

electrical resistivity has been observed previously by some other groups also[6,14], but those authors have not done any analysis to find the cause of this upturn. Lofland *et al.*[6] made some initial efforts to understand the cause of this upturn but due to the lack of precision in their data they could not make much progress and left this work for future studies.

7A.2.2 Electron tunneling conductance

Electron-electron interactions are known to cause significant corrections to the density of states. It has been shown previously[7,8] that e-e interactions cause a cusp in the density of states near the Fermi energy. If e-e interactions are really affecting the electrical resistivity of $La_{0.7}A_{0.3}MnO_3$ then they should affect the density of states also. So we felt that an investigation of the density of states near the Fermi energy would be quite informative in understanding the strongly interacting nature of charge carriers.

Tunneling conductance $G(V)=dI/dV$ of a metal-insulator-metal tunnel junction is a direct measure of the single particle density of states of the metal [15] at energy $E=q_eV$ from the Fermi energy i.e. $G(V) \propto N(E+E_F)$. To investigate the density of states of $La_{0.7}A_{0.3}MnO_3$ near the Fermi energy we performed electron tunneling experiments on $La_{0.7}A_{0.3}MnO_3$-Insulator-Pb(superconductor) tunnel junctions. Figure 7.2 shows the tunneling conductance data for these samples in the range 10 mV < |V| < 100 mV. We have normalized the data to unity at 100 mV and have shifted them vertically for clarity. In all the three cases a well defined superconductivity gap is observed. Inset of figure 7.2 shows the tunneling data of $La_{0.7}Sr_{0.3}MnO_3$ in the range |V| < 10mV; the superconductivity gap is clearly seen. Tunneling conductance data of all the samples show a dip at low bias voltages, indicating a reduction in the density of states at the Fermi energy.

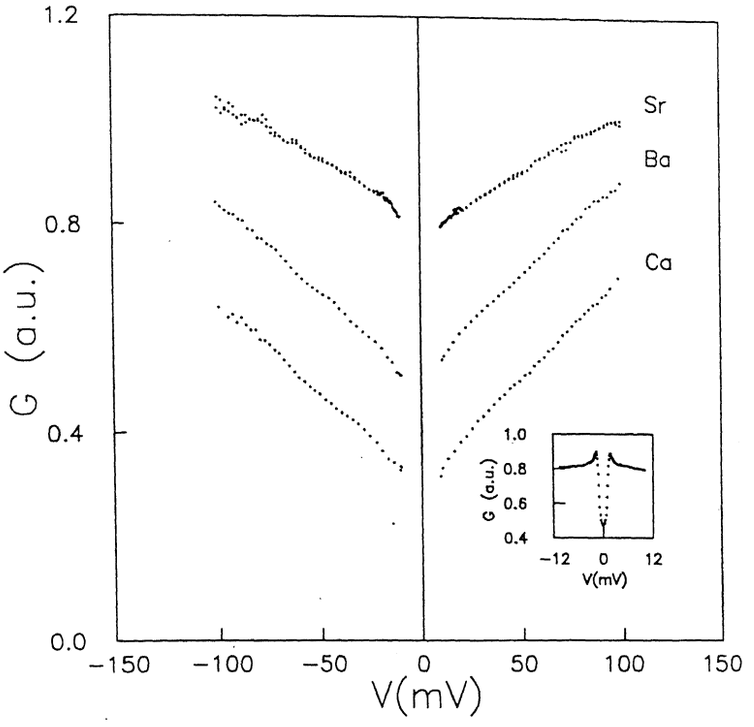

Figure 7.2: Tunneling conductance vs. bias voltage for $La_{0.7}A_{0.3}MnO_3$ (A: Ca, Sr, Ba) at 1.2 K. The data have been normalized to unity at 100mV and shifted vertically for clarity. Information about the absolute values is given in table 7.2. The inset shows the superconductivity gap of Pb as seen in the low bias (|V| < 10 mV) tunneling conductance data of $La_{0.7}Sr_{0.3}MnO_3$.

Table 7.2: Parameters used in fitting the tunneling conductance data of $La_{0.7}A_{0.3}MnO_3$ (A: Ca, Sr, Ba) at 1.2 K to $G(V) = G_0\left[1+\left(\frac{|V|}{\Delta}\right)^n\right]$. Data in the range 10 mV < V < 100 mV were used for fitting. Number of data points used for fitting, N ≈ 100.

A	G_0(S)	Δ(meV)	n	χ^2
Sr	0.0224(2)	401(17)	0.80(4)	193
Ba	0.0131(4)	162(4)	0.86(5)	175
Ca	0.0033(1)	151(3)	0.93(4)	156

The tunneling conductance data of all the samples is found to follow the relation $G(V) = G_0\left[1+\left(\frac{|V|}{\Delta}\right)^n\right]$ with $n \approx 0.8$-0.9 (see Table 7.2). This relation is quite similar to that predicted by Altshuler and Aronov[8] for correlated disordered metals except for the observed higher values of n. The value of n predicted by them, is 0.5. These predictions are based on a perturbative approach, valid in the weakly disordered metallic regime. In the case of highly disordered metals the perturbative analysis may not be valid. There is no theory[16] which describes the e-e interactions in the entire regime (weakly disordered metal, highly disordered critical regime and insulating regime). However recent experimental results[17] have shown that as the disorder in the metallic system increases the square root dip in the density of states near the Fermi energy deepens and changes to a linear form for highly disordered systems in the critical regime and becomes a quadratic gap just on the insulating side. Therefore the values of n close to unity puts these manganates into the class of highly disordered metals[26].

B. Metal-Insulator transition in $La_{0.7}Sr_{0.3}Mn_{1-x}Fe_xO_3$

7B.1 Introduction

In past a lot of work have been done to understand the nature of GMR materials. Most of these studies were done by replacing La by other rare earth elements. There are very few studies where doping is done on the Mn site[18-20]. We feel that the partial replacement of Mn, which plays a key role in the conduction process, by other transition metals may give important information about the nature of this system. For this purpose we doped Fe in $La_{0.7}Sr_{0.3}MnO_3$ and performed precise measurements of electrical resistivity and electron tunneling conductance measurements. Fe was chosen as the dopant because Mn^{3+} and Fe^{3+} have identical ionic sizes[20,21] and hence the crystal structure of the material remains unaltered .

7B.2 Results and discussion

Electrical resistivity data of $La_{0.7}Sr_{0.3}Mn_{1-x}Fe_xO_3$ samples with $0.0 \leq x \leq 0.25$ are shown in figure 7.3. The data of the undoped sample (x=0) has already been discussed in the first part of this chapter. For this sample ρ first increases with decrease in temperature, exhibits a peak at $T=T_p$ ($\approx T_c$) and then decreases as T is further reduced below T_p. As the Fe is doped into the system the resistivity increases and T_P falls (see table 7.2). For $x \leq 0.2$ all the samples show a peak in ρ, characteristic of an M-I transition, and samples are metallic at lower temperatures. For x=0.25, material shows insulating behavior throughout the whole temperature range.

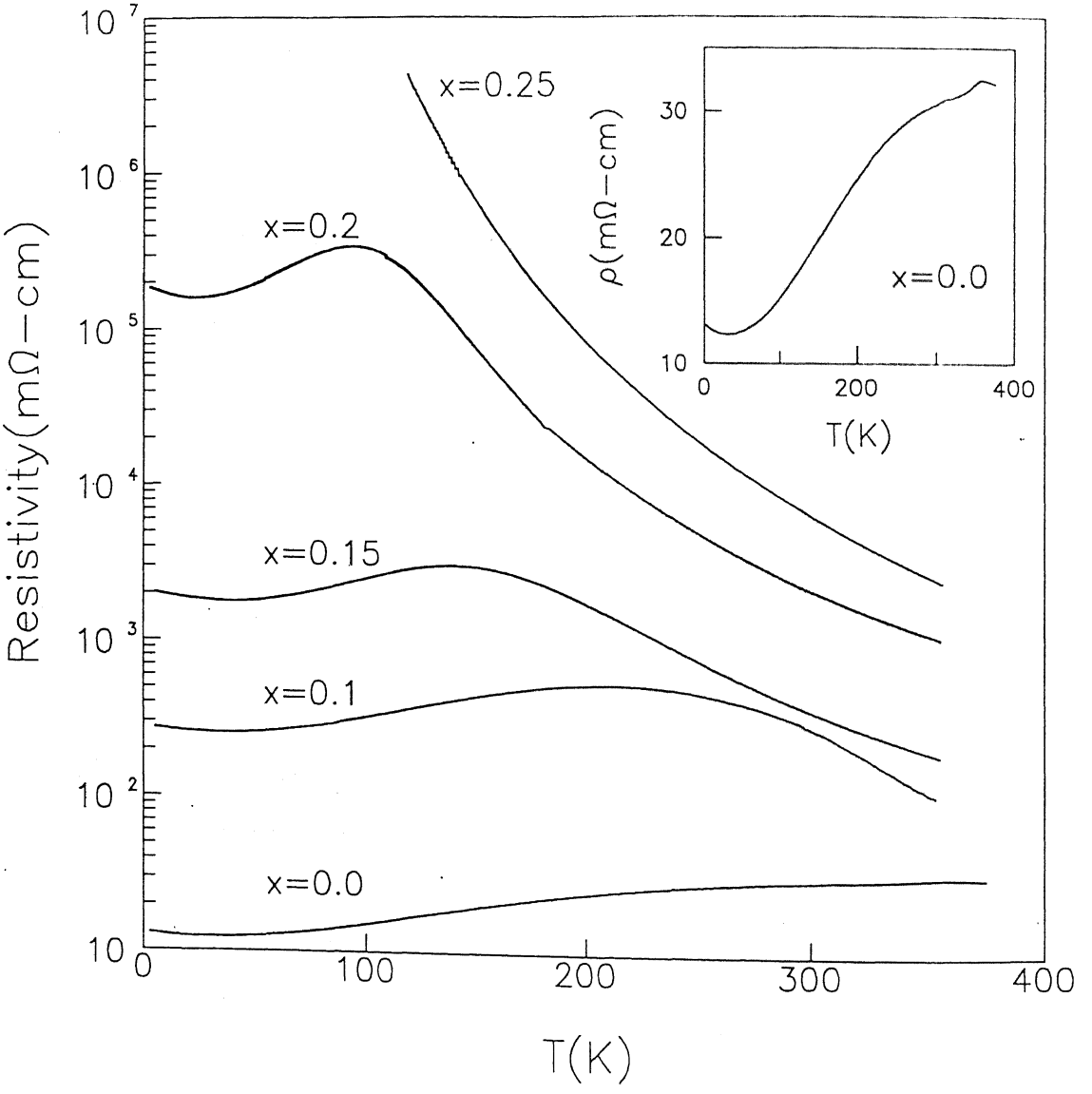

Figure 7.3: Electrical resistivity of $La_{0.7}Sr_{0.3}Mn_{1-x}Fe_xO_3$ ($x \leq 0.25$). Inset shows the electrical resistivity of x=0.0 sample in an enlarged scale.

The behavior of the system can be explained by considering the electronic band structure of the material. The configuration of d-electrons in transition metal oxides is determined by the internal crystal fields. In an octahedral field, the d-levels split into $t_{2g}\uparrow$, $e_g\uparrow$, $t_{2g}\downarrow$, and $e_g\downarrow$ as shown in figure 7.4(a). In solids these energy levels form bands. The electronic configuration for Mn^{3+} is $t^3_{2g\uparrow}e^1_{g\uparrow}$ and for Mn^{4+} it is $t^3_{2g\uparrow}$. In $La_{0.7}Sr_{0.3}MnO_3$, Mn exists both as Mn^{3+} as well as Mn^{4+}. So $t_{2g}\uparrow$ band is full and $e_g\uparrow$ band is less than half filled. The schematic band structure of $La_{0.7}Sr_{0.3}MnO_3$ can be represented as in figure 7.4(b). The $e_g\uparrow$ band of Mn is electronically active, where electron hopping occurs between Mn^{3+} and Mn^{4+}. Separation between $t_{2g}\uparrow$ and $e_g\uparrow$ has been estimated[22]to be ≈1.5 eV. The Fermi level lies ≈3.0 eV above the top of the 2p oxygen band[22].

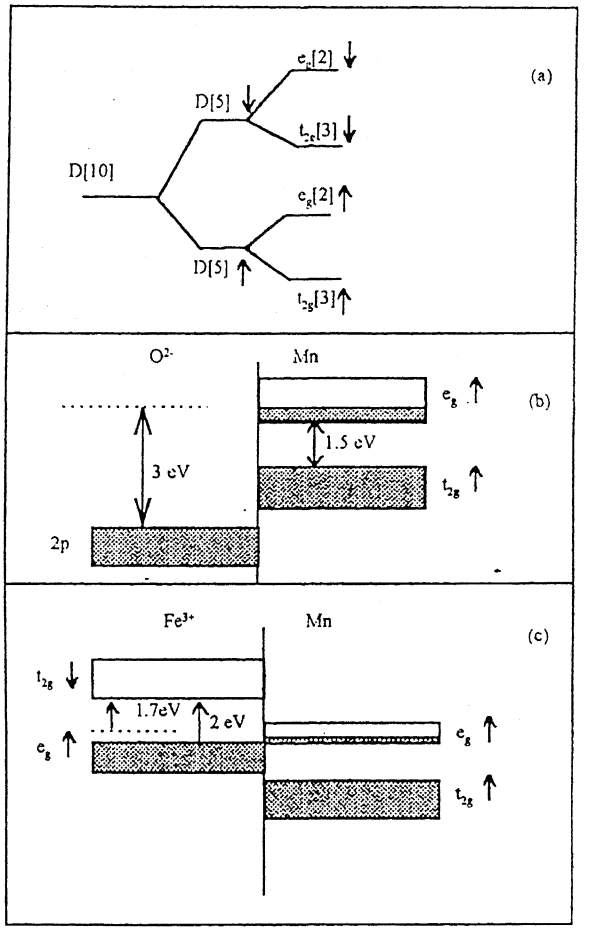

Figure 7.4 : (a) Octahedral field splitting of d levels (b) schematic band structure of $La_{0.7}Sr_{0.3}MnO_3$ (c) band structure of Fe and Mn in $La_{0.7}Sr_{0.3}Mn_{1-x}Fe_xO_3$.

Jonker *et al.*[18] have studied the electrical conductivity of an Fe doped manganate, $La_{0.85}Ba_{0.15}Mn_{1-x}Fe_xO_3$ and showed that for $0 < x < 0.85$ the system has Fe^{3+}, Mn^{3+} and Mn^{4+} ions and for $0.85 < x < 1.00$ the system has Fe^{3+}, Fe^{4+} and Mn^{4+} ions. The electronic configuration for Fe^{3+} is $t^3_{2g\uparrow}e^2_{g\uparrow}$ and for Fe^{4+} it is $t^3_{2g\uparrow}e^1_{g\uparrow}$. Simultaneous existence of Fe^{3+}, Mn^{3+} and Mn^{4+} indicate that Fe $e_{g\uparrow}$ band is full and Mn $e_{g\uparrow}$ band is less than half filled. While the existence of Fe^{3+}, Fe^{4+} and Mn^{4+} implies a more than half filled Fe $e_{g\uparrow}$ band and an empty Mn $e_{g\uparrow}$ band. The Fe $e_{g\uparrow}$ band remains fully filled only if the Mn $e_{g\uparrow}$ band has charge carriers. This implies that the Mn $e_{g\uparrow}$ band should be at the same level as, or higher than the, top of the Fe $e_{g\uparrow}$ band. Recently Ahn *et al.*[19], using the results of Banks and Tashima[20], found that there is a slight overlap (less than 3 %) between the $e_{g\uparrow}$ bands of Fe and Mn in $La_{1-x}Ca_xMn_{1-y}Fe_yO_3$ (x=0.37 and 0.53, $y < 0.20$).

The nominal stoichiometry of our samples is $La^{3+}_{0.7}Sr^{2+}_{0.3}Mn^{4+}_{0.3}Mn^{3+}_{0.7-x}Fe^{3+}_xO_3$. The $t_{2g\uparrow}$ band of Fe and Mn and $e_{g\uparrow}$ band of Fe are totally filled. There are (0.7-x) electrons in Mn $e_{g\uparrow}$ band which has a capacity of two electrons, hence (0.7-x)/2 part of the Mn $e_{g\uparrow}$ is also filled. The width of Mn $e_{g\uparrow}$ is about 1eV. So (assuming uniform filling of band) the highest filled state in Mn $e_{g\uparrow}$ (Fermi level) will be at $\approx$ [(0.7-x)/2]eV above the top of the Fe $e_{g\uparrow}$ band. In our system x lies between 0 and 0.25, so the Fermi level will be about $\approx$ 0.3 eV above the top of the Fe $e_{g\uparrow}$ band. In an earlier report[23] it has been shown that in $LaFeO_3$, Fe $t_{2g\downarrow}$ band lies about 2 eV above the top of the Fe $e_{g\uparrow}$ band. Assuming same situation in our case, the Fe $t_{2g\downarrow}$ band will lie $\approx$ 1.7 eV above the Fermi level(see figure 7.4(c)). It is clear from this energy diagram that there are no states on Fe^{3+} which can participate in electron hopping from Mn. So the doping of Fe results in a depletion in the number of hopping electrons and available hopping sites and hence weakens the double exchange interaction.

Although above simple band structure considerations give a qualitative account of the electrical conduction in the system, there are some issues which need further consideration. It is to be noted that although for low Fe dopings ($x \leq 0.2$) the material is metallic (as far as the temperature coefficient of resistivity, TCR, is concerned) the magnitude of resistivity (ρ) is very high. These ρ values are larger than the Mott's maximum metallic resistivity for the system, which is of the order of 1-10 mΩ-cm. If we assume that each Mn^{4+} ion provides one hole, then with a molar volume V $\approx$ 36 cm^3, charge carrier density is 10^{22} /cm^3. For this

typical metallic carrier density a low conductivity value implies a low diffusivity for the carriers. Under such conditions charge carriers are expected to be strongly correlated. Furthermore, the electrical resistivity of these samples show an upturn at low temperatures, a characteristic of disordered metallic systems with strong electronic interactions. In strongly interacting systems the density of states at the Fermi level gets modified. So we feel that an investigation of the density of states near the Fermi level will be quite informative in understanding the nature of this system.

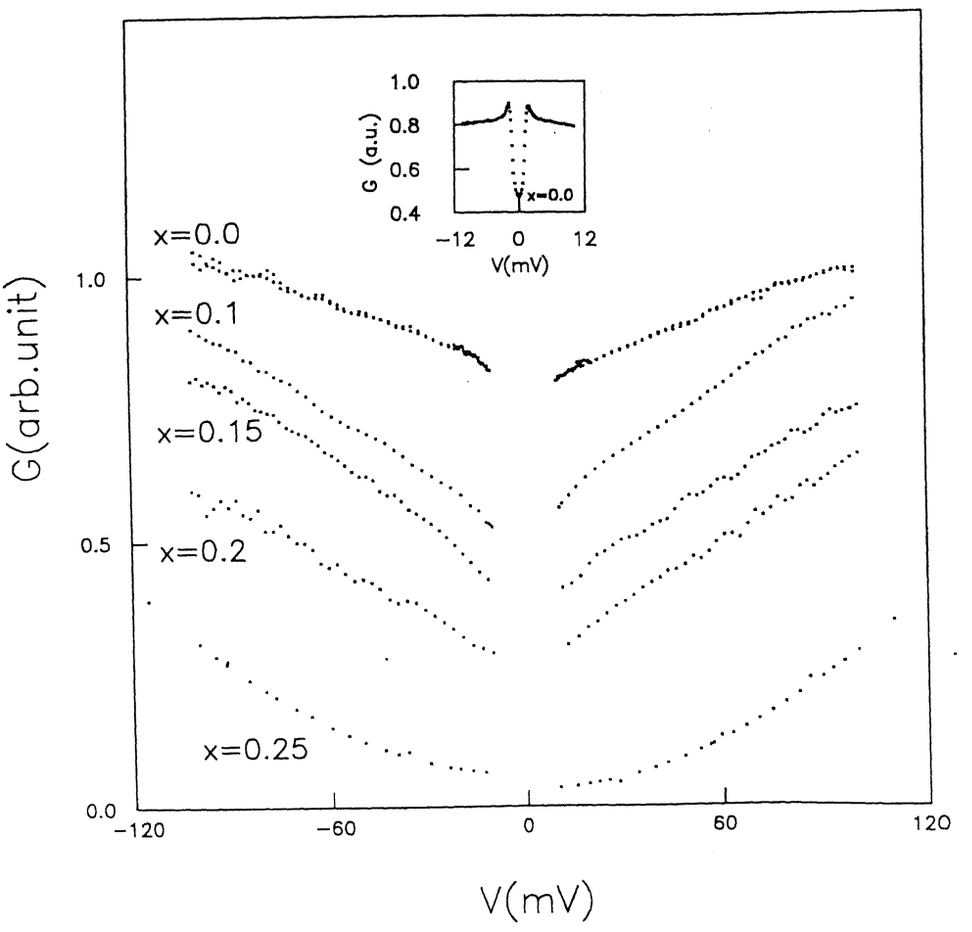

Figure 7.5: Tunneling conductance G(V) vs. bias voltage for $La_{0.7}Sr_{0.3}Mn_{1-x}Fe_xO_3$ ($x \leq 0.25$) at 1.2K. The data have been normalized to unity at 100 mV and shifted vertically for clarity. Information about the absolute values are given in table 7.3. Inset shows the superconductivity gap of Pb as seen in the low bias ($|V| < 10mV$) tunneling conductance data of $La_{0.7}Sr_{0.3}MnO_3$.

Table 7.3 : T_P and the fit parameters for the tunneling conductance data of $La_{0.7}Sr_{0.3}Mn_{1-x}Fe_xO_3$ ($x \leq 0.20$) at 1.2 K to $G(V) = G_0[1 + (|V| - \Delta)^n]$. Data in the range 10 mV < V < 100 mV were used for fitting. Number of data points used for fitting, N ≈ 100.

x	T_P (K)	G_0 (S)	Δ (meV)	n	χ^2
0.00	365	0.0224(2)	401(17)	0.80(4)	194
0.10	210	0.0161(4)	127(3)	0.85(3)	279
0.15	140	0.0133(1)	161(4)	0.85(4)	507
0.20	95	0.0045(1)	152(3)	0.94(4)	346

To investigate the density of states of $La_{0.7}Sr_{0.3}Mn_{1-x}Fe_xO_3$ near the Fermi energy we have performed electron tunneling experiments on $La_{0.7}Sr_{0.3}Mn_{1-x}Fe_xO_3$-Insulator-Pb(superconductor) tunnel junctions. Figure 7.5 shows the G(V) vs. V for all the samples in the range 10 mV < |V| < 100 mV. We have normalized the tunneling conductance data of all the samples to unity at 100mV and vertically shifted them for clarity. In all the cases a well defined superconductivity gap is observed. Inset of figure 7.5 shows the typical tunneling data of $La_{0.7}Sr_{0.3}MnO_3$ in the range |V| < 10 mV, a superconductivity gap can easily be recognized.

All the metallic samples ($x \leq 0.2$) show a dip in the density of states near the Fermi energy. As the value of x increases the dip deepens. The tunneling conductance data of $x \leq 0.2$ samples follow the relation $G(V) = G_0\left[1+\left(\frac{|V|}{\Delta}\right)^n\right]$ with n ≈ 0.80-0.94 (see table 7.3). The values of n close to unity puts these manganates ($x \leq 0.2$) into the class of highly disordered metals. Furthermore as the value of x increases the value of n also increases implying the increasing disorder in the system. Finally for x=0.25 a gap opens up at the Fermi level and tunneling data follows a parabolic dependence, a characteristic of insulating samples. It is to be noted that in x=0.25 sample Mn exists both as Mn^{3+} as well as Mn^{4+} so even in this sample sufficient number of hopping electrons as well as hopping sites are available. We believe that the observed metal-insulator transition in the system is the consequence of the disorder driven localization of charge carriers (i.e. Mott-Anderson transition).

The source of disorder

The disorder in the system is expected to arise mainly because of the random potential fluctuations seen by the conduction electrons due to different electronegativities of La^{3+} and A^{2+}[13]. Also recent pulsed neutron diffraction experiments[24] have shown that the local atomic structure of $La_{1-y}Sr_yMnO_3$ is significantly different from the long range structure. Although the overall crystal structure suggests that JT distortion is absent for $y > 0.16$, the pair distribution function analysis of neutron diffraction data shows that locally JT distortions are always present[25]. Doped charge carriers introduce local anti-JT distortions and disrupt the long range JT distortion. In the paramagnetic phase ($T>T_c$), the anti-JT distortions localize the conduction band electrons as polarons. At low temperatures ($T < T_c$) the charge carriers are delocalized, but local lattice distortions are still present. These local lattice distortions may also contribute to the strongly disordered nature of the low temperature metallic phase. Any substitution of Mn by other elements is likely to enhance the disorder in the system.

References:

[1] A. Asamitsu, Y. Moritomo, Y. Tomioka, T. Arima and Y. Tokura, Nature **373**, 407 (1995).

[2] S. Jin, T. H. Tiefel, M. McCormack, R. A. Fastnacht, R. Ramesh and L. H. Chen, Science **264**, 413 (1994).

[3] C. N. R. Rao, A. K. Cheetham and R. Mahesh, Chem. Mater. **8**, 2421 (1996).

[4] C. Zener, Phys. Rev. **82**, 403 (1951).

[5] A. J. Millis, P. B. Littlewood and Boris I. Shraiman, Phys. Rev. Lett. **74**, 5144(1995).

[6] S. E. Lofland, S. M. Bhagat, H. L. Ju, G. C. Xiong, T. Venkatesan and R. L. Greene, Phys. Rev. B **52**, 15058 (1995).

[7] P. A. Lee and T. V. Ramkrishnan, Rev. Mod. Phys. **57**, 287 (1985).

[8] B. L. Altshuler and A. G. Aronov, in A. L. Efros and M. Pollak (Eds.), Electron-Electron Interactions in Disordered Systems (North Holland, Amsterdam, 1985).

[9] H. Fukuyama, in A. L. Efros and M. Pollak (Eds.), Electron-Electron Interactions in Disordered Systems (North Holland, Amsterdam, 1985).

[10] $\tilde{F}_\sigma$ may be expressed in terms of the exact static amplitude of interaction (F) by the relation: $\tilde{F}_\sigma = \frac{-32}{F}\left[1+\frac{3F}{4}-\left(1+\frac{F}{2}\right)^{3/2}\right]$. Where F depends on the screening length and other details of the static screened potential between the electrons. Under Thomas-Fermi approximation it can be expressed as: $F = (1+Y)\ln(1+Y)$ where $Y = \frac{4\varepsilon_0 k_F^2}{e^2 N(E_F)}$. Under free

electron approximation the value of k_F for these samples is $k_F = (3\pi^2 n)^{1/3} \approx 5.32 \times 10^{10}$ m^{-1}. By an earlier specific heat study the value of $N(E_F)$ for these samples is found to be $\approx 1.9 \times 10^{47}$ J^{-1} m^{-3}. Using these values of k_F and $N(E_F)$ in above expression we find $\tilde{F}_\sigma \approx 0.808$ for all these samples.

[11] H. E. Fischer, S. K. Watson and D. G. Cahill, Comments Condens. Matter Phys. **14**, 65 (1988).

[12] K. P. Rajeev and A. K. Raychaudhuri, Phys. Rev. B **46**, 1309 (1992).

[13] J. M. D Coey, M. Viret, L. Ranno and K. Ounadjela, Phys. Rev. Lett. **75**, 3910 (1995).

[14] R. Mahendiran, S. K. Tiwary, A. K. Raychaudhuri, T. V. Ramakrishnan, R. Mahesh, N. Rangavittal and C. N. R. Rao, Phys. Rev. B **53**, 3348 (1996).

[15] E. L. Wolf, Principles of electron tunneling spectroscopy (Oxford University Press, Newyork, 1985).

[16] P. P. Edwards, T. V. Ramakrishnan, C. N. R. Rao, J. Phys. Chem. **99**, 5228 (1985).

[17] A. K. Raychaudhuri, K. P. Rajeev, H. Srikanth, R. Mahendiran, Physica B **197**, 124 (1994); A. K. Raychaudhuri, Phys. Rev. B, **44**, 8572 (1991).

[18] G. H. Jonker, Physica (Amsterdam) **20**, 1118 (1954).

[19] E. Banks and N. Tashima, J. Appl. Phys. **41**, 1186 (1970).

[20] K. H. Ahn, X. W. Wu, K. Liu and C. L. Chien, J. Appl. Phys. **81**, 5505 (1997).

[21] R. D. Shannon, Acta Crystallogr. Sec. A **32**, 751 (1976).

[22] J. F. Lawler, J. G. Lunney and J. M. D. Coey, Appl. Phys. Lett. **65**, 3017 (1994).

[23] A. Chainani, M. Mathew and D. D. Sarma, Phys. Rev. B **48**, 14818 (1993).

[24] Despina Louca and T. Egami, J. Appl. Phys. **81**, 5484 (1997).

[25] B. H. Toby and T. Egami, Acta Crystallogr. Sec.A **48**, 336 (1992).

[26] A. Tiwari and K. P. Rajeev, Phys. Rev. B (Accepted for publication).

Chapter 8

Conclusions

The main objective of this thesis was to study the effect of disorder on the electrical transport properties of transition metal perovskite oxides. We studied two different families of transition metal perovskite oxides, namely, nickelates and manganates. In this chapter we summarize some of the important findings of the present work.

Nickelates

The very first system investigated in this thesis is $LaNiO_{3-\delta}$ ($0.0 \leq \delta \leq 0.14$). Stoichiometric $LaNiO_3$ shows a positive temperature coefficient of resistivity throughout the whole temperature range, a characteristic of metals. However the residual resistivity of this sample is quite high ($\approx$1 mΩ-cm). Assuming that each Ni atom provides one conduction electron, this material has an electron density of $\approx 10^{22}$ /cm^3. The combination of reasonably high electron density and high residual resistivity indicates low diffusivity of electrons. This implies that even the stoichiometric sample has some disorder in it. As the oxygen deficiency is increased in the system the material becomes more disordered; the electrical resistivity starts showing an upturn at low temperature and the tunneling density of states shows a dip near the Fermi energy. A quantitative analysis of the low temperature electrical resistivity and tunneling density of states data shows the presence of enhanced e-e interactions in the system.

The next system investigated in this thesis is $NdNiO_{3-\delta}$ ($0.08 \leq \delta \leq 0.22$). The main issue that is addressed in this study is whether the sol-gel prepared nonstoichiometric $NdNiO_{3-\delta}$ is really an insulator at low temperature. In all the previous reports, guided by the fact that the temperature coefficient of resistivity is negative, $NdNiO_{3-\delta}$ has been claimed as an insulator at low temperature. But as a result of a careful quantitative analysis of our low

temperature electrical conductivity data we found that the $NdNiO_{3-\delta}$ samples have a nonzero extrapolated zero temperature conductivity and hence they can not be termed as insulators in the real sense of the word.

In another study we investigated the effect of substituting La by Nd in $LaNiO_3$. When Nd is doped in $LaNiO_3$ the electrical resistivity of $La_{1-x}Nd_xNiO_{3-\delta}$ system shows a minimum at low temperature which gradually shifts to higher temperature with increase in Nd concentration. In the low temperature limit the correction to electrical conductivity follows a power law behavior with an exponent ≈ 0.5 and the tunneling density of states of these samples show a cusp like dip near the Fermi energy. Both these features are attributed to enhanced e-e interaction in the system. Magnetoresistance of these samples is negative which indicates the possibility of the simultaneous presence of weak localization effects in the system.

After this we studied the effect of replacing Ni by Fe in $NdNiO_{3-\delta}$. $NdFeO_3$ is an insulator so it is expected that when Fe is doped in $NdNiO_{3-\delta}$ the resistivity of the system should increase. But contrary to this, for 10 atomic percentage doping of Fe the resistivity of the system is less than the undoped sample. This indicates the presence of weak localization effects in $NdNiO_{3-\delta}$. The partial suppression of the localization tendency by the spin flip scattering of electrons from Fe^{3+} centers may possibly be the cause of the unexpectedly lower electrical resistivity of 10 atomic percent Fe doped sample. As the Fe concentration is further increased the resistivity of the system increases but till 20 atomic percentage of Fe, all the samples have nonzero extrapolated zero temperature conductivity and hence are metallic. On further increasing Fe concentration the system undergoes an M-I transition and becomes insulating. The presence of a quantum correction to the density of states, due to e-e interactions, and the eventual opening up of a gap at E_F near the M-I transition are clearly seen in the electron tunneling conductance data.

Manganates

In this section we have undertaken two studies. In the first study we have investigated the low temperature electrical resistivity and electron tunneling conductance of $La_{0.7}A_{0.3}MnO_3$ (A: Ca, Sr, Ba) and in the second study we have examined the effect of the partial replacement of Mn by Fe in $La_{0.7}Sr_{0.3}MnO_3$.

Electrical resistivity of $La_{0.7}A_{0.3}MnO_3$ (A: Ca, Sr, Ba) samples shows a peak at a temperature close to ferromagnetic-paramagnetic transition temperature (T_c). Above T_c the material behaves as an insulator and below T_c it behaves as a metal. Though these materials are metallic at low temperature the magnitude of resistivity is rather high. We find that the residual resistivity of these materials is larger than or comparable to the estimated Mott's maximum metallic resistivity for the system. Electrical resistivity of all the samples show a slight upturn at around 30K, At low temperature the electrical conductivity follows a $\sqrt{T}$ dependence; a characteristic of disordered metallic systems with enhanced electron-electron interactions. Tunneling density of states of these materials show a dip near the Fermi energy and follows a $|E|^n$ energy dependence with n≈ 0.8-0.9. This behavior is quite similar to that observed in highly disordered systems close to metal-insulator transition.

When Fe is doped in $La_{0.7}Sr_{0.3}MnO_3$, the double exchange interaction between $Mn^{3+}$and Mn^{4+} is suppreseed and the resistivity of $La_{0.7}Sr_{0.3}Mn_{1-x}Fe_xO_3$ system increases. However, for $x \leq 0.2$ all the samples are found to be metallic. The magnitude of resistivity of these samples is quite high which is suggestive of the strongly disordered nature of these samples. Tunneling density of states of these materials show a dip near the Fermi energy and its energy dependence resembles that of highly disordered systems in the critical regime. As the concentration of Fe is further increased for $x \geq 0.25$ the system enters the insulating regime. It is found that even for the x = 0.25 sample, Mn exists both as Mn^{3+} as well as Mn^{4+} and hence sufficient number of the hopping electrons as well as the hopping

sites are available. We believe that the observed metal-insulator transition in the system is due to the disorder driven localization of charge carriers i.e. the Anderson transition.

After this we have discussed various causes that might be responsible for the disorder in Manganates. The random potential fluctuations seen by the conduction electrons due to different electronegativities of La^{3+} and A^{2+} (A: Ca, Sr, Ba) is understood to be the main cause of the disorder. Another cause of the disorder may be the local lattice distortions present in the system. Any substitution of Mn by other atoms is likely to further increase the disorder in the system.

The overall conclusion of this thesis is that the transition metal oxides are quite sensitive to disorder. When disorder is introduced into the system, by creating oxygen deficiency or by substituting one or more of the constituents, the diffusivity of the electrons goes down drastically and they start interacting with each other quite strongly and this causes significant corrections in the electrical transport and density of states. The oxide metals, even when they are 'clean', show a conductivity close to the Mott's minimum metallic conductivity. This means that these metals are quite close to the critical regime between good clean metals and insulators. And we find that this is especially so in the case of GMR oxides. The GMR metals at low temperatures, as shown by the electron tunneling conductance and resistivity data, are indeed lying deep inside the critical regime between metals and insulators, on the verge of a metal-insulator transition.

Appendix-I

Design and construction of a calorimeter

AI.1 introduction

Measurement of specific heat provides a lot of information about the lattice and electronic properties of a material. A device used for measuring the specific heat of samples is known as a calorimeter. History of the development of calorimeters is almost a century old. In 1910 Nernst and Eucken[1] for the first time measured the specific heat of solid materials using an adiabatic technique. In 1968 Sullivan and Seidel[2] devised an ac calorimeter to measure the specific heat of very small samples. Although this method allows the measurement of the specific heat of small samples, it has the drawback that it can be used only at very low frequencies and over limited temperature ranges. In the year 1980 Forgan and Nedjat[3] described a relaxation method to measure the specific heat of samples. In this method the sample is raised to an equilibrium temperature above a heat reservoir and then allowed to relax to the reservoir temperature with no heat input. In this method the time derivative of the temperature during the decay process is necessary for extracting the specific heat and hence it requires extensive calibration of heat losses of the sample as a function of temperature between the reservoir and final sample temperature. In the year 1986 Riegel and Weber[4] measured the specific heat of samples by using a technique which is a slight variation of the relaxation method. In this method they use an extremely weak thermal link to a reservoir and record the temperature of the sample while heating at constant power for one half of the cycle, then allow the sample to relax while recording the temperature during the second half of the cycle with zero power input. In the year 1990 Xu, Watson and Goodrich[5] devised a calorimeter that is a hybrid of ac calorimeter and relaxation calorimeter. This method uses some of the general ideas of the calorimeter of Riegel and Weber.

In the course of this thesis work a calorimeter has been designed and constructed to measure the specific heat of solids in the range 77-300K. This calorimeter is quite similar to the low temperature calorimeter of Xu *et al.*[5]. Because of the improved electronics and

data acquisition software, our calorimeter can be used to measure the specific heat of the solids at higher temperatures with good accuracy.

AI.2 Principle of operation

Suppose P_1 power is given to the sample, which is at the temperature T; a part of it will be lost to the surrounding while the rest of it will be spent in increasing the temperature of the sample. This can be expressed by the relation

$$p_1 = m \cdot C(T) \cdot \frac{dT}{dt}|_1 + p_{Loss} \qquad \text{(AI.1)}$$

Here m is the mass, $C(T)$ is the specific heat of the sample at temperature T, $\frac{dT}{dt}|_1$ represents the rate of change of temperature with time for the input power P_1, P_{Loss} represents the power lost to surrounding.

Now suppose that the sample is again at the temperature T and P_2 power is given to the sample then

$$p_2 = m \cdot C(T) \cdot \frac{dT}{dt}|_2 + p_{Loss} \qquad \text{(AI.2)}$$

For both the power inputs P_1 and P_2 the power lost to the surrounding P_{Loss} will remain same, because it depends on the temperature of the sample only (provided the other conditions are same in both the cases).

Subtracting eq.(AI.1) from eq.(AI.2) we get

$$C(T) = \frac{p_1 - p_2}{m \cdot \left(\frac{dT}{dt}|_1 - \frac{dT}{dt}|_2 \right)} \qquad \text{(AI.3)}$$

It is clear from the eq.(AI.3) that if at any particular temperature we know the values of the power inputs P_1 and P_2 and the corresponding derivatives $\frac{dT}{dt}|_1$ and $\frac{dT}{dt}|_2$ the value of the specific heat at that temperature can easily be determined.

AI.3 Experimental Set-up

Cryostat :

The schematic diagram of the cryostat is shown in figure AI.1. This consists of a vacuum

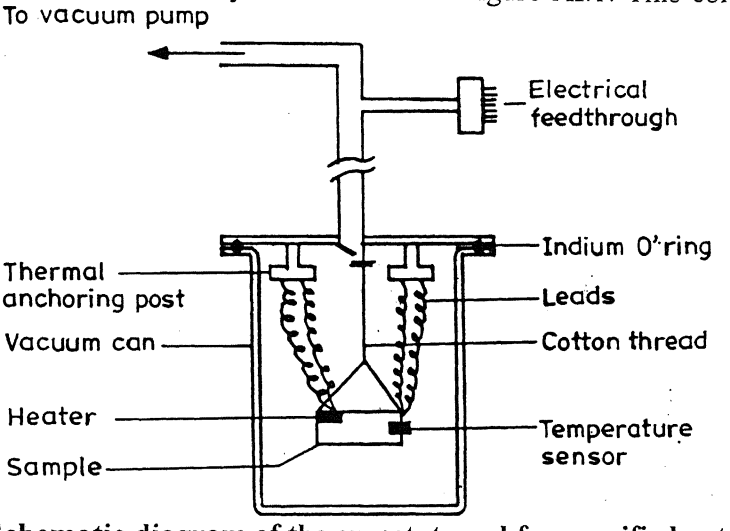

Figure AI.1: Schematic diagram of the cryostat used for specific heat measurement.

chamber sealed by indium O'ring. Sample is suspended from the top of this chamber with the help of a thin cotton thread. A miniature Platinum resistance (Pt 110 from Lake Shore Cryotronics) is used as the temperature sensor and a small Zener diode (dia=1.9mm, mass=69.4 mg, V_Z=4 V) is used as heater. The heater and the temperature sensor are placed on the sample directly. To minimize the heat loss, very thin phospher-bronze wires (SWG 40) were used for electrical connections.

Electronics:

The accuracy of specific heat measurement depends on the accuracy with which the temperature and time (i.e. $\frac{dT}{dt}$) can be measured. To measure the temperature with high accuracy we have constructed an electronic circuit using easily available operational amplifiers and transistors. The block diagram of the electronic circuit is shown in the figure AI.2. It consists of three important parts namely (a) bi-directional current source (b) Instrumentation amplifier (c) constant current source for heater.

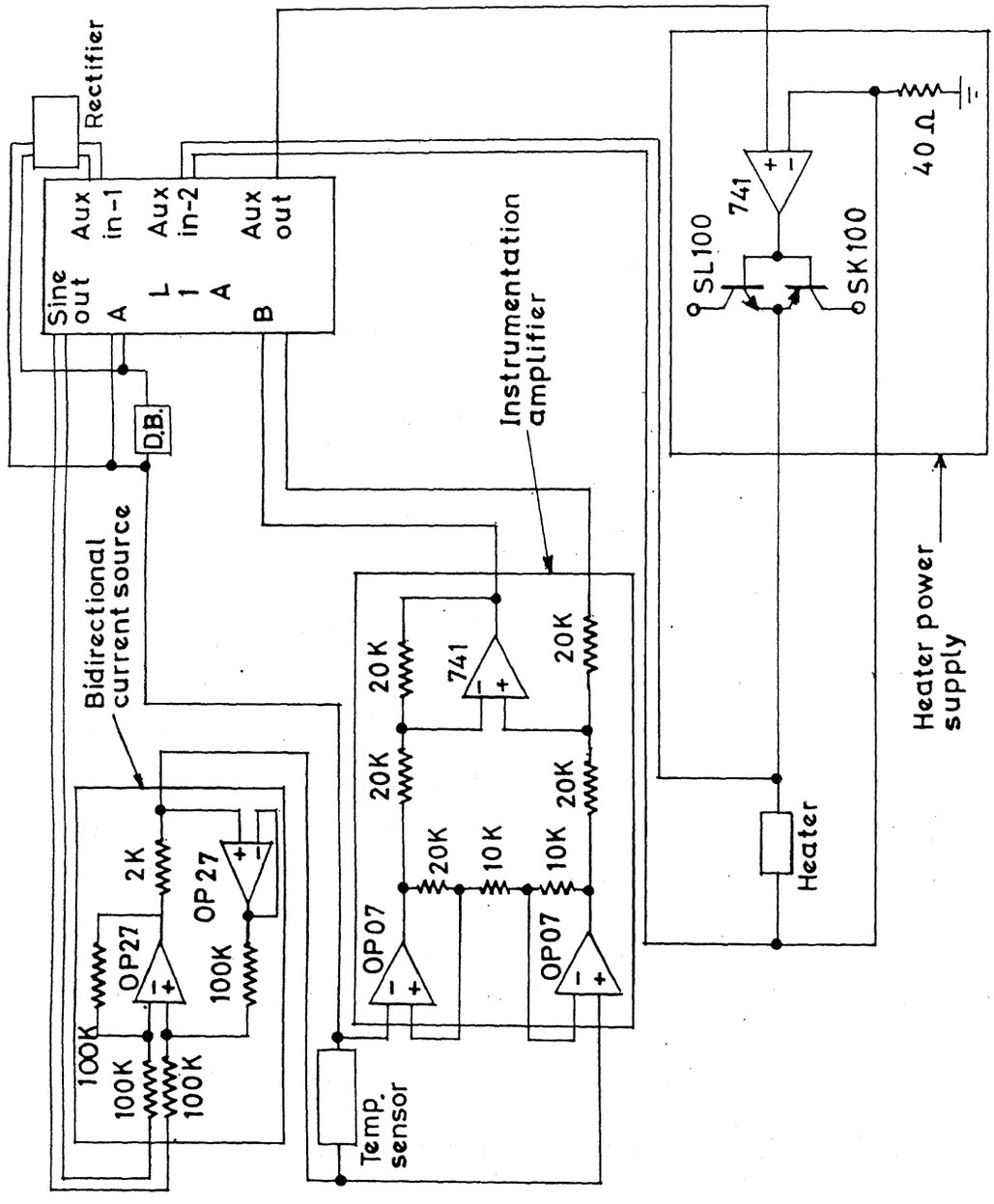

Figure AI.2:Detailed diagram of the electronic circuit used for specific heat measurement.

Bi-directional current source is driven by the Lock-in amplifier's (MODEL SR830 DSP Lock-In Amplifier) sineout and provides a constant ac current (freq.=997.7 Hz). Ac current (2 mA) is sent to the platinum resistance in series with a decade box. The voltage developed across the platinum resistance (V_s) is fed to the B-input (through the instrumentation amplifier) and the voltage across the decade box (V_D) is fed to the A-input of the Lock-in amplifier. The gain of the instrumentation amplifier is 5. The voltage difference (V_D - $5V_s$) is measured by the Lock-in amplifier in the A-B mode. The resistance of the decade box is adjusted in such way that the voltage difference (V_D - $5V_s$) is always less than 3 mV and the full-scale sensitivity of the Lock-In amplifier is kept at 3 mV. The resistance of the decade box is measured separately also by the aux-input of the Lock-in amplifier. For this purpose rectifier and filter circuits have been made which convert the ac voltage across the D.B. into dc voltage and this voltage is measured by the aux-input of the Lock-in amplifier. The value of (V_D-$5V_s$) in assistance with the separately measured value of the decade box resistance gives the resistance of platinum with a resolution $\approx$ 1 part in 10^6.

The heater current (0-500 mA) is provided by the constant dc current source, which is driven by the aux-out voltage of the Lock-in amplifier. The voltage developed across the heater is measured by the aux-input of the Lock-in amplifier.

AI.4 Data acquisition and Timing:

Reduction in the measurement of dT/dt calls for the accurate measurement of time. In this work we tackled this problem by having the PC acquire the temperature data at precisely equal intervals of time. This was done by using the timer interrupt which comes every 55 ms. An interrupt handler routine collects the temperature (resistance) data from the Lockin amplifier at every 20'th clock tick. This ensured that we measured an interval of $\approx$ 1 s to an accuracy better than 0.1 %. During the rest of the clock ticks the interrupt handler measures the power being delivered to the heater. To make sure that the interrupt handler gets control at precisely equal intervals of time we have to make sure that (a) the program should not be run in a multitasking environment (like windows, linux etc.) (b) no other program catches the timer interrupt (c) measurements inside the interrupt handler are completed well before the 55 ms time limit. To take care of (a) and (b) we ran the program under DOS (6.22) as a single task with a minimum of memory

resident utilities, none of which used the timer interrupt. To take care of (c) we timed the lock-in amplifier to find that it takes a measurement in 6 ms. Not more than 2 lock-in accesses were allowed inside the interrupt handler.

Operation and performance of the calorimeter

The sample is weighed before mounting it in the calorimeter. The temperature sensor (a miniature platinum resistance) and a heater (a miniature Zener diode) are fixed on the sample itself with a thin layer of GE varnish. (For the smaller samples, the sample can be placed on the one side of a thin sapphire plate and the temperature sensor and heater on the other side of the plate.) The sample is suspended from the top of the vacuum can with the help of a thin cotton thread. After mounting the sample, the vacuum can is pumped down to 1 μ Hg. After pumping the vacuum can is immersed in the liquid nitrogen.

To start with a heater-input power is given to the sample. A part of this power is lost to the surrounding and the rest is spent in increasing the temperature of the sample. Once the temperature has increased by 2-3 K the heater power is decreased and the temperature starts decreasing. When the temp. comes to the initial value the heater power is again increased and the whole process is repeated several times. The heater power and the temperature of the sample are continuously monitored as a function of time (see figure AI.3).

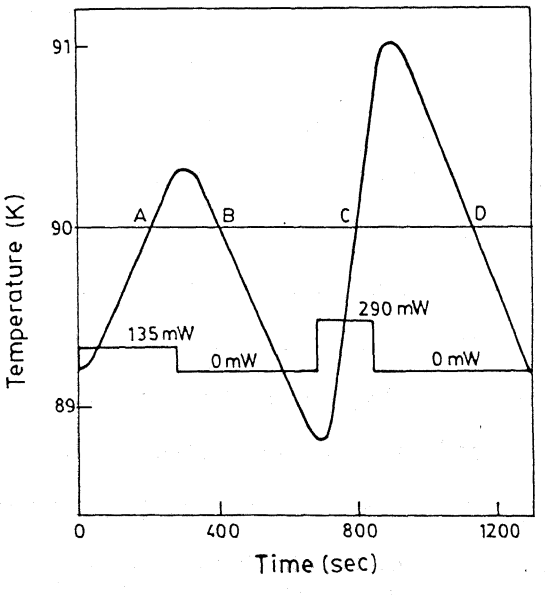

Figure AI.3 : Sample temperature and heater power as a function of time.

Specific heat can very easily be calculated from this figure. For this a horizontal line corresponding to the temperature of interest is drawn. This line cuts the temperature curves at points A,B,C..etc., all these points correspond to the condition when the sample was at the same temperature however the heater power was different. The value of the heater power input is known at all these points and the value of dT/dt at these points can be calculated numerically. Using these values of power inputs (P) and dT/dt in eq.(AI.3) we get the value of the specific heat of the samples. To check the performance of the instrument the specific heat of pure copper was measured and it was found to be in excellent agreement with the previously reported values (see figure AI.4a). Figure AI.4b shows the specific heat of $La_{0.7}Sr_{0.3}Mn_{0.9}Cu_{0.1}O_3$. This is a giant magnetoresistive material and undergoes a ferromagnetic to paramagnetic transition at T = 340 K (see inset of figure AI.4b) . Specific heat of the sample also shows a peak at the transition temperature.

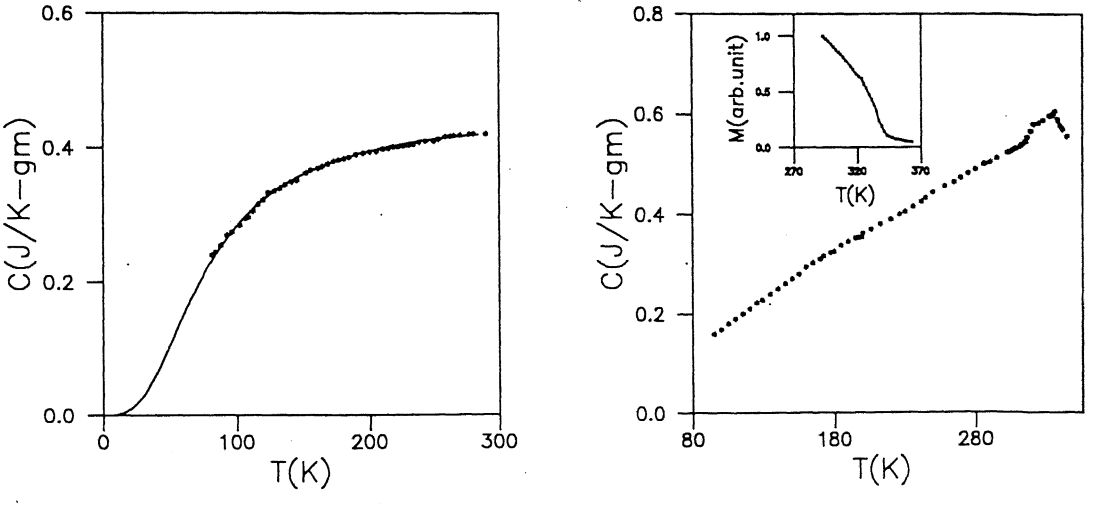

Figure AI.4 (a) Specific heat of Copper (b) specific heat of $La_{0.7}Sr_{0.3}Mn_{0.9}Cu_{0.1}O_3$, inset shows the magnetization vs. T.

References:

[1] G. K. White, Experimental techniques in low temperature physics (Clarendon press, Oxford, 1957).

[2]P. F. Sullivan and G. Seidel, Phys. Rev. **173**, 679 (1968).

[3]E. M. Forgan and S. Nedjat, Rev. Sci. Instrum. **51**, 411 (1980).

[4] S. Riegel and G. Weber, J. Phys. E. **19**, 790 (1986).

[5] Jing-chun Xu, C. H. Watson and R. G. Goodrich, Rev. Sci. Instrum. **61**, 814 (1990).

Appendix-II

Electron tunneling conductance and the density of states

Electron tunneling spectroscopy is a powerful technique to study the behavior of the density of states in materials at low temperature. There are some other techniques also like optical conductivity measurements, photoelectron spectroscopy, x-ray absorption spectroscopy etc., which are frequently used to determine the electronic density of states of materials. But the electron tunneling spectroscopy is unique in the sense that it probes the electronic states very close to the Fermi level and provides important information about the density of states near the Fermi energy. The energy resolution of the electron tunneling spectroscopy is a few times the thermal energy, so if the experiments are performed at liquid helium temperature, it has the resolution of millivolts or less.

The most crucial part of an electron tunneling experiment is to make a tunnel junction. One electrode of this junction is made of the material whose electronic states are to be studied and the second electrode (reference electrode) is made of a standard material whose density of states are already known. Next step in this experiment is to apply a bias voltage between the two electrodes. Now the bias voltage between the two electrodes is varied so that the electron tunneling between the different energy states of electrodes occur. This allows us to extract the information about the electronic density of states in the electrodes.

Fig AII.1 represents a typical diagram of a tunnel junction showing the electron tunneling process between the two electrodes. The tunneling conductance depends on the density of states of both, the sample electrode as well as the reference electrode. If the reference electrode is so chosen that it have constant density of states near the Fermi energy then at sufficiently low temperature the tunneling conductance data closely resemble the density of states of the sample i.e. $G(V) \propto N(q_e V + E_F)$.

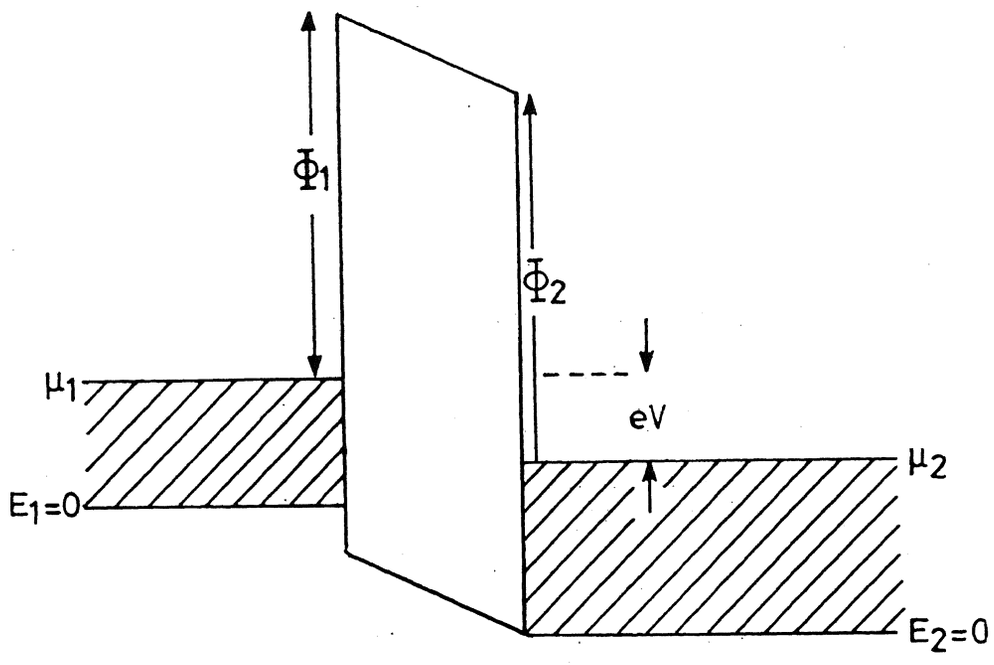

Figure AII.1 : Schematic illustration of the electron tunneling process. A thin insulating barrier separates the reference electrode and the sample. Φ_1 and Φ_2 represent the work functions and μ_1 and μ_2 represent the Fermi levels of the reference and sample respectively. V is the potential difference between the two electrodes. Conventionally if the sample voltage is greater than the reference electrode voltage, it is considered as a case of positive V. In this case the right side of the graph of dI/dV vs. V will represent empty states.

References:

[1] E. L. Wolf, Principles of electron tunneling spectroscopy (Oxford university press, New York, 1985).

Appendix-III

Local Environment of Fe in $NdNi_{1-x}Fe_xO_{3-\delta}$

Mössbauer spectroscopy[1-3] is an important spectroscopic technique for local structure determination via hyperfine interactions, i.e. the interactions between the nuclear charge distribution and extranuclear electric and magnetic fields. These hyperfine interactions give[2] rise to the isomer shift (IS), the quadrupole splitting (QS) and the magnetic Zeeman splitting. In this appendix a systematic study of the local environment of Fe in $NdNi_{1-x}Fe_xO_{3-\delta}$ using Mössbauer spectroscopy has been presented.

All the samples are orthorhombic and their unit cell parameters along with the oxygen stoichiometries are tabulated in table AIII.1. Room temperature Mössbauer spectra of various $NdNi_{1-x}Fe_xO_{3-\delta}$ samples are shown in figure AIII.1 and figure AIII.2. The experimental values of the isomer shift (relative to metallic iron), quadrupole splitting and internal magnetic fields for various samples are summarized in table AIII.2.

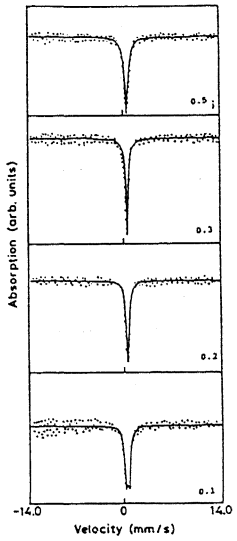

Figure AIII.1: Room temperature Mössbauer spectrum of $NdNi_{1-x}Fe_xO_{3-\delta}$ for x<0.5.

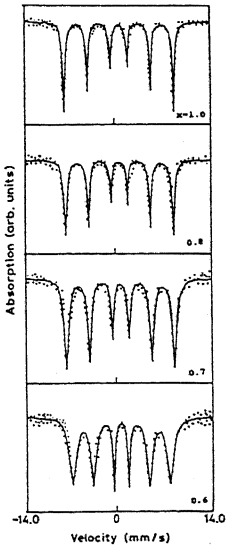

Figure AIII.2: Room temperature Mössbauer spectrum of $NdNi_{1-x}Fe_xO_{3-\delta}$ for x ≥0.5.

This appendix is based on the published work of A. Tiwari, J. of Alloys and Compounds **274**, 42 (1998).

Table AIII.1: Lattice parameters and oxygen contents of $NdNi_{1-x}Fe_xO_{3-\delta}$ samples.

x	parameters			3-δ
	a(Å)	b(Å)	c(Å)	
0.0	5.423	5.431	7.556	2.92
0.1	5.436	5.452	7.540	2.93
0.2	5.441	5.473	7.546	2.94
0.3	5.449	5.482	7.554	2.95
0.5	5.454	5.502	7.573	2.96
0.6	5.464	5.512	7.591	2.97
0.7	5.474	5.532	7.612	2.98
0.8	5.484	5.562	7.630	2.99
1.0	5.509	5.602	7.671	3.00

AIII.1 Isomer shift

The isomer shift results from the electrostatic interaction between the charge distribution of the nucleus and those electrons which have a finite probability of being found in the region of the nucleus[2,3]. Only s-electrons have a finite probability of overlapping with the nuclear charge density and thus of interacting with it. Although the p- and d-electrons do not interact directly with the nuclear charge density, they may cause a slight change in the s-electron density and thus cause a slight change in the isomer shift. The value of the isomer shift (in velocity units) is given by the well known relation[2,3]:

$$\text{I.S.} = 10.5 \frac{ZA^{2/3}}{E_\gamma} \frac{\Delta R}{R} [\rho_s(\text{A}) - \rho_s(\text{S})] \qquad \text{(AIII.1)}$$

where E_γ is the energy of the nuclear transition (keV), Z and A the electron number and mass number, respectively, R is the nuclear radius, ΔR the change in the nuclear radius for a transition from the excited state to the ground state, ρ_s(A) and ρ_s(S) are the s-electron densities in atomic units at the nucleus of the absorber and the source, respectively.

Table AIII.2 : Isomer shift (IS), quadrupole splitting (QS), internal magnetic field and effective s-electron density at the iron nucleus for various $NdNi_{1-x}Fe_xO_{3-\delta}$ samples.

Sample	IS (mm/s)	QS(mm/s)	Internal Magnetic Field (T)	$\rho_s(Fe^{3+})$ (a.u.)
0.1	0.506	0.48	-	7533.150
0.2	0.554	0.27	-	7533.055
0.3	0.575	0.15	-	7533.013
0.5	0.600	0.13	-	7532.963
0.6	0.639	0.04	45.42	7532.885
0.7	0.644	-0.01	50.38	7532.875
0.8	0.649	-0.025	50.44	7532.865
1.0	0.650	-0.03	51.27	7532.863

In $NdFeO_3$, Fe is in the 3+ state with the electronic configuration $3d^5$. By Hartree-Fock calculations the s-electron density for Fe^{3+} is found to be 7533.02 a.u.[3]. In the case of Fe atom ($3d^74s^1$) the s-electron density at the nucleus is found to be 7534.16 a.u.[3]. Using these values of charge densities with $\Delta R/R = -(18\pm4)\times10^{-4}$ in eq.(AIII.1) we obtain I.S.=0.66 mm/s, which is in excellent agreement with the observed isomer shift of 0.65 mm/s.

Table AIII.2 summarizes the values of s-electron densities at the iron nucleus for various samples. As the concentration of Ni increases the isomer shift decreases, implying an increase in the effective density of s-electrons at the nucleus. The increase in the effective s-electron density is equivalent to a decrease in the localized d-electron density (the 3d-electrons have a finite probability of lying within 3s-electrons, causing 3s-electrons to expand and thus reduce the s-electron density at the nucleus). So as the concentration of Ni increases the d-electrons become more delocalized.

AIII.2 Quadrupole splitting

Another important quantity from which information can be obtained is the quadrupole splitting (QS). Any nuclear state with $I>1/2$ has a quadrupole moment Q, which can interact with a noncubic extranuclear field to lift the degeneracy of the state. The quadrupole splitting (QS) is directly proportional to Q and the electric field gradient

A very small quadrupole splitting value is observed for $NdFeO_3$, which suggests an almost octahedral environment for Fe. This small quadrupole splitting may be because of the polycrystalline nature of the sample (Goldanski-Karayagin effect)[2,3]. As the concentration of Ni increases the QS remains very small and varies very slightly till 40 atomic percent of Ni . For Ni concentration more than 50 atomic percent the QS becomes quite appreciable and increases with further increase in Ni concentration. The increase in QS with increasing Ni concentration can be attributed to the increasing oxygen deficiency in the sample. Because of the oxygen deficiency the environment of Fe is not purely octahedral, i.e. FeO_6 octahedra are not regular and hence the Fe atom experiences a noncubic electric field which gives rise to QS.

AIII.3 Nuclear magnetic Zeeman splitting

The third hyperfine interaction that affects the Mössbauer spectrum is the nuclear magnetic Zeeman splitting. When the nucleus is subject to an internal or an external magnetic field the nuclear energy levels split. The extent of the energy separation depends, both on the nuclear magnetic moments of the ground and excited states and also on the magnitude of the magnetic field. For instance, for ^{57}Fe the $I=1/2$ ground state splits into two sublevels and the $I=3/2$ excited state splits into four sublevels. Transitions between these are subject to the selection rule $\Delta m=0, \pm 1$. So, because of the nuclear magnetic Zeeman splitting of Fe six resonance lines are expected.

For $NdFeO_3$ six resonance lines are observed. This shows that the Fe ions experience an internal magnetic field. It has been reported[4,5] that $NdFeO_3$ is an antiferromagnet with T_N=620 K. The Fe ions are arranged as two sublattices coupled antife-

rromagnetically. These sublattices are slightly canted with respect to the antiferromagnetic axis, resulting in a small net ferromagnetic moment. For $NdFeO_3$ an internal magnetic field of 51.3 T has been observed, which is in very good agreement with the previously reported value[5].

$NdNiO_3$ is a paramagnet. So, as the concentration of Ni increases in the system the strength of the antiferromagnetic interaction decreases, which causes a decrease in the internal magnetic field experienced by the Fe ion. For Ni concentration more than 50 atomic percent, the internal magnetic field vanishes completely causing the disappearance of six line resonance spectra.

References:

[1] N. N. Greenwood, Angew. Chem. Int. Ed. **10** , 716 (1971) .

[2] G. M. Bancroft, Mössbauer spectroscopy: An Introduction for Inorganic Chemists and Geochemists (Mcgraw-Hill, New York, 1973).

[3]G. K. Shenoy, F. E. Wagner (Eds.), Mössbauer Isomer Shift (North-Holland, Amsterdam, 1978).

[4] J. Blasco, J. García, J. Phys. Chem. Solids **55**, 843 (1994)

[5] M. Eibschutz, S. Shtrikman, D. Treves, Phys. Rev. B **48**, 11666 (19993).

Appendix-IV

$LaMnO_{3+\delta}$

One of the most important parameters that affects the behavior of any oxide material is the oxygen stoichiometry. Since in manganates it is the ratio of Mn^{3+} and Mn^{4+} that determines the whole behavior, the role of oxygen stoichiometry becomes more crucial. In this section an effort has been made to see how does the material behaves when the oxygen stoichiometry is varied.

$LaMnO_{3+\delta}$ samples were prepared by the citrate precursor decomposition method. Appropriate amounts of Lanthanum nitrate, manganese nitrate and citric acid were dissolved in water so as to maintain La:Mn:citric acid ratio of 1:1:2.05. The resulting solution was refluxed at 360 K for 12 hours. After refluxing the solution was gently warmed to get citrate precursor powder. The precursor powder was ground and given heat treatment at 823 K. The sample thus prepared was pressed into five pellets and each pellet was annealed under different condition. The oxygen stoichiometries of these samples were determined by iodometric titration. Table AIV.1 shows the annealing conditions and oxygen stoichiometry in various samples.

Table AIV.1: Mn^{3+}/Mn^{4+} ratio for different annealing conditions.

Annealing atmosphere	Annealing temperature	Duration	Mn^{3+}/Mn^{4+} ratio	Stoichiometry
O_2	1075 K	12 hours	0.30/0.70	$LaMnO_{3.15}$
Air	1075 K	24 hours	0.24/0.76	$LaMnO_{3.12}$
Air	975 K	24 hours	0.20/0.80	$LaMnO_{3.10}$
Air	975 K	12 hours	0.16/0.84	$LaMnO_{3.08}$
Vacuum	975 K	24 hours	0.08/0.92	$LaMnO_{3.04}$

This appendix is based on the published work of A.Tiwari and K.P.Rajeev, Journal of Material Science Letters **16**, 521 (1997).